

2018

Whispering-Gallery Mode Microsphere Resonators for Applications in Environmental Sensing

Arun Mallik

Technological University Dublin, arun.mallik@tudublin.ie

Follow this and additional works at: <https://arrow.tudublin.ie/engdoc>

 Part of the [Electrical and Computer Engineering Commons](#)

Recommended Citation

Mallik, A. K. (2018) *Whispering-Gallery Mode Microsphere Resonators for Applications in Environmental Sensing*. Doctoral thesis, DIT, 2018. doi.org/10.21427/jjkc-kq78

This Theses, Ph.D is brought to you for free and open access by the Engineering at ARROW@TU Dublin. It has been accepted for inclusion in Doctoral by an authorized administrator of ARROW@TU Dublin. For more information, please contact arrow.admin@tudublin.ie, aisling.coyne@tudublin.ie, vera.kilshaw@tudublin.ie.

Whispering-Gallery Mode Microsphere Resonators for Applications in Environmental Sensing

A thesis submitted in partial fulfilment of the requirement
for the degree of Doctor of Philosophy

by

ARUN KUMAR MALLIK



**Supervisors: Prof. Yuliya Semenova
Prof. Gerald Farrell
Dr. Qiang Wu**

School of Electrical and Electronic Engineering
Dublin Institute of Technology
Dublin, Ireland
August 2018

*To my beloved wife and son, parents and siblings,
teachers and friends*

Abstract

Humidity, temperature and volatile organic compounds (VOCs), particularly ammonia, are key environmental conditions that have a major impact on human comfort, well-being and productivity, as well as on agriculture, food processing and storage, electronic manufacturing and many other industries. This results in the urgent need for the development of sensing technologies allowing rapid detection and accurate measurement of these environmental parameters. Over the past decades many electrical as well as optical sensors have been proposed and demonstrated for environmental applications. However, challenge always exists for these sensors in terms of sensitivity, selectivity, detection limit, speed of response and robustness, where researchers and engineers are still working continuously on improving the performance of these sensors.

Whispering gallery mode (WGM) optical micro-resonators have been shown to be able of detecting minute changes in their environment. This has made them a well-established platform for highly sensitive physical, chemical and biological sensors. Silica micro-resonators with high quality factors and low absorption loss can be fabricated easily at the tip of an optical fiber, and the WGMs in such resonators can be excited by evanescent light coupling using tapered fibers.

The aim of this PhD thesis is the development of novel ultra-high sensitivity sensors based on silica micro-spheres functionalized with specific coatings with a particular focus on measurement of water vapor and ammonia concentration in air. A numerical simulation model has been analysed based on perturbation theory to facilitate deep understanding of WGMs in coated micro-sphere resonators and the results of the simulations have been validated by experimental studies.

Relationship between key design parameters of the sensor such as microsphere size, thickness of the coating layer, tapered fiber waist diameter, its Q factor and sensitivity has been investigated and established.

A novel high sensitivity relative humidity (RH) sensor based on an agarose-coated spherical micro-resonator has been proposed and experimentally demonstrated. The sensor's spectrum shows a wavelength shift of approximately 518 pm corresponding to a relative humidity change of 40% RH. Detailed experimental investigation of the influence of the agarose coating thickness on the sensor's humidity response has been carried out and correlated with the analytical model results. Sensor's performance in very low humidity environments (<10% RH) has been studied. It has been demonstrated that the proposed sensor is capable of detecting water molecules concentration in air in the order of parts per million (ppm) with good repeatability, low hysteresis and long-term stability.

A novel ultra-sensitive ammonia sensor has been proposed and developed by coating a porous silica gel on a microsphere acting as the sensing head. The sensor offers high resolution and the lowest reported to date detection limit of 0.16 ppb with response and recovery times of 1.5 s and 3.6 s respectively.

Finally, a novel approach to simultaneous measurement of ammonia vapors and humidity in air with high resolution has been proposed and demonstrated experimentally. In the proposed two-parameter sensor WGMs are excited at the same time in an array of two micro-spheres coated with different polymers, namely, silica gel and agarose hydrogel, coupled to a single adiabatic fiber taper. The method can be further expanded to achieve sensing of multiple chemical and biological quantities utilizing various coatings and possibly increasing the number of sensors within the array, thus reducing the cost of sensors interrogation.

Declaration

I hereby declare that this thesis is entirely my own original work. All other sources of information presented which are not part of my own work have been properly cited in the bibliography. No part of this thesis has been submitted for any degree at any other university or academic institution. This thesis was prepared according to the regulations for postgraduate study by research of the Dublin Institute of Technology.

The work reported on in this thesis conforms to the principles and requirements of the Dublin Institute of Technology's guidelines for ethics in research.

DIT has permission to keep, lend or copy this thesis in whole or in part, on condition that any such use of the material of the thesis is duly acknowledged.

Signature 

22 Aug 2018

Date

Acknowledgements

This four years PhD study at DIT Photonics Research Center (PRC) has become the most significant period of time in my life. I would like to express my gratitude to the following people, without whose help this thesis could not have been complete. Prof. Yuliya Semenova, my supervisor, whose constant guidance and sympathetic encouragements has been indispensable. She always inspired me and manage to motivate me with her ingenious suggestions. I reserve my gratitude for her constant guidance and support over all these years. I am also grateful to her for creating good lab facilities that helped me to carry out my research work smoothly and independently. Her enthusiasm, encouragement, advice, inspiration, patience, and great efforts for explaining things simply and clearly, made my thesis work more effective.

Prof. Gerald Farrell and, Dr. Qiang Wu my co-supervisors, who made valuable suggestions during my work on WGM sensing application. Their positive attitude and advice gave me the confidence to approach many problems both in research and life. I also want to sincerely thank them for the careful reading, comments and perspectives given to my thesis.

Special thanks to my fellow colleagues at the PRC: Wei Han, Dejun Liu, Fang Fang Wei, Vishnu Kavungal, Xiaokang Lian, Manjusha Ramakrishnan, Lin Bo, Youqiao Ma for their support and friendship and making a pleasant atmosphere during research carrier. I would also like to thank to all visiting students Aseel Ibrahim, Zhe Kang, Sun Lei, K Tian, Michal Skalsky, Diego Lopez, Yo Xuan Tiang for their unconditional friendship and encouragement during each stage of my PhD career.

I acknowledge the financial support from “Fiosraigh Dean of Graduate Research School” for my research study.

Many thanks to my friends in Ireland, Sithara, Shivananda, Sanjay, Prabhdeep, Sobin, Sony who have motivated me a lot and given their help from time to time, especially for the occasional dinner parties, which made my life more enjoyable in Ireland.

Last, but not least, I would like to acknowledge my indebtedness to my family, specially to my wife Sonali Mallik, whose understanding and love have sustained me at times when living in foreign country far from home has proven difficult. Special love to my son Aarush Mallik, born in the first year of my PhD studentship. I also would like to thank my entire extended family, cousins, uncles, and aunties.

Arun Kumar Mallik

List of Publications

Peer-Reviewed Journal Articles:

- [1] **A. K. Mallik**, G. Farrell, M. Ramakrishnan, V. Kavungal, D. Liu, Q. Wu and Y. Semenova, “Whispering gallery mode micro resonators for multi-parameter sensing applications”, **Optics Express**, accepted for publication.
- [2] **A. K. Mallik**, G. Farrell, D. Liu, V. Kavungal, Q. Wu and Y. Semenova, “A coated spherical micro resonator for measurement of water vapor concentration at ppm levels in very low humidity environments,” **Journal of Lightwave Technology**, Vol. 36, 2667-2674 (2018).
- [3] **A. K. Mallik**, G. Farrell, D. Liu, V. Kavungal, Q. Wu and Y. Semenova, “Silica gel coated spherical micro resonator for ultra-high sensitivity detection of ammonia gas concentration in air,” **Scientific Reports**, 8, 1620 (2018).
- [4] **A. K. Mallik**, Q. Wu, G. Farrell and Y. Semenova, “Study of the influence of the Agarose hydrogel layer thickness on sensitivity of the coated silica microsphere resonator to humidity,” **Applied Optics**, Vol. 56, 4065-4069 (2017).
- [5] **A. K. Mallik**, D. Liu, V. Kavungal, Q. Wu, G. Farrell and Y. Semenova, “Agarose Coated Spherical Micro Resonator for Humidity Measurements,” **Optics Express**, Vol. 24, 21216-21227 (2016).
- [6] V. Kavungal, G. Farrell, Q. Wu, **A. K. Mallik** and Y. Semenova, “Studies of geometrical profiling in fabricated tapered optical fibers using whispering gallery modes spectroscopy” **Optical Fiber Technology**, Vol. 41, 82-88 (2018).
- [7] V. Kavungal, G. Farrell, Q. Wu, **A. K. Mallik** and Y. Semenova, “Thermo-optic tuning of a packaged whispering gallery mode resonator filled with nematic liquid crystal” **Optics Express**, Vol. 26, 8431-8442 (2018).
- [8] V. Kavungal, G. Farrell, Q. Wu, **A. K. Mallik** and Y. Semenova, “A comprehensive experimental study of whispering gallery modes in a cylindrical micro-resonator excited by a tilted fiber taper,” **Microwave and Optical Technology Letters**, Vol. 60, 1495-1504 (2018).
- [9] V. Kavungal, G. Farrell, Q. Wu, **A. K. Mallik** and Y. Semenova, “A packaged whispering gallery mode strain sensor based on a polymer wire

- cylindrical micro resonator,” **Journal of Lightwave Technology**, Vol. 36, 1757-1765 (2018).
- [10] D. Liu, R. Kumar, F. Wei, W. Han, **A. K. Mallik**, C. Yu, Z. Kang, F. Li, Z. Liu, H.Y. Tam, G. Farrell, Y. Semenova and Q. Wu “Highly sensitive twist sensor based on partially silver coated hollow core fiber structure,” **Journal of Lightwave Technology**, Vol. 36, 3672 - 3677 (2018).
 - [11] D. Liu, R. Kumar, F. Wei, W. Han, **A. K. Mallik**, J. Yuan, S. Wan, X. Hei, Z. Kang, F. Li, C. Yu, Y. Semenova, G. Farrell, and Q. Wu, “High sensitivity optical ber sensors for simultaneous measurement of methanol and ethanol”, **Sensors and Actuators B: Chemical**, Volume 271, 1-8 (2018).
 - [12] D. Liu, Q. Wu, C. Mei, J. Yuan, X. Xin, A. K. Mallik, F. Wei, W. Han, R. Kumar, C. Yu, S. Wan, X. He, B. Liu, G.-D. Peng, Y. Semenova, and G. Farrell “Hollow Core Fiber Based Interferometer for High Temperature (1000 °C) Measurement,” **Journal of Lightwave Technology**, Vol. 36, 1583-1590 (2018).
 - [13] V. Kavungal, **A. K. Mallik**, G. Farrell, Q. Wu and Y. Semenova, “Strain-induced spectral tuning of the whispering gallery modes in a cylindrical micro-resonator formed by a polymer optical fiber,” **Applied Optics**, Vol. 56, 1339-1345 (2017).
 - [14] F. Wei, **A. K Mallik**, D. Liu, Q. Wu, G.-D. Peng, G. Farrell and Y. Semenova, “Magnetic field sensor based on a combination of a microfiber coupler covered with magnetic fluid and a Sagnac loop,” **Scientific Reports**, 7 , 4725 (2017).
 - [15] D. Liu, W., **A. K. Mallik**, J. Yuan, C. Yu, G. Farrell, Y. Semenova and Q. Wu, “High sensitivity sol-gel silica coated optical fiber sensor for detection of ammonia in water,” **Optics Express**, Vol. 24, 24179-24187 (2016).
 - [16] D. Liu, **A. K. Mallik**, J. Yuan, C. Yu, G. Farrell, Y. Semenova and Q. Wu, “High sensitivity refractive index sensor based on a tapered SCSMF structure,” **Optics Letters**, Vol. 40, 4166-4169 (2015).

Conference Proceedings:

- [1] **A. K. Mallik**, D. Liu, Vishnu Kavungal, X. Lian, G. Farrell, Qiang Wu, Yuliya Semenova, “Compact relative humidity sensor based on an agarose coated silica micro resonator,” [Proc. SPIE 10323, 25th International Conference on Optical Fiber Sensors Jeju, South Korea \(2017\).](#)
- [2] **A. K. Mallik**, D. Liu, Vishnu Kavungal, Qiang Wu, G. Farrell and Yuliya Semenova, “Porous silica coated spherical microresonator for vapor phase sensing of ammonia at a sub-ppm level,” [Proc. SPIE 9916, Sixth European Workshop on Optical Fibre Sensors Limerick, Ireland \(2016\).](#)
- [3] **A. K. Mallik**, G. Farrell, Qiang Wu, Yuliya Semenova, “Refractive Index Sensor Based on a Silica Microsphere Whispering Gallery Mode Resonator,” [IEEE Worksop in Recent Advance Photonics \(WRAP\), India \(2015\).](#)
- [4] **A. K. Mallik**, Yuliya Semenova, Qiang Wu, G. Farrell, “Numerical and Experimental Study of Whispering Gallery Mode Resonator based on a Silica Microsphere,” [12th International Conference on Fiber Optics and Photonics, India \(2014\).](#)
- [5] F. Wei, **A. K. Mallik**, D. Liu, Wei Han, X. Lian, G. Farrell, Q. Wu, G.-D. Peng, Y. Semenova, “Simultaneous measurement of both magnetic field strength and temperature with a microfiber coupler-based fiber laser sensor,” [Proc. SPIE. 10323, 25th International Conference on Optical Fiber Sensors, 103230H Jeju, South Korea \(2017\).](#)
- [6] D. Liu, X. Lian, **A. K. Mallik**, W. Han, F. Wei, J. Yuan; C. Yu, G. Farrell, Y. Semenova, Q. Wu, “Detection of volatile organic compounds using an optical fiber sensor coated with a sol-gel silica layer containing immobilized nile red,” [Proc. SPIE. 10323, 25th International Conference on Optical Fiber Sensors, 103232 Jeju, South Korea \(2017\).](#)
- [7] D. Liu, **A. K. Mallik**, Wei Han, F. Wei, Lei Sun, J. Yuan, C. Yu, G. Farrell, Y. Semenova and Q. Wu, “Sol-gel silica coated optical fiber sensor for ammonia gas detection,” [ICO CN 2016, China \(2016\).](#)
- [8] Wei Han, D. Liu, X. Lian, **A. K. Mallik**, F. Wei, Lei Sun, G. Farrell, Y. Semenova and Q. Wu, “A spherical-structure-based fiber sensor for measuring simultaneous measurement of both ammonia gas concentration and temperature,” [Proc. SPIE. 10025, Advanced Sensor Systems and Applications VII, 100251J China \(2016\).](#)

Table of Contents

Abstract	I
Declaration	III
Acknowledgements	IV
List of publications	VI
Table of contents	IX
List of Figures	XII
List of Tables	XVI
List of Abbreviations	XVII
1. Introduction	1
1.1. Background	1
1.2. Overview of optical fiber sensing	1
1.3. Whispering gallery mode (WGM) optical resonators	3
1.4. WGM field distribution	8
1.4.1. WGM field distribution in an uncoated microsphere	8
1.4.2. Field distribution for a microsphere with a functional coating ...	12
1.4.3. Light coupling from the tapered fiber in to the microsphere	14
1.4.4. Quality factor of a microsphere resonator	19
1.5. Motivation for the research	20
1.6. Research aim and objectives	22
1.7. Research Methodology	23
1.8. Layout of thesis	28
2. Spherical microresonator for relative humidity (RH) measurement	36
2.1. Agarose Coated Spherical Micro Resonator for humidity Measurement.	37
2.2. Introduction	38
2.3. Experimental setup and sensor fabrication	40
2.3.1. Fiber taper fabrication	40
2.3.2. Microsphere fabrication	41
2.3.3. Agarose gel coating preparation	42
2.3.4. Experimental set up for RH measurements	43
2.3.5. Sensor characterization	44
2.4. Results and discussion	44

2.4.1. Spectrum characterization	44
2.4.2. RH dependency	46
2.4.3. Coating thickness dependency	47
2.5. Sensor characterization	51
2.5.1. Sensor stability	52
2.6. Conclusion	54
3. Study of the influence of the functional coating thickness on sensitivity of the WGM sensor	59
3.1. Study of the influence of the agarose hydrogel layer thickness on sensitivity of the coated silica microsphere resonator to humidity.....	60
3.2. Introduction	60
3.3. Theoretical analysis	63
3.4. Experimental results and discussion	65
3.5. Conclusion	70
4. Sensing of low humidity levels with the agarose-coated WGM microresonator	72
4.1. A Coated Spherical Microresonator for Measurement of Water Vapor Concentration at PPM Levels in Very Low Humidity Environments	73
4.2. Introduction	74
4.3. Sensing Principle	76
4.4. Experiments and discussion	78
4.4.1. Experimental investigation of the humidity response	78
4.4.2. Stability tests	86
4.4.3. Response time	88
4.4.4. Temperature effects	89
4.5. Conclusion	91
5. Spherical microresonator for ammonia sensing	96
5.1. Silica gel coated spherical micro resonator for ultra-high sensitivity detection of ammonia gas concentration in air	97
5.2. Introduction	98
5.3. Methods	100
5.3.1. Preparation of porous silica gel	100
5.3.2. Microsphere resonator fabrication	101
5.3.3. Two methods for characterization of the sensor performance. .	102
5.4. Results	103

5.4.1. Experimental investigation of the sensor in a wider range of low (>4-30 ppm) ammonia concentrations using an OSA	103
5.4.2. Experimental investigation of the sensor in the ultra-low ammonia concentrations range using frequency detuning method	106
5.5. Discussion	108
5.6. Conclusion	114
6. Spherical microresonators for multi-parameter sensing	119
6.1. Whispering gallery mode micro resonators for multi-parameter sensing applications	120
6.2. Introduction.....	120
6.3. Sensor Fabrication and Experimental setup	124
6.4. Results and discussion	126
6.5. Conclusion	135
7. Conclusions and Future work.....	140
7.1. Conclusions	140
7.1.1. Conclusions regarding the agarose coated spherical microsphere resonator for sensing of humidity.....	141
7.1.2. Conclusions regarding the influence of the agarose coating thickness on the sensitivity of the WGM sensor to relative humidity.....	142
7.1.3. Conclusions regarding application of the proposed agarose coated microsphere for sensing of low relative humidity	143
7.1.4. Conclusions regarding the silica gel coated spherical microsphere resonator for ammonia sensing applications	144
7.1.5. Conclusions regarding the multi-parameter sensing with silica microsphere resonators	146
7.2. Future Work	147
7.2.1. Improving the accuracy of measurement for the sensor's response time	147
7.2.2. Sensor packaging and protection	148
7.2.3. More detailed study of multi parameter sensors based on the WGM effect for different applications	149
8. Appendix A: Statement of contribution.....	153
9. Appendix B: WGMs field distributions in an uncoated microsphere resonator	154
10. Appendix C: WGM field distribution in a microsphere resonator coated with a thin functional layer	160

List of Figures

Fig. 1.1 Schematic of the mode propagation constants along the surface of a sphere...	9
Fig. 1.2 Schematic of a WGM resonance in spherical coordinates.	10
Fig. 1.3 Schematic diagram of a coated microsphere	13
Fig. 1.4 Schematic diagram of WGMs excitation in a sphere by evanescent coupling with a tapered fiber	14
Fig. 1.5 Simulated transmission for the fiber taper coupled to 104 μm diameter sphere, $k=0.002434, l = m = 298, n = 1$	18
Fig. 1.6 Schematic diagram of a WGM microresonator as a relative humidity/ammonia sensor	24
Fig. 1.7 Optical microscope images of a bare fiber and microsphere	26
Fig. 1.8 Schematic diagram of a typical coupling and characterization setup for a WGM microsphere resonator	27
Fig. 2.1 Application areas of humidity sensors.....	36
Fig. 2.2. Schematic diagram of the tapered fiber used for coupling the light into the microsphere. The waist diameter $W = 3.3 \mu\text{m}$, waist length $L_1=2 \text{ mm}$, full taper length $L_2=12 \text{ mm}$ and the length of the taper between the cured epoxy droplets on the microscope slide $L_3=4 \text{ cm}$	40
Fig. 2.3. Optical microscope image of the microsphere with the diameter of 171 μm used in the experiment.....	41
Fig. 2.4. Experimental set-up used for RH measurement using spherical microresonator.....	43
Fig. 2.5. Transmission spectrum recorded with an Agarose coated microsphere with a diameter of 171 μm	45
Fig. 2.6 Experimental results for the WGM resonator based on a 171 μm diameter microsphere coated with 2.25% Agarose gel coupled with a 3.3 μm tapered fiber in the range of humidity from 35 % to 81% RH at a constant temperature of 25 $^{\circ}\text{C}$. (a) WGM spectra at different RH levels; (b) wavelength shift of the WGM spectrum versus RH; (c) humidity response of the WGM spectrum for an uncoated microsphere resonator; (d) spectral shift versus RH for the sensors based on the same diameter microsphere coated with the Agarose solutions of different concentrations.....	47
Fig. 2.7. Experimental spectra and Lorentzian fitting for a 100 μm diameter microsphere coated with 2.25% Agarose hydrogel: a) after one coating cycle; b) after three coating cycles; c) Q factor versus the number of coating cycles.....	49
Fig. 2.8 (a) RH response of the sensor based on a 100 μm diameter microsphere with a different number of Agarose layers: (b) Q factor and estimated RH sensitivity	

for the 100 μm diameter microsphere with a different number of Agarose coating layer.....	50
Fig. 2.9 (a) Relative humidity responses of the sensor, measurements recorded seven days apart; (b) studies of the sensor hysteresis: humidity response for the 171 μm microspheres coated with different Agarose concentration coatings during RH increase-decrease cycle at 25 ^o C.....	52
Fig. 2.10. Resonance wavelength shift versus temperature for the 171 μm microsphere coated with 2.25% wt./vol. Agarose solution at 41% RH.....	53
Fig. 3.1 Schematic diagram of the Agarose coated microsphere.....	64
Fig. 3.2 Radial field distributions for the fundamental WGM with $l = m = 757$ and different Agarose coating thickness values:(a) $t = 0$; (b) $t = 0.5 \mu\text{m}$ and (c) $t = 2 \mu\text{m}$	64
Fig. 3.3 Simulated dependence for the RI sensitivity of the fundamental WGM above versus the Agarose coating layer thickness.....	65
Fig. 3.4 Experimental setup for RH measurements;.....	66
Fig. 3.5 Transmission spectra with the selected WGM resonances: (a) for uncoated silica microsphere with a 260 μm diameter and (b) for the same microsphere after application of four Agarose coating layers. Insets illustrate fitting of the selected resonances and estimated Q factors.....	67
Fig. 3.6 Experimental WGM spectra for the microsphere coated with a single Agarose layer recorded at different humidity levels varying from 25 to 50% RH. Inset graph illustrates the WGMs spectral shift versus changes in RH.....	68
Fig. 3.7 Transmission spectra with the selected WGM resonances: (a) for uncoated silica microsphere with a 260 μm diameter and (b) for the same microsphere after application of four Agarose coating layers. Insets illustrate fitting of the selected resonances and estimated Q factors and (c) experimental Q factor and calculated agarose coating layer thickness as a function of the number of coatings.....	69
Fig. 4.1 Schematic diagram of the Agarose coated microsphere.....	77
Fig. 4.2 Schematic representation of experimental setup for humidity measurements. The dotted line of the box indicates the location of microsphere and the coupling taper, shown in the inset image.....	79
Fig. 4.2 Q factor estimate for the 162 μm diameter silica sphere (a) before and (b) after its coating with Agarose.....	80
Fig. 4.4 SEM image of the Agarose coated-fiber cross section.....	82
Fig. 4.5 Wavelength shift of the WGM resonance versus RH for the micro-resonator before and after its coating with Agarose. Inset graph illustrates the experimental transmission spectra of the coated micro-resonator corresponding to different RH values.....	83

Fig. 4.6 (a) Simulated electric field intensity distributions for the fundamental WGM; (b) change of the Agarose layer RI corresponding to the RH changes (calculated using the theoretical model) with $n = 1$, $l = m = 463$ with $a_0 = 81.0 \mu\text{m}$ and Agarose layer thickness $t = 3.55 \mu\text{m}$	85
Fig. 4.7 (a) RH responses of the sensor taken within 2 weeks; (b) Studies of repeatability and estimates for response and recovery times; (c) WGM spectra at different RH levels at increasing and decreasing humidity at 17°C ; (d) WGM resonance shift versus RH at 17°C	87
Fig. 4.8 Temporal response of the sensor.....	88
Fig. 4.9 Resonant wavelength shift versus temperature for the $162 \pm 0.15 \mu\text{m}$ microsphere coated with 2.25% wt./vol. Agarose solution: (a) 10% RH, 15 % RH and 25% RH; (b) Hysteresis of temperature response at 15% RH.....	90
Fig. 5.1 SEM image of porous silica coated microsphere used in experiment.....	101
Fig. 5.2 Experimental setup for ammonia sensing using (a) OSA interrogation system; (b) frequency detuning method.....	103
Fig. 5.3 Transmission spectrum recorded by the OSA for a coated microsphere with a $282 \mu\text{m}$ diameter.....	104
Fig. 5.4 (a) WGM spectral shift during sensor's exposure to different concentrations of NH_3 ranging from 4 ppm to 30 ppm. (b) Sensor's temporal response to the ammonia concentration of 8 ppm. Inset figure illustrates the wavelength shift for a selected WGM resonance in response to exposure to 8 ppm concentration of ammonia. (c) Sensor's response as a function of NH_3 concentration.....	105
Fig. 5.5 Q factor estimates for the $282 \mu\text{m}$ diameter silica sphere (a) before and (b) after its coating with porous silica gel.....	106
Fig. 5.6 (a) Wavelength shifts of the WGM resonance versus time during the sensor's exposure to various vapor phase ammonia concentrations. (b) A linear fit of the wavelength shift data.....	107
Fig. 5.7 (a) Sensor's response to various volatile organic compounds.....	108
Fig. 5.8 (a) Time responses of the sensor to NH_3 recorded with a 10-days interval. (b) Sensor's responses to 12 ppm of ammonia during three consecutive tests at constant humidity and temperature.....	109
Fig. 5.9 WGM spectral shift versus RH change from 30-65% RH silica gel coated on $282 \mu\text{m}$ microsphere at 23°C	110
Fig. 5.10 WGM spectral shift versus different RH change from 30-70% RH silica gel coated on $282 \mu\text{m}$ microsphere at 23°C against 5 ppb of ammonia.....	111
Fig. 5.11 Dynamic response-recovery curve of the sensor to NH_3 at constant room temperature 23°C and constant humidity of 50% RH.....	113
Fig. 6.1 SEM images of cross sections of singlemode fibers coated with (a) silica sol-gel; (b) 0.5\% wt. vol. agarose hydrogel.....	124

Fig. 6.2 Experimental setup for multi parameter sensor characterization.....	125
Fig. 6.3 Transmission WGM spectra for both sensors separately and when both microspheres are coupled simultaneously.....	126
Fig. 6.4 Transmission spectrum for sensors A and B simultaneously at different humidity levels inside the chamber. The inset graphs are enlarged selected portions of the overall spectrum for sensors 'A' and 'B' at constant temperature of $25 \pm 0.1^\circ$	128
Fig. 6.5 Linear fitted graph of the selected WGM wavelengths versus relative humidity for both the silica gel coated (sensor A) and agarose coated (sensor B) microspheres.....	129
Fig. 6.6 (a) Transmission spectrum for the sensor system recorded at different times after injection of ammonia vapor in concentration of 46 ppm inside the chamber at constant temperature of $25 \pm 0.1^\circ\text{C}$ and humidity 40% RH. Insets represent the enlarged portions of the spectrum corresponding to sensors A and B; (b) A and B WGM spectral shifts in response to three different concentrations of ammonia (0.46 ppm, 1.46 ppm and 2.19 ppm) after injection of the vapors inside the chamber. Inset figure illustrates the response to 0.46 ppm concentration of ammonia only; (c) WGM spectral shifts for the sensors A and B as a function of ammonia concentration.....	130
Fig. 6.7 K_{12} as a function of RH at constant temperature of 25°C	132
Fig. 6.8 Temperature dependence of the WGM spectral shift for sensors A and B at constant humidity of 40% RH.....	134
Fig. 7.1 Schematic diagram of one of the possible approaches to packaging of spherical micro resonator.....	149
Fig. 7.2 Schematic diagram of the set up for simultaneous measurement of three different gases (NH_3 , O_2 and NO_2) using an array of the WGM sensors.....	150
Fig. B.1 Simulated WGM radial field intensity distributions for the 1 st order mode $n = 1$, $l = 24$, $\lambda = 1.608 \mu\text{m}$ and 2 nd order mode $n = 2$, $l = 24$, $\lambda = 1.388 \mu\text{m}$ for a sphere of radius $R=5 \mu\text{m}$, $n_s = 1.4682$, $n_0 = 1$	156
Fig. B.2 Simulated electric field distribution in the polar angular direction $l = 24$, $m = 24, 23, 22, 21$, $n = 1$	158
Fig. B.3 The contour plot of electric field distribution in the $r - \varphi$ plane, $n = 1$, $l = m = 24$, $\lambda = 1.608 \mu\text{m}$, $R_0=5 \mu\text{m}$	159

List of Tables

Table 5.1 Detection limit calculation for the silica gel coated microsphere sensor...[112](#)

Table 5.2 Comparative study of performance of various optical ammonia sensors...[114](#)

Table 6.1 Detection limit estimates for sensor A and B.....[133](#)

List of Abbreviation

WGM	Whispering Gallery Mode
VOCs	Volatile Organic Compounds
OFS	Optical Fiber Sensor
RI	Refractive Index
Q factor	Quality factor
TE field	Transverse Electric field
TM field	Transverse Magnetic field
RH	Relative Humidity
NH ₃	Ammonia
SMF	Single Mode Fiber
UV	Ultra Violet
OSA	Optical Spectrum Analyser
F.S. R	Free Spectral Range
FWHM	Full Width Half Maximum
DI water	Deionized water
SLED	Superluminescent light diode
R.I.U.	Refractive Index Unit
DL	Detection Limit
ppm	Parts per million
ppb	Parts per billion
TEOS	Tetra-Ethyl Ortho Silicate
H ₂ SO ₄	Sulfuric Acid
SEM	Scanning Electronic Microscope
F. G	Function Generator
NH ₄ OH	Ammonium Hydroxide
LPG	Long Period Grating
FBG	Fiber Bragg Grating
HCL	Hydrochloric acid
SO ₂	Sulphur Dioxide
NO _x	Nitrogen oxides derivatives

NO ₂	Nitrogen dioxide
CO	Carbon mono oxide
LuPc ₂	Lutetium bisphthalocyanine
PAH	Poly Allylamine Hydrochloride
PAA	Poly Acrylic Acid

1 Introduction

1.1 Background

The environmental conditions surrounding us have a major impact in our day-to-day well-being and health and also significantly influence agriculture, food manufacturing and processing industries and food storage. The measurement and monitoring of environmental conditions or parameters are key requirements in many situations. Examples of the parameters to be monitored include humidity, temperature, the presence of pollutants and the concentration of other containments, such as volatile organic compounds (VOCs).

The core chapters of this thesis are presented as a series of limited journal publications. For this reason, this chapter provides not only an introducing optical fiber sensor but also an overview of the sensor structures, applications and fundamental principles involved relevant to this thesis.

1.2 Overview of Optical Fiber Sensing

In order to measure and monitor qualitative and/or quantitative information about a parameter, some form of sensor is needed. Sometimes a particular parameter of interest will coexist with other parameters and it is difficult for a sensor to identify accurately and selectively. To date, many sensing techniques have been developed to measure the chemical and physical properties of the environment. Electronic sensors are one of the most popular choices to measure such parameters. The

fundamental sensing principle of such sensors relies on a detectable change in either voltage or current as a function of the environmental conditions.

However electronic sensors can be difficult to use in harsh environments and may require substantial physical protection, increasing the effective sensor size and fabrication cost. It is thus important to develop sensors that are both durable in harsh environments and can operate reliably over long time periods. OFSs have been widely studied as sensors to monitor a wide range of parameters such as displacement, vibration, strain, temperature, humidity, viscosity, pressure, current, electric field strength and others [1], [2] many of which are environmental parameters. OFSs possess some inherent advantages over their electrical counterparts such as immunity to electromagnetic interference, radioactivity; safe operation in explosive environments; light weight, high sensitivity and the potential for remote real time monitoring over long distances of tens or even hundreds of kms.

Over the past 50 years, OFSs have become a popular choice in many existing application areas and have stimulated the development of a wide variety of novel sensing applications. OFSs are categorized into four major categories depending on which property of light is influenced. These properties are light intensity, phase, frequency and polarization. A variety of fiber structures and sensing principles have been utilized to realize such measurements including fiber resonators, fiber gratings, micro-structured, polarization-maintaining, D-shaped, multi-core fibers, fiber hetero-structures and other special types of optical fibers.

Recent rapid progress in micro- and nanotechnologies has led to the development of novel miniature fiber sensors with improved sensitivity [3]–[5]. Among those, micro-fibers are one of the technologies that have attracted many researchers in

the fields of physical, chemical and biological sensing [6], [7]. Compared to traditional fiber based sensors, in a micro-fiber based sensor a large portion of light, travelling outside of the fiber in the form of evanescent field, interacts with the surrounding medium, leading to possibility of new sensor types and to an improved sensitivity to the ambient changes. Most commonly microfiber-based sensors detect minute changes in the surrounding refractive index (RI) by measuring changes in, for example, optical transmission power through the sensor or shifts in transmitted or reflected spectra, which is widely used in identification of many biological or chemical species by functionalizing microfiber surfaces to convert the changes in the bio-/chemical analyte into RI variations. Microfiber resonators, in the shape of rings, loops, knots or coils, have been studied extensively as RI sensors owing to their miniature dimensions, high sensitivity and simple fabrication [8]–[10]. However, microfiber loop resonators often lack mechanical stability due to the existence of overlapping coupling regions. Fiber knot resonators possess better stability than the micro fiber loop resonators but their fabrication process is more complex and such structures have higher scattering losses.

There are a number of outstanding issues that need to be addressed for the fiber-based resonator sensors related to improving their sensitivity, stability, accuracy and resolution, further development of packaging and miniaturization techniques, reducing of fabrication and interrogation costs etc.

1.3 Whispering gallery mode (WGM) optical resonators

An optical resonator (resonant optical cavity) consists of two or more mirrors that form a standing wave cavity for light waves, so that light is confined and stored

within the cavity by circulating along a closed path via multiple reflections from these mirrors. Typically the main design objective for an optical resonator for sensing applications is to achieve high quality (Q) factor, leading to high measurement resolution. The Q factor is a parameter that represents a ratio between stored energy and energy loss per cycle of reflections. The simplest and most common optical resonator is a Fabry-Perot (FP) type resonator, where two opposing flat mirrors are used to create multiple reflections and interferences within the cavity. To achieve high Q factor these mirrors should have high reflectivity and furthermore losses inside the cavity must be minimized. The Q factor of practical FP resonators is often limited by the losses introduced by both diffraction and mirror imperfections, which has significant impact on the Q factor. This means that for state-of-the-art mirror surfaces with even minor roughness, the Q factor is typically low. In addition, FP resonators are typically expensive devices and are difficult to assemble and miniaturize due to offer necessary resistance to their low vibrations [11].

In the last few decades, another type of optical microresonator has been extensively studied as the basis for the next generation of ultra-high sensitivity sensors. Whispering gallery mode (WGM) optical resonators are dielectric structures with a circular symmetry capable of trapping light inside the micro-sized cavity by almost total internal reflections. The high- Q optical WGMs (at specific resonant frequencies) circulating around the cavity can interact with the local environment through the evanescent field. Lord Rayleigh was the first to introduce the term “whispering gallery waves” for description of an acoustic phenomenon in the 19th century [12]. He observed that a whisper uttered at one end of the circular dome of St. Paul’s Cathedral in London could be heard very

clearly at the distant opposite end of the dome. This meant that in a “whispering gallery” at certain conditions sound intensity decreased much slower with the distance from the source than in free space. In 1909, Debye had proposed a theoretical solution for resonant eigen-frequencies of dielectric and metallic spheres [13] based on Mie scattering [14]. Subsequently the generalized properties of electromagnetic resonances in dielectric spheres were widely discussed, with emphasis on microwave modes [15].

To illustrate the operation of a microcavity, assume the cavity has a circular symmetry, found for example in a sphere. Typically light is coupled into the microcavity from an external evanescent light field and is trapped within the microcavity due to total internal reflections at the boundary of the microcavity material and surrounding medium. Within the microcavity, for specific optical frequencies, constructive interference takes place for the trapped light along the equatorial path of the microresonator. The trapped light propagates over a distance equal to the circumference equal to one round trip. If λ_R is the resonance wavelength, n_{eff} is the effective RI of the resonant mode, then the integer l number of multiple wavelengths (λ_R) that satisfy the resonance condition for a circular microcavity with radius R_0 is given approximately as

$$l\lambda_R \approx 2\pi R_0 n_{eff} \quad (1.1)$$

The free spectral range (F.S.R) is the wavelength interval that separates the mode number l from the next mode of higher number $l + 1$ and the quantity may be expressed as

$$FSR = \frac{\lambda_R^2}{2\pi R_0 n_{eff}} \quad (1.2)$$

It is clear from Eq. (1.1) that the resonance wavelength. (λ_R) depends not only the radius of the microsphere but also on the effective RI of the optical mode. The change in the resonant wavelength due to changes in the spherical microcavity radius and of the effective RI of the optical mode can be expressed as:

$$\frac{\Delta\lambda_R}{\lambda_R} = \frac{\Delta R_0}{R_0} + \frac{\Delta n_{eff}}{n_{eff}} \quad (1.3)$$

Since environmental variations near the resonator surface may lead to changes in the effective RI, Eq. (1.3) essentially illustrates the operating principle of a sensor based on such a WGM resonator, where the measured change in the resonant wavelength is related to changes influenced by external factors in the resonator dimensions and the effective RI. The Q factor of such a resonator is associated with photon lifetime of the resonance mode, which means a higher Q factor is equivalent to a longer photon life time [16]. A longer photon lifetime increases the length of the path of interaction between photons and the surrounding environment as they circulate within the microcavity. By using highly transparent, low scattering loss material, such as silica, WGM resonators can achieve extremely high values of Q factor (10^8 - 10^9) [17] in a small mode volume. The Q is mainly limited by the material attenuation and scattering loss contributed by surface roughness and geometrical imperfections. Due to their miniature size and high sensitivity, WGM resonators are one of the most attractive forms of optical sensors, for example in bio-sensing they can provide ultra-high sensitivity down to single molecule detection [18], as well as real-time analysis often without the need for fluorescent labels, a multiplexed sensing ability and cost-effective integration with fiber optics [19][20].

Various geometries of WGM resonators have been explored to date for sensing applications including micro pillars [21], micro rings [22], [23], micro

disks [24]–[26], microtoroids [27], [28] and photonic crystal cavities [29], [30]. Among these structures, microspheres are the simplest and are easy to fabricate in laboratory conditions from a single piece of silica fiber. The fabrication can be carried out without the need for sophisticated instruments or a cleanroom environment, which results in a low fabrication cost, compared to microtoroid and micro ring structures fabricated using mechanical polishing or microfiber manipulation of photolithographic patterning. Given their simplicity and high Q -factors silica microsphere resonators are among the most popular optical resonators and have been studied widely for many applications. Many researchers have successfully demonstrated silica microsphere resonators coated with analyte-selective functional layers in various chemical, physical and bio sensing applications involving molecular adsorption [18], [31], RI [32]–[35], temperature [36], [37], force [38] and electromagnetic field strength sensing [39]. However, while experimental prototypes of the sensors have demonstrated the great potential of the WGM technique, there is an urgent need to gain a deeper understanding of the WGM phenomenon in the microresonators for practical realization of ultra-sensitive sensors with high measurement resolution, long term stability, selectivity and fast response.

The impact of the coating layer on a WGM microsphere was studied earlier by Teraoka et al. [40]. They examined the properties of WGMs in a microsphere using perturbation theory when a high RI coating material is applied to the microsphere surface. Later, Nai Lin et al. simulated the performance of a microsphere sensor with a particular coating, in that case polymer zeolite, a high RI polymer used for gas sensing applications [41]. Much less common are experimental studies carried out to establish a correlation between the sensitivity

of the WGM microresonator and the thickness of coating whose RI is lower than that of the microsphere using same perturbation theory [42].

As mentioned previously, this thesis for the first time focuses on sensing of environmental parameters with WGM silica microsphere resonators, specifically, sensing of relative humidity levels and concentrations of vapor phase ammonia. The detailed impact of coating thickness on the sensitivity is also analyzed theoretically and validated experimentally. An array of two microspheres with different coatings has been demonstrated experimentally in order to explore the potential for multi parameter sensing applications as a very significant step towards independent and simultaneous measurement of several parameters within a single sensing system with a common interrogator.

The core chapters of the thesis are presented as a series of linked journal publications. For this reason in this introduction chapter, it is useful as a starting point to provide a more detailed numerical analysis which follows in section 1.3 for the electric field distribution of a fundamental WGM mode and its sensing characteristics in both uncoated microsphere and a microsphere coated with a suitable functional coating layer.

1.4 WGM field distribution

1.4.1 WGM field distribution in an uncoated microsphere

WGM modal structure has been studied by many researchers [43]–[45]. Whispering gallery modes can be thought of as ray tracing out a “zig-zag” path around the sphere with the equatorial plane being the mean plane of propagation (Fig. 1.1). A WGM mode is conventionally described in terms of a three-integer set l, m and n , which represent angular (polar), azimuthal (equatorial), and radial

mode numbers, respectively. The integer values $2m$, $l - |m| + 1$ and n are equal to the number of field maxima in the angular, polar and radial directions. A WGM for which $n = 1$ is the first order radial mode that lies closest to the surface of the sphere. The angular mode number l represents the number of modes of the fields that fit in to the circumference of the equatorial plane.

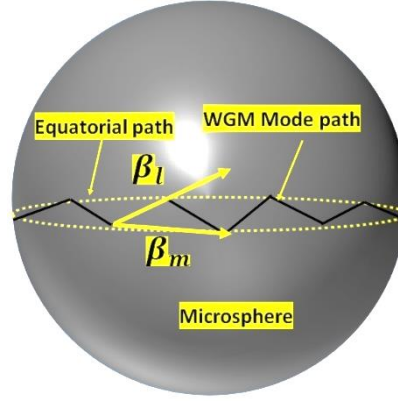


Fig. 1.1 Schematic of the mode propagation constants along the surface of a sphere

The value of the resonant wavelength is obtained based on the mode number l , which is supported by the sphere radius R . Each value of l is associated with a different resonant mode starting from first-order mode ($n = 1$), second order mode ($n = 2$), etc. In other words, we can say that for each value of the radial mode number, there are l number of resonant wavelengths travelling parallel to the surface, in a zig-zag path with the propagation constant $\beta_l = \frac{\sqrt{l(l+1)}}{R_0}$, where R_0 is the radius of the sphere. The projection of β_l on to the equator $\beta_m = m/R$ is commonly referred to as the propagation constant because it is the wave vector in the net direction of propagation [45]. For any fixed value of l , m can take a value $|m| \leq l$. Different values of m represent modes travelling in zig-zag paths with different inclinations with respect to the equatorial plane. For the fundamental mode ($m = l$ and $n = 1$), the inclination is the smallest, with a value of

approximately $1/\sqrt{l}$ radians. Modes with higher m values correspond to larger inclinations of the zig-zag paths corresponding to the same resonant wavelength for a constant value of l . This is because modes that take longer excursions away from the equator need to propagate over shorter distances to complete a revolution around the sphere (which is possible because higher latitude circles have a smaller circumference than that at the equator). Each WGM can support either TE or TM polarization, and the two polarizations can be selectively excited. The resonant mode distribution in the microsphere can be derived analytically.

Consider a sphere of radius R_0 with a RI n_s , surrounded by a uniform background with the RI n_0 . The coordinate system for the sphere is represented by r along the radial direction, by θ in the polar direction and by ϕ in the azimuthal direction as shown in Fig. 1.2.

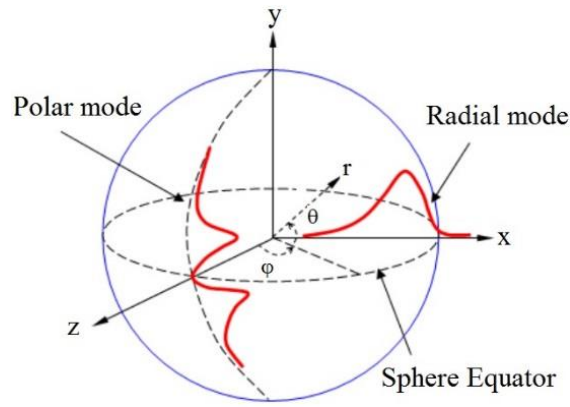


Fig. 1.2 Schematic of a WGM resonance in spherical coordinates.

The WGM spherical resonator should satisfy the Helmholtz equation in r, θ, ϕ planes. The scalar wave equation in spherical coordinates can be written as

$$\frac{1}{r^2} \frac{\partial}{\partial r} \left(r^2 \frac{\partial \psi}{\partial r} \right) + \frac{1}{r^2 \sin \theta} \left(\sin \theta \frac{\partial \psi}{\partial \theta} \right) + \frac{1}{r^2 \sin^2 \theta} \frac{\partial^2 \psi}{\partial \phi^2} + k^2 \psi = 0 \quad (1.4)$$

where k is the wave number and ψ is the electric field intensity of the spherical mode. The solution of Eq. (1.4) is found by the variables separation method

described in [46]. For TE polarization the electric field has only a θ component and the electric field distribution is given as:

$$\psi_{l,m,n}(r, \theta, \varphi) = N_s \psi_r(r) \cdot \psi_\theta(\theta) \cdot \psi_\varphi(\varphi) \quad (1.5)$$

where ψ_r , ψ_θ and ψ_φ are the electric fields in radial, polar and azimuthal directions respectively. Detailed derivations of the radial, azimuthal and polar modes are presented in Appendix B. Eq. (1.6) is the combined equation for the WGM electric field distribution within a microsphere as follows

$$\begin{aligned} \psi_\varphi(\varphi) &= \exp[\pm jm\phi] \\ \psi_\theta(\theta) &= \exp\left[\frac{m}{2}\theta^2\right] H_N(\sqrt{m}\theta), \quad m \gg 1 \gg \theta \\ \psi_r(r) &= \begin{cases} j_l(kn_s r), & r \leq R_0 \\ j_l(kn_s R_0) \exp(-\alpha_s(r - R_0)), & r > R_0 \end{cases} \end{aligned} \quad (1.6)$$

The coefficient N_s is derived as

$$\begin{aligned} N_s &= \left\{ \sqrt{\frac{\pi}{m}} 2^{N-1} N! R_0^2 \left[\left(1 + \frac{1}{\alpha_s R_0}\right) j_l^2(kn_s R_0) - \right. \right. \\ &\quad \left. \left. j_{l-1}(kn_s R_0) j_{l+1}(kn_s R_0) \right] \right\}^{-\frac{1}{2}} \\ \alpha_s &= \sqrt{\beta_l^2 - k^2 n_0^2} \\ \beta_l &= \frac{\sqrt{l(l+1)}}{R_0}, \quad N = l - m, \quad k = \frac{2\pi}{\lambda} \end{aligned} \quad (1.7)$$

where β_l is the propagation constant parallel to the surface of the sphere, α_s is the decay constant away from the sphere. The characteristic equation can be derived after matching the tangential electric and magnetic fields across the surface of the sphere. For the TE mode $E_\theta(r, \theta, \phi) = \psi_{l,m,n}(r, \theta, \phi)$ because the transverse field is parallel to the surface of the microsphere so $E_\phi = 0$. Similarly, for the TM mode, $H_\theta(r, \theta, \phi) = \psi_{l,m,n}(r, \theta, \phi)$. The characteristic equation can be derived as [45]:

$$\left(\eta_s \alpha_s + \frac{l}{R_0}\right) j_l(kn_s R_0) = kn_s j_{l+1}(kn_s R_0) \quad (1.8)$$

where $\eta_s = \begin{cases} 1 & TE \text{ mode} \\ \frac{n_s^2}{n_0^2} & TM \text{ mode} \end{cases}$

For a large sphere, where the radius is much larger than the wavelength, l can be calculated approximately as $l \approx \frac{2\pi R_0 n_{eff}}{\lambda}$, where n_{eff} is the effective RI of the microsphere which refers to the cavity path length of each mode of the microsphere. The exact resonance wavelength can be calculated by finding the zeros of the asymptotic Eq. (1.8).

1.4.2 Field distribution for a microsphere with a functional coating

In order to detect various biological and environmental parameters, the surfaces of microspheres are often functionalized with various polymer coating layers. The penetration depth of the evanescent field into the medium surrounding the coating is typically greater in a coated microsphere than that for an uncoated microsphere, so that a greater fraction of the mode energy interacts with the surrounding medium. The electromagnetic field distribution for a coated microsphere has been studied by Teraoka et al. in [40], where the application of a high-RI layer coating was proposed to enhance the sensitivity of the resonator several times. Perturbation theory was used to analyze the sensing performance of the coated micro resonator. For coated microspheres, knowledge of the evanescent wave penetration depth and its relation to the radial mode number can provide the key to an understanding of the experimental results and lead to an improvement in sensitivity of the WGM sensor. The same approach based on the perturbation

theory has been applied in this thesis in the analysis of the WGM modes in microspheres coated with lower RI surface layer.

For simplicity, the present analysis is limited to the electric field associated with the 1st order radial mode in a coated microsphere, shown in Fig. 1.3. In this model the RI of the sphere, its coating layer and the surrounding medium are set as n_s , n_f and n_0 , respectively.

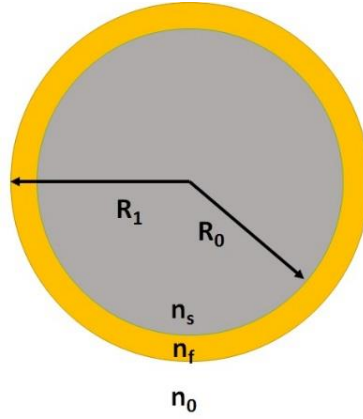


Fig. 1.3 Schematic diagram of a coated microsphere

The radial distribution of the transverse electromagnetic (TE) WGMs in the coated microsphere can be described by Mie theory [16, 17]:

$$E_l = \begin{cases} A_l \psi_l(n_s k r) & r \leq R_0 \\ B_{1l} \psi_l(n_f k r) + B_{2l} \chi_l(n_f k r) & R_0 \leq r \leq R_1 \\ C_l \chi_l(n_0 k r) & r \geq R_1 \end{cases} \quad (1.9)$$

where ψ_l and χ_l are the l_{th} orders of spherical Ricatti-Bessel and spherical Ricatti-Neumann functions, respectively. Each value of l represents multiple values of λ_R that satisfy the characteristic equation. The A_l , B_{1l} , B_{2l} and C_l are the constants that can be determined after finding the azimuthal value l corresponding to the resonance wavelength.

The characteristic equation for the coated microsphere can be derived from Eq. (1.9) as

(1.10)

$$\frac{B_{1l}}{B_{2l}} = \frac{\eta_1 \psi_l'(n_s k R_0) \chi_l(n_f k R_0) - \psi_l(n_s k R_0) \chi_l'(n_f k R_0)}{\psi_l'(n_s k R_0) \psi_l(n_s k R_0) - \eta_1 \psi_l(n_s k R_0) \psi_l'(n_s k R_0)}$$

1.4.3 Light coupling from the tapered fiber in to the microsphere

(circulated power before coupling) a_2

α, φ

$Sphere$
 n_s

t^*

b_2 (circulated power after coupling)

H TM
 E

a_1 (input power)

S_0

K

K^*

t

r

E TE
 H

b_1 (output power)

$fiber$ n_f

14 | Page

Fig. 1.4 schematically illustrates coupling of light into a microsphere using a tapered fiber. The interaction of evanescent field of the tapered fiber and WGM modes of the sphere gradually decreases with the increase in the distance between them [45]. In the diagram (Fig. 1.4), S_0 is the minimum distance at which the fundamental modes of the tapered fiber and the sphere are coupled to each other. The strength of interaction between the fiber mode F and the sphere mode $\psi_{l,m,n}$ at the minimum separation distance S_0 is given by the overlap integral of these two modes described by Eq.(1.11) [45]:

$$K(S_0) = \frac{k^2}{2\beta_f} \iint_{x,y} (n_s^2 - n_0^2) F \psi_{l,m,n} dx dy \quad (1.11)$$

where $K(S_0)$ is the rate of increase in the amplitude of the sphere mode at the minimum separation from the fiber, β_f is the propagation constant of the fiber, F and $\psi_{l,m,n}$ are the normalized electric fields in the fiber and sphere, respectively. The amount of power coupled from the fiber to the sphere is termed as the coupling factor κ , which can be determined as:

$$\kappa^2 = K^2(S_0) \frac{\pi}{\gamma_t} \exp \left[-\frac{\Delta\beta^2}{2\gamma_t} \right] \quad (1.12)$$

where, $\Delta\beta = \beta_f - \frac{m}{R_0}$, $\gamma_t = \frac{\gamma_f}{2R_0}$, γ_f = Decay constant in fiber

Maximum coupling efficiency is obtained at zero separation distance S_0 and decreases exponentially with the increase of the separation distance. Higher order modes are likely to be coupled with lower efficiency than the fundamental mode and the coupling efficiency decreases rapidly with the separation distance. The coupling efficiency is also influenced by the diameter of the tapered fiber,

becoming gradually higher with the decrease of the waist diameter of a tapered fiber. The quality factor associated with coupling between tapered fiber and the microsphere for a resonance wavelength is denoted as Q_{ext} and is expressed as [45]:

$$Q_{ext} = \frac{m\pi}{\kappa^2} \quad (1.13)$$

Assume that a unidirectional coupling has been established between the tapered fiber and microsphere shown in Fig. 1.4. Then the optical power transfer equation can be written as [22]:

$$\begin{bmatrix} b_1 \\ b_2 \end{bmatrix} = \begin{bmatrix} t & \kappa \\ -\kappa^* & t^* \end{bmatrix} \begin{bmatrix} a_1 \\ a_2 \end{bmatrix} \quad (1.14)$$

where t is the transmission coefficient determined by the value of the field transmitted from input fiber to the output fiber, κ is the cross-coupling factor of the fiber to sphere. a_1 , b_1 , the field amplitudes at the input and the output of the fiber, respectively, while the circulated field amplitudes in the sphere immediately before and after the coupling region are a_2 and b_2 , respectively. κ^* , t^* are the complex conjugates of the coupling factor and transmission coefficient respectively.

From the energy conservation law

$$\begin{aligned} t^2 + \kappa^2 &= 1 \\ |t| &= \sqrt{1 - |\kappa|^2} \end{aligned} \quad (1.15)$$

The power-transfer equation for transmission through the fiber to the total inner circulating loss factor inside the sphere can be written as

$$\frac{p_t}{p_i} = \left| \frac{b_1}{a_1} \right|^2 = \frac{\alpha^2 - 2\alpha|t|\cos(\varphi) + |t|^2}{1 - 2\alpha|t|\cos(\varphi) + \alpha^2|t|^2} \quad (1.16)$$

$$\frac{p_r}{p_i} = \left| \frac{a_2}{a_1} \right|^2 = \frac{\alpha^2(1 - |t|^2)}{1 - 2\alpha|t|\cos(\varphi) + \alpha^2|t|^2}$$

where p_i is the incident power at the fiber input, p_t is the transmitted power at the fiber output. p_r is the circulating power inside the sphere. The inner circulation loss factor α can be expressed as

$$\alpha = 1 - \pi R_0(\alpha_{surf} + \alpha_{mat} + \alpha_{rad}) \quad (1.17)$$

The phase shift φ during circulation can be calculated as

$$\varphi = \frac{2\pi^2 D n_{eff}}{\lambda} \quad (1.18)$$

where D is the sphere diameter and n_{eff} is the effective RI of the resonance mode.

But the resonant wavelength, φ is equal to $2\pi l$, where l is an integer value,

Eq. (1.16) is to simplified to become:

$$\frac{p_t}{p_i} = \left| \frac{b_1}{a_1} \right|^2 = \frac{(\alpha^2 - |t|)^2}{(1 - \alpha|t|)^2} \quad (1.19)$$

$$\frac{p_r}{p_i} = \left| \frac{a_2}{a_1} \right|^2 = \frac{\alpha^2(1 - |t|^2)}{1 - 2\alpha|t|\cos(\varphi) + \alpha^2|t|^2}$$

The Q factor of the resonator can be defined from the full width half maxima (FWHM) of the resonant wavelength and is expressed as [8]:

$$Q = \frac{\lambda_{resonance}}{\Delta\lambda_{FWHM}} = \frac{\pi^2 D n_{eff}}{\lambda} \times \frac{\sqrt{\alpha t}}{1 - \alpha t} \quad (1.20)$$

$$\Delta\lambda_{FWHM} = \frac{\lambda^2}{\pi^2 D n_{eff}} \times \frac{1 - \alpha t}{\sqrt{\alpha t}}$$

where α is the circulation loss factor inside the sphere and t is the transmission coefficient. Fig. 1.5 illustrates an example of transmission through a 3 μm waist diameter fiber taper coupled to a sphere, simulated using the power transfer equation Eq. (1.16).

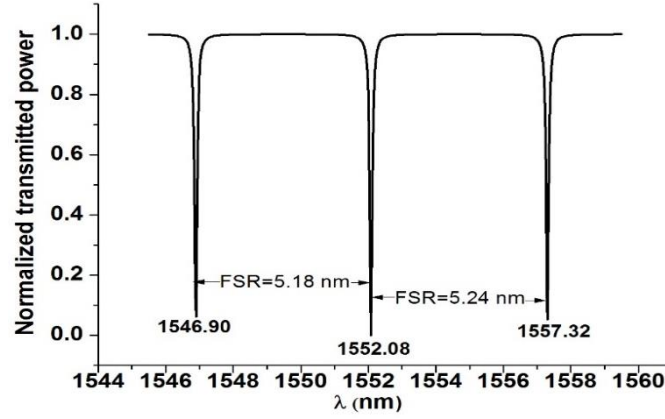


Fig. 1.5 Simulated transmission for the fiber taper coupled to 104 μm diameter sphere, $k=0.002434$, $l = m = 298$, $n = 1$.

The gap between the tapered fiber and the microsphere was assumed zero. The value of coupling factor κ was derived from Eq. (1.9). The transmission coefficient t was calculated from Eq. (1.15). The RIs of the sphere and the tapered fiber were assumed equal to 1.4682. Assuming $\alpha = 0.95$ for simplicity, the calculated $t = 0.99$. It can be seen from the figure that the resonant wavelengths are located at 1546.90 nm, 1552.08 nm and 1557.32 nm respectively. The spectral separation between these two dips is known as the free spectral range (F.S.R) of the microresonator and it can be calculated using Eq. (1.2). The effective RI of the resonant mode n_{eff} calculated as $n_{eff} = l\lambda/\pi D$, where l is the azimuthal mode number and D is the diameter of the sphere. For the value of $l = 298$ and resonance wavelength $\lambda = 1552.08$ nm, the calculated n_{eff} is 1.415 for the sphere with the diameter of 104.0 μm

1.4.4 Quality factor of a microsphere resonator

The quality (Q) factor of any resonator is a very important parameter that provides a convenient measure of energy stored by the resonator. It is defined as

$$Q = 2\pi \times \frac{\text{Stored energy}}{\text{Energy lost per cycle}} \quad (1.21)$$

The Q factor of an optical resonator is proportional to the photon lifetime in the cavity for the resonant mode. In other words, in a resonator with high Q -factor photons interact with the surrounding analyte multiple times along their re-circulating path due to total internal reflections from the surface of the microcavity. However, several sources of losses exist in a WGM resonator reducing the life time of photons, such as material loss, radiative loss, surface scattering loss and coupling loss [17]. The Q factor thus can be expressed as

$$Q^{-1} = Q_{mat}^{-1} + Q_{rad}^{-1} + Q_{s.s}^{-1} + Q_{ext}^{-1} \quad (1.22)$$

Q_{mat} is related to absorption and Rayleigh scattering within the material of the resonator which can be estimated as:

$$Q_{mat} = \frac{4.3 \times 10^3}{\alpha_a} \frac{2\pi n_s}{\lambda} \quad (1.23)$$

where α_a is the attenuation constant (0.17 dB/km for silica), n_s is the sphere's material RI and λ is the resonant wavelength. $Q_{mat}=10^{11}$ at 1550 nm [17].

Q_{rad}^{-1} is associated with radiative losses and it vanishes when the ratio of diameter of the sphere to the resonance wavelength is greater than or equal to 15 [17].

The surface scattering loss is estimated from the formula:

$$Q_{s.s} = \frac{\lambda^2}{2\pi^2 \sigma^2 B} \quad (1.24)$$

where σ and B are the roughness and the length of surface inhomogeneities respectively. $Q_{s,s}$ is expected to be less than 10^{10} when the diameter of the resonator is greater than $100\text{ }\mu\text{m}$ [17].

The loss due to the optical mismatch between the fiber and sphere modes, can be determined as:

$$Q_{ext} = \frac{m\pi}{\kappa^2} \quad (1.25)$$

where κ is the coupling factor between the sphere mode and fiber mode [45].

Based on known values for $Q_{mat}, Q_{rad}, Q_{s,s}, Q_{ext}$, the total Q factor can be found from the Eq. (1.22).

1.5 Motivation for the research

WGMs in silica microsphere resonators have become a well-established approach used in refractometric sensors for a wide range of bio-sensing applications and for measurement of chemical composition or concentration changes [3][23][36][39]. Most of the microsphere sensors reported to date detect the change in the ambient RI due to interactions of the evanescent “tail” of the WGMs with the surrounding medium. A most typical case involves a silica microsphere surrounded by air, so that there is a large RI contrast, leading to a very small radiation loss and, in turn, very high Q factor. Vollmer et al. reported specific detection of proteins absorbed on a spherical surface down to single molecules by observing the resonant wavelength shift of WGMs [18]. Although they didn’t understand precisely the nature of the interaction between WGMs and protein molecules bound to the microsphere surface, it was predicted that when a layer of protein accumulates on the surface of the sphere, the optical field of the mode protrudes further outward,

increasing the light path at the molecules binding site. Teraoka et al. [40] described the perturbation theory for the wavelength shift of WGM resonances in a microsphere coated with a high RI index layer and demonstrated that such a layer enhances the sensitivity of WGM frequency-shift sensors when used to detect adsorption of molecules and a change in RI in the surroundings. Later, Nai Lin et al. used this approximate model to calculate the thickness-dependent sensitivity of a zeolite coated microsphere to ammonia gas [42].

However, only a very few studies have been concerned with WGM microsphere resonators for measurement of humidity and gas concentration in air, particularly for ammonia gas [42], [51]–[53]. In this thesis the use of different functional coatings, based on the hygroscopic agarose gel and a porous silica gel, have been explored for realizing measurements of water vapor and ammonia gas concentration in air with high sensitivity, high accuracy and low detection limits, using the WGM principle.

To the best of the author's knowledge no detailed theoretical analysis has been carried out in relation to sensitivity of agarose-coated spherical microresonators to relative humidity and no related experimental studies have been reported to date, which prevents the development of practical devices for highly demanding environmental applications. Similarly, no studies were reported in relation to detection and quantification of ultra-low concentrations of ammonia gas with WGM sensors using silica gel coatings. Although the coating materials based on agarose and silica gel previously showed promise as functional coatings for various fiber sensors in terms of high sensitivity, repeatability, long-term stability, there is a lack of knowledge in relation to design and fabrication of WGM sensors with such coatings.

Finally, the concept of multi-parameter sensors, where two or more microspheres functionalized with different coating materials to target different gas analytes are combined using a common coupling and interrogation system, has not been sufficiently explored in the literature to date. Development of such a sensor array could help address the challenges of simultaneous measurement of multiple parameters with minimum cross-sensitivity and to reduce the cost of interrogation.

1.6 Research aim and objectives

The main goal of this research is to:

“Develop and investigate novel ultra-high sensitivity sensors for environmental applications based on the WGM effect in polymer-coated WGM silica fiber microsphere resonators with a particular focus on relative humidity and ammonia gas sensing”.

Achieving this goal requires the acquisition of a deeper knowledge of the fundamental principles of the WGM effect in this type of microresonators, the development of relevant numerical models, functional coatings, coating applications methods and addressing a range of sensor design issues, such as compactness, long term stability combined with ultra-high resolution and fast response. The specific objectives of this doctoral research are as follows:

- A simulation platform for predicting the WGMs behaviour in coated microspherical resonators based on perturbation theory and validate with experimental outcomes. The purpose of this analysis is to correlate the simulated WGM spectra with those measured experimentally in order to determine the unknown physical parameters of the coatings and to gain a better understanding of the sensing behaviour of the WGMs.

- Based on the above model and an improved understanding of the WGM phenomena, enhance the performance of the WGM sensors by using different types/thickness of functional coatings and by optimizing the parameters of the microsphere (e.g., diameter) and the coupling tapered fiber (waist diameter and length), to achieve the highest possible Q factors, most efficient coupling and ultra-high sensitivity to address challenging environmental sensing applications.
- Develop a simple and reliable fabrication process for this type of sensor based on the dip coating method for functionalizing the microsphere's surface with a particular focus on sensing of relative humidity and gas/analyte concentrations in air.
- Investigate different sensor interrogation methods; compare their performance and relative merits in practical applications for the WGM sensors.
- Develop and demonstrate experimentally a new approach to simultaneous sensing of multiple physical parameters by coupling an array of microspheres to a single adiabatic fiber taper using common interrogation system.

1.7 Research Methodology

As mentioned previously the core chapters of the thesis are presented as a series of linked journal publications. For this reason, in this introduction chapter it is useful to provide an overview of the general methodology employed for the research.

This research is focused on investigation and demonstration of ultra-high sensitivity sensors for measurement of relative humidity and gas concentrations in

air based on whispering gallery mode effect in spherical WGM microresonators. For all the experiments in this thesis the sensors consisted of a silica microsphere placed in direct physical contact with an adiabatic tapered fiber, as shown schematically in Fig. 1.6. A portion of light transmitted within the tapered fiber will be coupled and trapped inside the microcavity via total internal reflections from the boundaries of the microsphere surface. The trapped light propagates as a WGMs which are noticeable in the transmission spectrum of the tapered fiber as narrow spectral dips. As mentioned previously if the surface of the microsphere is modified with an appropriate functionalization layer so that it can adsorb and desorb water or other analyte molecules, this will introduce changes of the optical path, cavity loss, effective RI and radius of the microsphere, resulting in the shift of the WGM resonant wavelengths as shown in the inset of Figure 1.6.

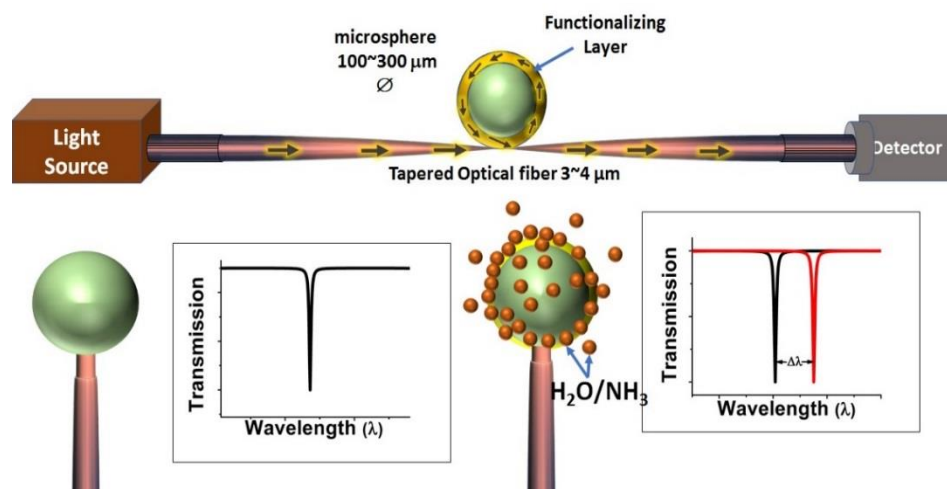


Fig. 1.6 Schematic diagram of a WGM microresonator as a relative humidity/ammonia sensor

The methodology employed throughout the research undertaken in this thesis typically consisted of a sequence of related steps as follows:

- Numerical investigations of the WGM microsphere-based sensors:

● **Develop understanding of fundamentals of WGMs in the coated microsphere with the functional coating materials for specific applications.** This involved:

- An analytic and theoretical study utilizing existing published knowledge as a foundation. Appropriate computer based models have been developed to simulate the spectral responses of the WGM resonators under a variety of conditions using a custom code in MATLAB, based on the perturbation theory and coupled mode theory for analysis of coupling between the tapered fiber and microsphere.
- Investigation and analysis of the influence of the optical fiber taper profile, waist diameter and surface roughness on the coupling loss between the microsphere and tapered fiber. This also involved optimization of these parameters to achieve high coupling efficiency, large Q factor and desired free spectral range for the sensor.
- Investigate the influence of the coating material's RI, layer thickness and surface roughness on the sensitivity of the sensors to relative humidity and ammonia gas concentration.
- Validate the developed models experimentally and subsequently apply them to refining the operation of the practical WGM sensors in order to improve their performance and to achieve the required sensitivity.

➤ **Fabrication of the WGM microsphere based sensors**

● **Fabrication of microspheres and tapered fibers**

- The tapered fibers were fabricated using customized micro-heater brushing technique described in [54]. The shape of a fiber taper which has significant influence on the sensitivity and Q factor of WGM sensors. The influence of heating temperature, heating zone length and motorized translation moving function and speed were investigated and these parameters were optimized to achieve a smooth surface and designed shape of the fiber tapers.
- The silica microsphere samples were fabricated from a tip of a single mode fiber using a standard fusion splicer in a manual mode by applying a controlled number of electric arc discharges or the micro-heater. In each case the fabrication parameters, such as the number of fusion splicer arcs or the micro-heater temperature/time of exposure were optimized to achieve smooth microsphere surface and the designed diameter. Fig 1.7 shows typical microscopic images of a cleaved single mode fiber (left) and fabricated microsphere (right).

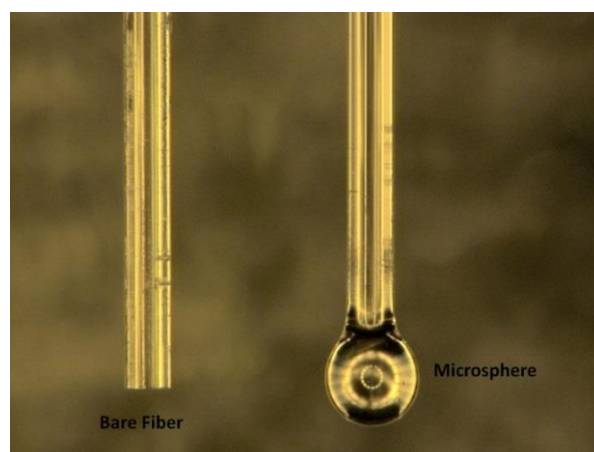


Fig. 1.7 Optical microscope images of a bare fiber and microsphere

● Microsphere surface modification

- Investigation of different processes for surface modification of the microspheres was performed for various sensing applications. The corresponding coatings preparation methods are described in the main body of the thesis. The coatings were typically applied using the dip-coating method, and the relevant details in each case are also provided for each of the experiments.
- The thickness of the coating materials and surface roughness were analyzed using scanning electron microscopy.

● Typical coupling and WGM microsphere characterization setup

- Fig.1.8 schematically illustrates a typical transmission spectrum characterization setup for a WGM sensor. The system consists of a broadband light source, polarization controller and optical spectrum analyzer. The microsphere, mounted on a XYZ nano-positioning stage, is gradually and carefully brought in direct contact with the tapered fiber until the WGM resonances are clearly observed in the transmission spectrum of the fiber taper. An optical microscope is used to guide the coupling process.

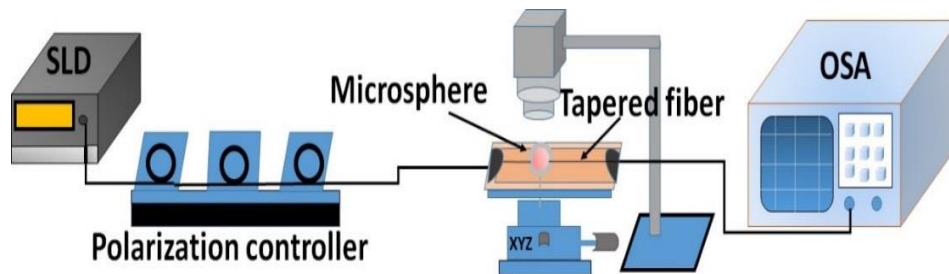


Fig. 1.8 Schematic diagram of a typical coupling and characterization setup for a WGM microsphere resonator

➤ **Experimental studies of the sensor's response to relative humidity/ammonia**

- Functional coatings were prepared and applied on the microsphere surface to measure the concentration of water vapors as well as ammonia in the humidity and temperature controlled chamber. Agarose hydrogel was utilized for relative humidity measurements and porous silica gel-coating was used to detect changes in the ammonia concentration in air.
- For each type of coating, the influence of the coating thickness on the sensors' performance was investigated separately for both relative humidity and ammonia concentrations in the chamber at constant temperature.
- Other important parameters associated with these sensors were investigated experimentally such RH/NH₃ measurement range, sensitivity, response times, temperature dependence, repeatability and hysteresis.
- High and ultra-low concentrations of water vapors as well as ammonia were investigated in detail using different interrogation techniques described in the main body of the thesis.

1.8 Layout of thesis

This thesis is based on a series of linked publications prepared during the period of this PhD research. The publications are all first author publications by the author of this thesis. As the research was carried out within a research group, there are several authors for each publication. A signed statement from all the co-

authors is included in Appendix A, confirming that the first author undertook all aspects of the research described in each paper, including preparation and submission of the paper, with the support and advice of the co-authors.

The layout of the thesis is as follows:

Chapter 1 is this introductory chapter containing the background for the research, a brief overview of fundamentals of WGMs in microsphere resonators, analytical models for uncoated and coated WGM microspheres, introductions to the concepts of coupling efficiency and Q factor, an outline of the research aim and objectives, research methodology and the layout of the thesis.

Chapter 2 presents a novel agarose coated silica microsphere resonator sensor for measurement of relative humidity (RH) and its experimental investigations. The proposed sensor offers a high sensitivity to humidity of 518 pm/ %RH within the range from 30% -70% RH. An experimental study of the humidity response for the sensors fabricated using three different concentrations of agarose gel is also presented. The results of the investigations of other important characteristics of the sensor such as repeatability, long-term stability of performance, measurement accuracy and temperature dependence are also presented in this chapter.

Chapter 3 presents an in-depth investigation, both theoretically and experimentally, of the influence of the agarose hydrogel layer thickness on sensitivity of the silica microsphere to humidity. Using perturbation theory, the influence of the agarose coating thickness on the sensitivity of the proposed sensor is analyzed and compared with experimental findings for different coating layer thicknesses. The results of the study are useful for the design and optimization of microsphere sensors' parameters to meet various performance specifications.

Chapter 4 is devoted to further experiments with the agarose-coated microsphere in the low relative humidity (RH) range (below 25 % RH). A detailed noise analysis, repeatability tests, hysteresis study, response time and temperature effects are also presented in this chapter.

Chapter 5 describes a novel ultra-high sensitivity ammonia gas sensor based on a silica gel coated microsphere resonator. This chapter also presents a comparative study of the sensor performance using two different interrogation systems (optical spectrum analyzer and frequency detuning). In addition it presents the results of the repeatability tests, temperature effect analysis and study of the sensor's cross sensitivity to other VOCs.

Chapter 6 describes a novel approach to simultaneous sensing of two physical parameters using the WGM sensors coupled to a single fiber. In this chapter, an array of two silica microspheres coated with different polymer layers has been proposed and demonstrated experimentally, capable of sensing ammonia in air and relative humidity simultaneously. A detailed performance analysis and studies of the coating's cross-sensitivity and temperature dependence are also presented.

Chapter 7 presents the overall conclusions from this work and an outlook into future research directions.

References:

- [1] H. E. Joe, H. Yun, S. H. Jo, M. B. G. Jun, and B.-K. Min, “A review on optical fiber sensors for environmental monitoring,” *Int. J. Precis. Eng. Manuf. Technol.*, vol. 5, no. 1, pp. 173–191, 2018.
- [2] B. Lee, “Review of the present status of optical fiber sensors,” *Optical Fiber Technology*, vol. 9, no. 2, pp. 57–79, 2003.
- [3] S. Editors, P. A. B. Bhushan, and K. V. K. H. Sakaki, “*NanoScience and Technology NanoScience and Technology*”, *Probe microscopy*, 2006.
- [4] I. S. Chronakis, “Micro-/nano-fibers by electrospinning technology: Processing, properties and applications,” in *Micro-Manufacturing Engineering and Technology*, 2nd Edition, book, 2015.
- [5] W. Jin, H. L. Ho, Y. C. Cao, J. Ju, and L. F. Qi, “Gas detection with micro- and nano-engineered optical fibers,” *Opt. Fiber Technol.*, vol. 19, pp. 741–759, 2013.
- [6] B. Lee, S. Roh, and J. Park, “Current status of micro- and nano-structured optical fiber sensors,” *Opt. Fiber Technol.*, vol. 15, no. 3, pp. 209–221, 2009.
- [7] L. Zhang, J. Lou, and L. Tong, “Micro/nanofiber optical sensors,” *Photonic Sensors*, vol. 1, no. 1, pp. 31–42, 2011.
- [8] L. Shi, Y. Xu, W. Tan, and X. Chen, “Simulation of optical microfiber loop resonators for ambient refractive index sensing,” *Sensors*, vol. 7, pp. 689–696, 2007.
- [9] F. Xu, V. Pruneri, V. Finazzi, and G. Brambilla, “An embedded optical nanowire loop resonator refractometric sensor,” *Opt. Express*, vol. 17, no. 2, pp. 1062–1067, 2008.
- [10] F. Xu, P. Horak, and G. Brambilla, “Optical microfiber coil resonator refractometric sensor,” *Opt. Express*, vol. 15, no. 12, pp. 7888–7893, 2007.
- [11] L. Chen, J. L. Hall, J. Ye, T. Yang, E. Zang, and T. Li, “Vibration-induced elastic deformation of Fabry-Perot cavities,” *Phys. Rev. A - At. Mol. Opt. Phys.*, vol. 74, no. 5, 2006.
- [12] W. S. Lord Rayleigh, “Theory of Sound,” in *Theory of Sound*, vol. 1, pp. 235, 1895.
- [13] P. Debye, “Der Lichtdruck auf Kugeln von beliebigem Material,” *Ann.*

Phys., vol. 335, no. 11, pp. 57–136, 1909.

- [14] G. Mie, “Contributions to the optics of turbid media, especially colloidal metal solutions,” *Ann. Phys. (N. Y.)*, vol. 330, no. 3, pp. 377–445, 1908.
- [15] M. Gastine, L. Courtois, and J. L. Dormann, “Electromagnetic Resonances of Free Dielectric Spheres,” *IEEE Trans. Microw. Theory Tech.*, vol. MTT-15, no. 12, pp. 694–700, 1967.
- [16] M. S. Luchansky, A. L. Washburn, T. A. Martin, M. Iqbal, L. C. Gunn, and R. C. Bailey, “Characterization of the evanescent field profile and bound mass sensitivity of a label-free silicon photonic microring resonator biosensing platform,” *Biosens. Bioelectron.*, vol. 26, no. 4, pp. 1283–1291, 2010.
- [17] M. L. Gorodetsky, A. A. Savchenkov, and V. S. Ilchenko, “Ultimate Q of optical microsphere resonators,” *Opt. Lett.*, vol. 21, no. 7, pp. 453–455, 1996.
- [18] F. Vollmer and S. Arnold, “Whispering-gallery-mode biosensing: label-free detection down to single molecules,” *Nat Methods*, vol. 5, no. 7, pp. 591–596, 2008.
- [19] M. R. Foreman, J. D. Swaim, and F. Vollmer, “Whispering gallery mode sensors,” *Adv. Opt. Photonics*, vol. 7, no. 2, pp. 168–240, 2015.
- [20] B. Bernhardt *et al.*, “Cavity-enhanced dual-comb spectroscopy,” *Nat. Photonics*, vol. 4, no. 1, pp. 55–57, 2010.
- [21] J. M. Gérard, B. Sermage, B. Gayral, B. Legrand, E. Costard, and V. Thierry-Mieg, “Enhanced spontaneous emission by quantum boxes in a monolithic optical microcavity,” *Phys. Rev. Lett.*, vol. 81, no. 5, pp. 1110–1113, 1998.
- [22] B. E. Little, S. T. Chu, H. A. Haus, J. Foresi, and J. P. Laine, “Microring resonator channel dropping filters,” *J. Light. Technol.*, vol. 15, no. 6, pp. 998–1005, 1997.
- [23] H. Okamura and K. Iwatsuki, “A Finesse-Enhanced Er-Doped-Fiber Ring Resonator,” *J. Light. Technol.*, vol. 9, no. 11, pp. 1554–1560, 1991.
- [24] N. Pornsuwancharoen *et al.*, “Micro-Current Source Generated by a WGM of Light Within a Stacked Silicon-Graphene-Au Waveguide,” *IEEE Photonics Technol. Lett.*, vol. 29, no. 21, pp. 1768–1771, 2017.
- [25] A. F. J. Levi, R. E. Slusher, S. L. McCall, J. L. Glass, S. J. Pearton, and R.

- A. Logan, "Directional light coupling from microdisk lasers," *Appl. Phys. Lett.*, vol. 62, no. 6, pp. 561–563, 1993.
- [26] S. L. McCall, A. F. J. Levi, R. E. Slusher, S. J. Pearton, and R. A. Logan, "Whispering-gallery mode microdisk lasers," *Appl. Phys. Lett.*, vol. 60, no. 3, pp. 289–291, 1992.
- [27] A. L. Martin, D. K. Armani, L. Yang, and K. J. Vahala, "Replica-molded high-Q polymer microresonators," *Opt. Lett.*, vol. 29, no. 6, pp. 533–535, 2004.
- [28] S. M. Spillane, T. J. Kippenberg, K. J. Vahala, K. W. Goh, E. Wilcut, and H. J. Kimble, "Ultrahigh-Q toroidal microresonators for cavity quantum electrodynamics," *Phys. Rev. A - At. Mol. Opt. Phys.*, vol. 71, no. 1, pp. 1–8, 2005.
- [29] P. T. Lee, T. W. Lu, F. M. Tsai, T. C. Lu, and H. C. Kuo, "Whispering gallery mode of modified octagonal quasiperiodic photonic crystal single-defect microcavity and its side-mode reduction," *Appl. Phys. Lett.*, vol. 88, no. 20, p. 201104, 2006.
- [30] P. T. Lee, T. W. Lu, F. M. Tsai, and T. C. Lu, "Investigation of whispering gallery mode dependence on cavity geometry of quasiperiodic photonic crystal microcavity lasers," *Appl. Phys. Lett.*, vol. 89, no. 23, p. 231111, 2006.
- [31] F. Vollmer, D. Braun, A. Libchaber, M. Khoshshima, I. Teraoka, and S. Arnold, "Protein detection by optical shift of a resonant microcavity," *Appl. Phys. Lett.*, vol. 80, no. 21, pp. 4057–4059, 2002.
- [32] P. Zijlstra, K. L. Van Der Molen, and A. P. Mosk, "Spatial refractive index sensor using whispering gallery modes in an optically trapped microsphere," *Appl. Phys. Lett.*, vol. 90, no. 16, 2007.
- [33] A. K. Mallik, Q. Wu, G. Farrell, and Y. Semenova, "Refractive index sensor based on a silica microsphere whispering gallery mode resonator," *Workshop on Recent Advances in Photonics, WRAP, 2015*.
- [34] N. M. Hanumegowda, C. J. Stica, B. C. Patel, I. White, and X. Fan, "Refractometric sensors based on microsphere resonators," *Appl. Phys. Lett.*, vol. 87, no. 20, pp. 1–3, 2005.
- [35] H. Wang, L. Yuan, C.-W. Kim, J. Huang, X. Lan, and H. Xiao, "Integrated microsphere whispering gallery mode probe for highly sensitive refractive

- index measurement,” *Opt. Eng.*, vol. 55, no. 6, p. 067105, 2016.
- [36] Q. Ma, T. Rossmann, and Z. Guo, “Micro-temperature sensor based on optical whispering gallery mode of fiber taper-microsphere coupling system,” in *Proceedings of SPIE - The International Society for Optical Engineering*, vol. 7420, 2009.
 - [37] A. Rahman, “Temperature sensor based on dielectric optical microresonator,” *Opt. Fiber Technol.*, vol. 17, no. 6, pp. 536–540, 2011.
 - [38] T. Ioppolo, M. Kozhevnikov, V. Stepaniuk, M. V. Ötügen, and V. Sheverev, “Micro-optical force sensor concept based on whispering gallery mode resonators,” *Appl. Opt.*, vol. 47, no. 16, pp. 3009, 2008.
 - [39] T. Ioppolo, J. Stubblefield, and M. V. Ötügen, “Electric field-induced deformation of polydimethylsiloxane polymers,” *J. Appl. Phys.*, vol. 112, no. 4, 044906, 2012.
 - [40] I. Teraoka and S. Arnold, “Enhancing the sensitivity of a whispering-gallery mode microsphere sensor by a high-refractive-index surface layer,” *J. Opt. Soc. Am. B*, vol. 23, no. 7, pp. 1434, 2006.
 - [41] N. Lin *et al.*, “Simulation and optimization of polymer-coated microsphere resonators in chemical vapor sensing,” *Appl. Opt.*, vol. 50, no. 28, p. 5465, 2011.
 - [42] N. Lin *et al.*, “Ultrasensitive chemical sensors based on whispering gallery modes in a microsphere coated with zeolite,” *Appl. Opt.*, vol. 49, no. 33, pp. 6463–6471, 2010.
 - [43] A. B. Matsko and V. S. Ilchenko, “Optical resonators with whispering-gallery modes-part I: basics,” *IEEE J. Sel. Top. Quantum Electron.*, vol. 12, pp. 3–14, 2006.
 - [44] R. L. Hightower and C. B. Richardson, “Resonant Mie scattering from a layered sphere,” *Appl. Opt.*, vol. 27, no. 23, pp. 4850–5, 1988.
 - [45] B. E. Little, J. P. Laine, and H. A. Haus, “Analytic theory of coupling from tapered fibers and half-blocks into microsphere resonators,” *J. Light. Technol.*, vol. 17, no. 4, pp. 704–715, 1999.
 - [46] C. Someda G., *Electro magnetic Waves*, 2006th ed. Taylor and Fransis.
 - [47] M. L. Gorodetsky and V. S. Ilchenko, “High-Q optical whispering-gallery microresonators: precession approach for spherical mode analysis and emission patterns with prism couplers,” *Opt. Commun.*, vol. 113, no. 1–3,

pp. 133–143, 1994.

- [48] V. S. Ilchenko, X. S. Yao, and L. Maleki, “Pigtail the high-Q microsphere cavity: a simple fiber coupler for optical whispering-gallery modes,” *Opt. Lett.*, vol. 24, no. 11, pp. 723–725, 1999.
- [49] J. C. Knight, G. Cheung, F. Jacques, and T. A. Birks, “Phase-matched excitation of whispering-gallery-mode resonances by a fiber taper,” *Opt. Lett.*, vol. 22, no. 15, pp. 1129, 1997.
- [50] M. Cai, O. Painter, and K. J. Vahala, “Observation of critical coupling in a fiber taper to a silica-microsphere whispering-gallery mode system,” *Phys. Rev. Lett.*, vol. 85, no. 1, pp. 74–77, 2000.
- [51] L. Huang, Z. Guo, T. Rossmann, and S. Member, “Whispering- Gallery Mode Silica Micro-Sensors for Temperature and Gas-Phase Concentration Measurements,” *Aerosp. Eng.*, no. July, pp. 1–11, 2010.
- [52] Q. L. Ma, L. Huang, Z. X. Guo, and T. Rossmann, “Spectral shift response of optical whispering-gallery modes due to water vapor adsorption and desorption,” *Meas. Sci. Technol.*, vol. 21, no. 11, pp. 7, 2010.
- [53] M. Qiulin, L. Huang, Z. Guo, and T. Rossmann, “Spectral shift response of optical whispering-gallery modes due to water vapor adsorption and desorption,” *Meas. Sci. Technol.*, vol. 21, no. 11, pp. 115206, 2010.
- [54] G. Brambilla, V. Finazzi, and D. J. Richardson, “Ultra-low-loss optical fiber nanotapers,” *Opt. Express*, vol. 12, no. 10, pp. 2258, 2004.

2. Spherical microresonator for relative humidity (RH) measurement

Humidity is the quantity of water vapor present in air. Absolute humidity and relative humidity (RH) are the two most commonly used measures of humidity. Absolute humidity is the amount of water vapor in a unit volume of air regardless of temperature. Relative humidity is the most popular measure used in both the scientific world as well as in industry. RH is defined as the percentage of water vapor present in air at a particular temperature and pressure with respect to the maximum amount of water vapor required to saturate the same volume of air at the same temperature. Humidity measurements play a very significant role in agriculture, food industry, clinical medicine, chemical, civil engineering, textile and semiconductor industries and many other fields, some of which are illustrated in Fig.2.1.

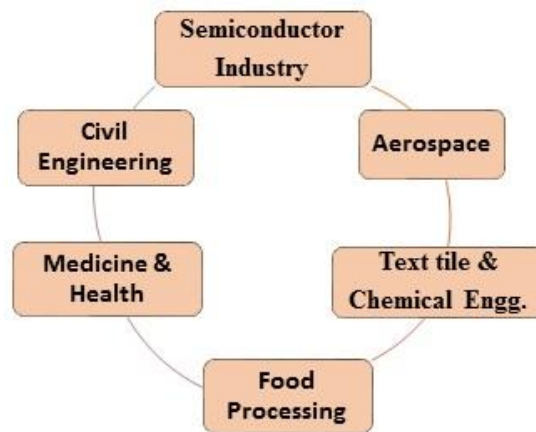


Fig. 2.1 Application areas of humidity sensors

In some industries humidity measurements are critical because it may affect the quality of products, for example the shelf-life of foodstuffs. Hence, humidity sensing is very important, especially in the control systems for industrial processes

and for human comfort. In recent decades, various humidity sensors have been proposed and developed, whose operation relies on sensing RH in terms of resistance or capacitance. However, development of a miniature humidity sensor that can offer a complete set of desired characteristics and parameters, such as high resolution and sensitivity, good linearity, low hysteresis and rapid response time, still remains a challenge.

This chapter addresses one of the main objectives of the thesis as it focuses on the development of a novel high sensitivity relative humidity sensor based on the WGM effect in a spherical microresonator coated with a layer of hygroscopic polymer material agarose. Its results demonstrate that the proposed sensor allows for the detection of RH with high sensitivity by measuring the WGM resonance wavelength shift due to the refractive index change of the agarose layer induced by changes in the surrounding RH. The chapter also examines the sensitivity of the sensor to RH and the Q factor of the resonator under different concentrations of agarose within the coating and for different coating thicknesses. The results of the experimental studies of the sensor's stability, hysteresis and RH detection limit are also presented and analysed.

2.1 Agarose Coated Spherical Micro Resonator for humidity Measurements¹

Abstract: A new type of fiber optic relative humidity (RH) sensor based on an Agarose coated silica microsphere resonator is proposed and experimentally demonstrated. Whispering gallery modes (WGMs) in the micro resonator are excited by evanescent coupling using a tapered fiber with $\sim 3.3 \mu\text{m}$ waist diameter.

¹ Arun Kumar Mallik, Dejun Liu, Vishnu Kavungal, Qiang Wu, Gerald Farrell, and Yuliya Semenova, "Agarose Coated Spherical Micro Resonator for Humidity Measurements," Optics express, Vol 24, 21216-21227 (2016).

A change in the relative humidity of the surrounding the resonator air induces changes in the refractive index (RI) and thickness of the agarose coating layer. These changes in turn lead to a spectral shift of the WGM resonances, which can be related to the RH value after a suitable calibration. Studies of the repeatability, long-term stability, measurement accuracy and temperature dependence of the proposed sensor are carried out. The RH sensitivity of the proposed sensor depends on the concentration of the agarose gel which determines the initial thickness of the deposited coating layer. Studies of the micro- resonators with coating layers fabricated from gels with three different agarose concentrations of 0.5%, 1.125% and 2.25 wt./vol.% showed that an increase in the initial thickness of the coating material results in an increase in sensitivity but also leads to a decrease of quality factor (Q) of the micro resonator. The highest sensitivity achieved in our experiments was 518 pm/%RH in the RH range from 30% to 70%. The proposed sensor offers the advantages of a very compact form factor, low hysteresis, good repeatability, and low cross sensitivity to temperature.

Key words: Optical Resonators; Micro-optical Devices; Fiber Optic Sensors; Micro structured fibers.

2.2 Introduction

Whispering gallery mode (WGM) based micro resonators have attracted significant attention from researchers for applications in various photonic devices and sensors due to their ultra-high-quality factors (Q), low absorption loss and easy and inexpensive fabrication methods. A significant amount of research work has been carried out on various micro resonator shapes, such as microspheres [1], [2], microdisks [3] and microtubes [4]. Inside such a circular-shaped resonator the

light propagates in the form of whispering gallery modes as a result of total internal reflection. Due to their extreme sensitivity to the size of the resonator and also to the refractive indices of the resonator and the surrounding medium, WGMs can be used for sensing of various parameters such as molecular adsorption [2], refractive index [5] and stress [6]. Polymer coated spherical microresonators have been previously developed for chemical vapor sensing [7]. When an optical microresonator is coated with a thin layer of polymer, WGM frequency shift occurs when the polymer undergoes a change in refractive index or thickness. This change can be induced for example by adsorption from the local environment by quantities such as the ammonia vapor [7].

Measurement of humidity is important in a wide range of applications, including meteorology, agriculture, food industry, clinical medicine, manufacturing, civil engineering and many other fields [8]–[10]. Several types of fiber optic humidity sensors have been proposed and demonstrated to date, including a scheme based on fluorescence [11], fiber Bragg gratings [12], interferometry [13] and surface plasmon resonance [14]. Many of these sensing techniques involve using humidity sensitive coatings or gels on the surfaces or end faces of the optical fiber. For example, hydrogel polymers, such as polyvinyl alcohol (PVA) [15], [16], polyethylene glycol [17] and agarose [18], have been previously proposed and studied as coating materials for optical fiber based humidity sensors. Such polymer coatings have the advantage of good reproducibility and long term stability. The coatings usually swell physically and experience a refractive index change in response to changes in relative humidity (RH). For example, Barian et al.[18] demonstrated a tapered fiber coated with agarose gel for humidity sensing

based on the refractive index change of agarose, which is linear over a wide range of RH values [19].

In this paper we propose a new type of fiber optic humidity sensor based on an agarose coated silica microsphere resonator. WGMs are excited in the agarose coated microsphere by coupling evanescent light to and from a tapered fiber. In this case the tapered fiber has a $\sim 3.3 \mu\text{m}$ waist diameter. Fabrication of the microsphere and the fiber taper is an inexpensive process and involves commercially available fibers. agarose gel is well known as a hygroscopic polymer commonly used in biological research[20][21], with an advantage of better long-term stability compared with materials used in[22] and [23]. Three sensor samples based on the silica microspheres dip-coated with agarose gel of different concentrations (0.5, 1.125 and 2.25 wt./vol. %) are experimentally investigated. A detailed study of the sensor in terms of its sensitivity, repeatability, long-term stability and measurement accuracy is reported.

2.3 Experimental setup and sensor fabrication

2.3.1 Fiber taper fabrication

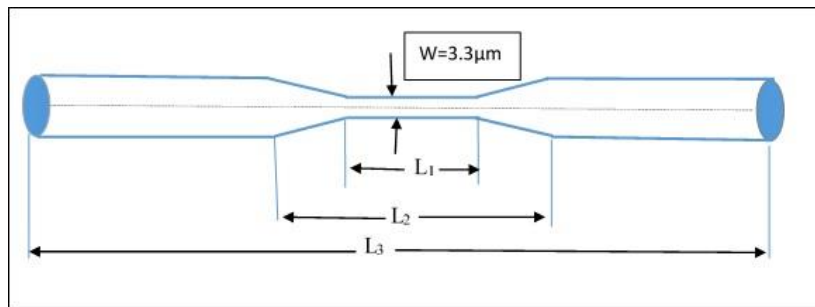


Fig. 2.2. Schematic diagram of the tapered fiber used for coupling the light into the microsphere. The waist diameter $W = 3.3 \mu\text{m}$, waist length $L_1 = 2 \text{ mm}$, full taper length $L_2 = 12 \text{ mm}$ and the length of the taper between the cured epoxy droplets on the microscope slide $L_3 = 4 \text{ cm}$.

Tapered fiber with a waist diameter of $\sim 3.3 \mu\text{m}$ was prepared from a standard single-mode telecommunications optical fiber (SMF-28 Corning) with core and cladding diameters of 8.3 and $125 \mu\text{m}$ respectively. For the experiments, a 1.5 m length of this fiber was used and a 3 cm-long section at the center was stripped off its coating by a mechanical stripper. The stripped part was cleaned with isopropyl alcohol and then fixed horizontally between two computer controlled XYZ translational stages. The tapered fiber was then fabricated by means of the customized micro-heater brushing technique described in [24]. A ceramic micro heater (CMH-7019, NTT-AT) was used to heat the fiber up to approximately 1300°C , making the silica material soft enough for tapering. A customized PC program allowed for an accurate control of the diameter, the length and the shape of the fabricated tapers [25]. In our experiment the tapered waist diameter is approximately 3.3 micron, the waist length is around $L_1 = 2 \text{ mm}$ and the full taper length is circa $L_2 = 12 \text{ mm}$ (as shown in Fig. 2.2). The fabricated fiber taper was then fixed on a glass slide at a height of $\sim 5 \text{ mm}$ from the slide surface using two drops of UV curable epoxy (Norrrland). The total length of the fiber between the cured epoxy droplets was $L_3 = 4 \text{ cm}$.

2.3.2 Microsphere fabrication

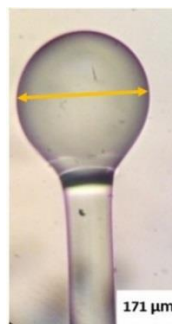


Fig. 2.3. Optical microscope image of the microsphere with the diameter of $171 \mu\text{m}$ used in the experiment

The microsphere for our experiments was fabricated at the tip of a standard single mode fiber SMF-28². A small length of fiber (~3.8 cm) was stripped from one end cleaned with isopropyl alcohol and cleaved. The cleaved end of the fiber was placed inside a fusion splicer (Sumitomo Type-36). A series of electric arc discharges was then applied to the cleaved end of the fiber so that the tip of the fiber was gradually melted, assuming a spherical shape as the glass softens due to surface tension. The diameter of the sphere increases with the number of arcs applied. In our experiment we used a silica microsphere with a diameter of 171 μm (Fig. 2.3). A variety of microsphere diameters were fabricated but it was found that for our purposes the diameter had little effect on the sensing performance.

2.3.3 Agarose gel coating preparation

Agarose is a complex sugar (polysaccharide) derived from the seaweed. agarose gel is porous in nature and is used widely to separate, identify and purify nucleic acid in the field of bio chemistry [26]. It is usually sold in a form of white powder soluble in water at 34-38°C. In our experiment agarose powder, obtained from Sigma Aldrich (A6013), was dissolved in water, in proportions of 0.5, 1.125 and 2.25 wt./vol.%. The solutions then were heated up to 65°C. To dissolve the agarose in distilled water, the beaker containing the mixture was placed on a heater combined with a magnetic stirrer. Microsphere samples were dipped into the hot agarose solution and pulled out very fast. When the agarose solution cools down and reaches room temperature, it polymerizes to form hydrogel and will not assume a liquid form again unless it is heated above the melting point. All coated microspheres were left to dry for 48 hours at room temperature.

² SMF-28 was tapered down to 80 μm .

2.3.4 Experimental set up for RH measurements

Fig. 2.4 shows the experimental set-up for the humidity sensor characterization. The system consists of a broadband light source (Thorlabs S5FC1005S), polarization controller, optical spectrum analyzer (OSA, Advantest Q8384) and a temperature controlled humidity chamber (ETS 5503). The fiber taper fixed on a glass slide is placed inside the humidity chamber. The environmental chamber consists of $\sim 0.11 \text{ m}^3$ air tight space with an inlet and an outlet. The upper inlet is made for the entry of the moist air into the chamber and the outlet is used for dragging the moist air to the dehumidifier through a pump. The dehumidifier box contains anhydrous calcium sulfate which absorbs moisture from the air. The compressed dry air is pumped to regulate the RH in the chamber. The humid air was obtained by bubbling dry air into the ultrasonic humidification system (ETS5462) controlling the ratio of humid air and compressed dry air in the chamber to achieve the required value of RH. This data is fed to the humidity controller through the reference sensor head. The chamber controller system allows for independent setup of both temperature and humidity inside the chamber. The accuracy of the chamber is $\pm 2\%$ RH. Each humidity measurement was recorded five minutes after the RH level reached a certain set value to allow the humidity level to stabilize throughout the chamber.

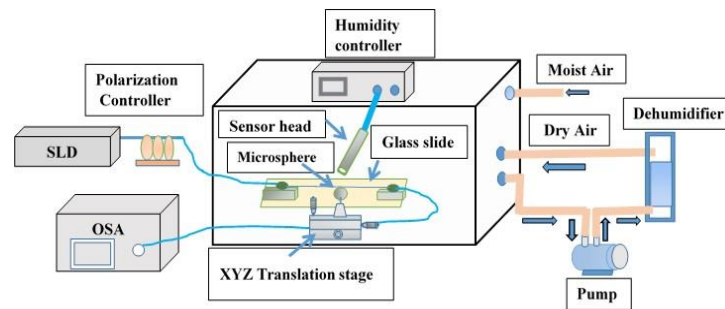


Fig. 2.4. Experimental set-up used for RH measurement using spherical microresonator.

2.3.5 Sensor characterization

The coated microsphere was placed in contact with the tapered fiber inside the humidity chamber. Light from the broadband superluminescent light source (SLD) operating in the wavelength range 1530-1570 nm was launched into the fiber taper and the corresponding transmission spectrum was observed at the taper output by means of the OSA. The wavelength resolution of the OSA was 10 pm. The microsphere, mounted on a XYZ nano-positioning stage, was gradually and carefully brought in direct contact with the tapered fiber until the WGM resonances were clearly observed in the transmission spectrum of the fiber taper. The polarization controller was also adjusted manually to achieve maximum light coupling efficiency. The humidity chamber was then closed and left to stand for one hour in order to stabilize the RH and temperature throughout its volume. In order to eliminate the effect of temperature variations, the temperature of the humidity chamber was set to a constant 25 °C (close to room temperature) throughout the entire RH measurement cycle.

2.4 Results and discussion

2.4.1 Spectrum characterization

Fig. 2.5 illustrates a typical fiber taper transmission spectrum achieved with the agarose coated microsphere. As can be seen from the figure, WGM resonances are clearly observed in the spectrum. The value of the free spectral range (F.S.R) determined from the graph (3.141 nm) can be used to estimate the microsphere diameter or its effective refractive index (RI) based on the approximate formula [27]:

$$\text{F.S.R} \approx \frac{\lambda_0^2}{\pi D n_{eff}} \quad (2.1)$$

where λ_0 , n_{eff} and D are the resonant wavelength, the effective refractive index of the fundamental WGM for the microsphere and the microsphere diameter, respectively.

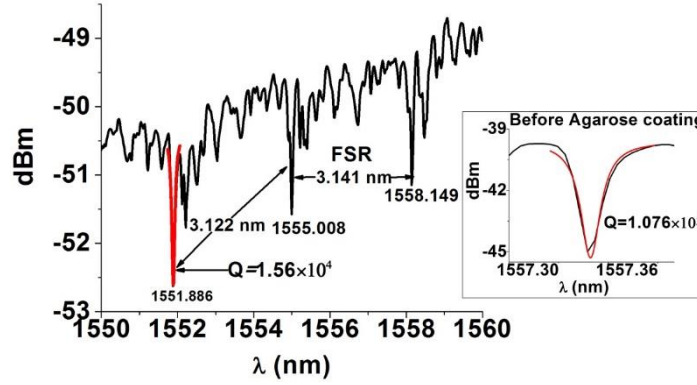


Fig. 2.5. Transmission spectrum recorded with an agarose coated microsphere with a diameter of 171 μm .

Effective RI can be calculated by solving the wave equation described in [28] considering the RIs of silica (1.4682) and the agarose layer (1.336). This numerical calculation resulted in the $n_{eff} = 1.4321$ for this case, so that resulting from the Eq. (2.1) microsphere diameter is 170.83 μm , which is in a good agreement with the result of the microscopic measurement (Fig. 2.3).

The Q factors for the microsphere before and after its coating with an agarose layer were estimated from the experimental spectra by measuring the full width at half maximum (FWHM) of the WGM resonance near 1551 nm (inset in Fig. 2.5 illustrates the corresponding WGM resonance and its Lorentz fitting in the spectrum of the microsphere before its coating with agarose). The FWHM for an uncoated microsphere was 14.47 pm at the wavelength of 1557.3493 nm. The corresponding value of the Q factor was calculated as 1.076×10^5 . After application of the agarose coating on the microsphere surface the Q factor decreased to 1.56×10^4 . Such a decrease in the Q factor is likely due to scattering

caused by the surface roughness and higher absorption and scattering within the agarose layer.

2.4.2 RH dependency

We recorded a series of transmission spectra for the sensor at different RH values in the range from 35% to 81% RH. The corresponding results for the microsphere coated with 2.25% concentration agarose solution are shown in Fig. 2.6 (a).

As can be seen from the figure, an increase in the surrounding RH leads to a red shift of the WGM spectrum. This could be explained by the fact that when the surrounding RH increases, the agarose coating absorbs more water from the environment which leads to an increase of the effective refractive index of the coating and also to an increase of the coating thickness, with both factors contributing to the spectral shift of the WGMs. Fig. 2.6 (b) illustrates the shift of a selected WGM resonant wavelength versus RH at a constant temperature of 25°C.

Two RH ranges within which the dependencies are almost linear but have different slopes can be identified as follows: lower RH range (38.7-65.7%) with lower sensitivity and a higher RH range (65.7-81%) with higher sensitivity. The corresponding RH sensitivity values estimated from the graph are 17.51 pm/%RH and 53 pm/%RH. It can also be noticed from Fig. 2.6 (a) that for the RH values above 70%, losses in the transmission spectrum increases rapidly. The main reason for such high losses may be the mechanical stress and resulting bend experienced by the tapered fiber due to accumulation of the water molecules on its surface. As mentioned in the previous section, the fiber taper was stretched in the air 5 mm above the microscopic glass slide inside the chamber so that accumulation of a quantity of water on the surface of the fiber taper may cause a

slight sagging of the fiber taper. Another possible reason for the increased loss is the increase of absorption by the micro resonator material due to the change of the agarose layer properties at high RH.

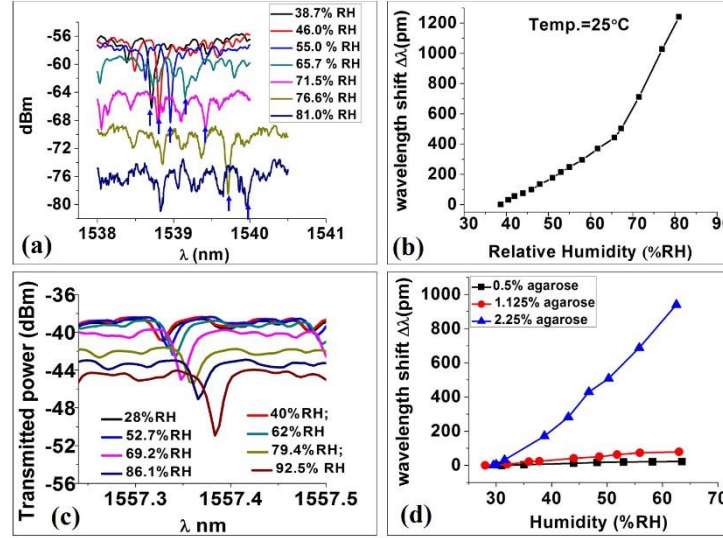


Fig. 2.6 Experimental results for the WGM resonator based on a 171 μm diameter microsphere coated with 2.25% agarose gel coupled with a 3.3 μm tapered fiber in the range of humidity from 35 % to 81% RH at a constant temperature of 25 $^{\circ}\text{C}$. (a) WGM spectra at different RH levels; (b) wavelength shift of the WGM spectrum versus RH; (c) humidity response of the WGM spectrum for an uncoated microsphere resonator; (d) spectral shift versus RH for the sensors based on the same diameter microsphere coated with the agarose solutions of different concentrations.

To further investigate the influence of the high RH levels on the sensor performance, an additional experiment was carried out with the same tapered fiber but with an uncoated microsphere of the same diameter in the RH range from 28% to 92%. The results are presented in Fig. 2.6 (c) where it can be seen that the overall loss increases by circa 5 dB when the RH changes from 69% to 92%. A small (~ 36 pm, equivalent to 0.56 pm/%RH) wavelength shift is also observed, possibly due to stress induced onto the fiber by the water weight.

2.4.3 Coating thickness dependency

It should be noted that the average transmission loss level also depends on other factors, such as the tapered fiber waist diameter and the coating thickness on the

surface of the microsphere. To investigate the effect of coating thickness, three different solutions with agarose concentrations of 0.5%, 1.125% and 2.25 wt./vol. % were prepared and applied to the microspheres of the same diameter (171 μm). Fig. 2.6 (d) shows that the RH sensitivity of the sensor depends significantly on the concentration of the agarose solution used to form a coating layer. As can be seen from Fig. 2.6 (d) the highest RH sensitivity is achieved with the 2.25% agarose solution in the range of RH from 25% to 65%.

The influence of the thickness of the polymer coating on the RH sensitivity of such a microsphere resonator can be analyzed as follows. It is known that the Q factor of an uncoated micro resonator is determined by the total loss including radiation loss, scattering loss from the surface irregularities and by material absorption, which can be expressed by Eq.(2.2) [27]:

$$\frac{1}{Q_{\text{in}}} = \frac{1}{Q_{\text{rad}}} + \frac{1}{(Q_{\text{abs}})_{\text{silica}}} + \frac{1}{(Q_{\text{abs}})_{\text{agarose}}} + \frac{1}{Q_{\text{s.s.}}} + \frac{1}{Q_{\text{coupling}}} \quad (2.2)$$

where $1/Q_{\text{rad}}$ denotes intrinsic radiative (curvature) losses of the resonator, $1/(Q_{\text{abs}})_{\text{silica}}$ and $1/(Q_{\text{abs}})_{\text{agarose}}$ denote the material absorption loss within the silica microsphere and the polymer layer, respectively, $1/Q_{\text{s.s.}}$ denotes scattering losses due to the microresonator surface inhomogeneities and $1/Q_{\text{coupling}}$ - losses due to coupling with the fiber taper. $1/Q_{\text{rad}}$ can be neglected in our case since this term vanishes exponentially for the resonators with $D/\lambda \geq 15$ [27]. The absorption limited Q factors can be calculated as $(Q_{\text{abs}})_{\text{silica}} = 2\pi n_s / \lambda_R \alpha_s$ and $(Q_{\text{abs}})_{\text{agarose}} = 2\pi n_a / \lambda_R \alpha_a$, where α_s , n_s and α_a , n_a are optical attenuation coefficients per unit length and refractive indices of silica and agarose layer respectively. Since optical attenuation within the agarose layer is several order of magnitude higher than that in silica, so the term $1/(Q_{\text{abs}})_{\text{agarose}}$ will be much higher than $1/(Q_{\text{abs}})_{\text{silica}}$. When the

polymer layer thickness increases, greater portion of light energy is distributed within the polymer and thus the change in the polymer's RI (n_a) in response to changing RH leads to a higher RH sensitivity of the micro resonator. However, as the thickness of the polymer layer increases, the larger material absorption loss in the polymer compared to silica contributes to an overall decrease of the Q factor for coated resonators. Another significant contribution to the overall losses is due to scattering on the surface inhomogeneities, which strongly depends on their rms size and correlation length. In practice the total Q factor for the agarose coated resonators considered in this study is limited by the last three terms of Eq (2.2).

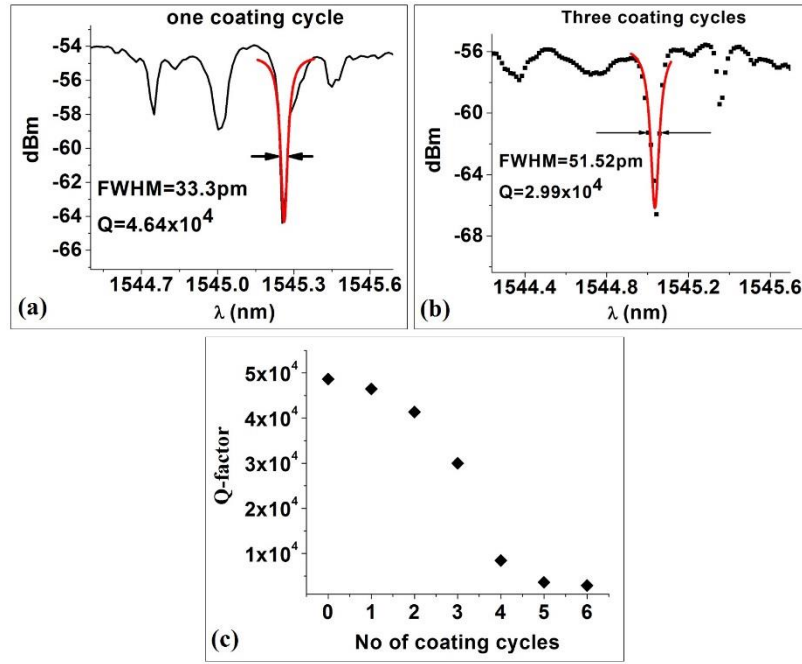


Fig. 2.7. Experimental spectra and Lorentzian fitting for a 100 μm diameter microsphere coated with 2.25% agarose hydrogel: a) after one coating cycle; b) after three coating cycles; c) Q factor versus the number of coating cycles

To further analyze the influence of the coating layer thickness, we carried out a series of experiments for a silica microsphere of a fixed diameter (100 μm) which was coated with 2.25 wt./vol.% agarose gel applied multiple times through repeated coating cycles, forming coatings with progressively larger thickness values. The WGM spectra of the coated sphere were recorded after one, two, three,

four, five and six coating cycles respectively using the same setup and the same tapered fiber at a constant temperature ($23 \pm 0.4^\circ\text{C}$) and humidity (66 %RH). The spectra were further analyzed to estimate the corresponding Q factors, as illustrated in Fig. 2.7 (a, b).

The quality factor can be calculated as $Q = \lambda_{res} / \Delta\lambda_{FWHM}$, where λ_{res} is the resonance wavelength and $\Delta\lambda_{FWHM}$ is the FWHM of the resonant lobe. We estimated the FWHM as 33.3 pm and 51.52 pm at the wavelengths of 1545.261 nm and 1545.035 nm, respectively. The corresponding Q factor values are thus estimated as 4.64×10^4 for the microsphere after the first coating cycle and 2.99×10^4 for the same microsphere after two coating cycles were carried out. As illustrated in Fig. 2.7 (c), the Q factor of the sphere gradually decreased with each consequent coating cycle. The RH sensitivity of the sensors based on the same silica microsphere with different thicknesses of the agarose coating was also investigated in the RH range from 30% to 70% RH and the results are presented in Fig. 2.8 (a). The resonance wavelength shift over the entire humidity range was 0.41 nm for the sensor with a single coating, 0.964 nm for the sensor coated twice and 1.54 nm for the same sensor after three coating cycles.

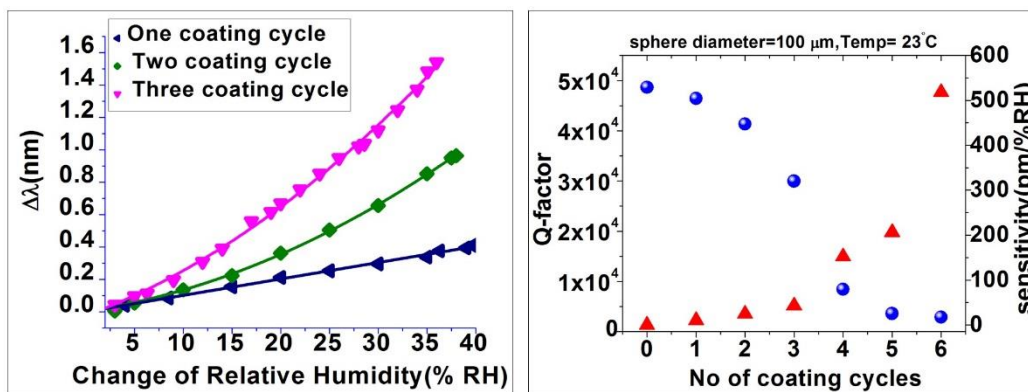


Fig. 2.8 (a) RH response of the sensor based on a 100 μm diameter microsphere with a different number of agarose layers: (b) Q factor and estimated RH sensitivity for the 100 μm diameter microsphere with a different number of agarose coating layers

Although the thickness of the agarose gel could not be controlled accurately, these results demonstrate that sensitivity gradually increases with the increase of the agarose layer thickness. The maximum sensitivity in our experiments was observed for the sensor coated six times and was estimated at 518 pm/%RH which is significantly higher than that of 10 pm/%RH for the sensor with single coating as illustrated in Fig. 2.8 (b).

This result is also, to the best of our knowledge, the highest sensitivity reported for agarose coated fiber optic sensors, including that of 114.7 pm/%RH in the range 25%-96% RH for an agarose-coated long-period grating (LPG) reported in [29] and for an agarose-coated photonic crystal fiber interferometer previously reported by our group in [30], where for the same number of coating cycles the sensitivity was ~200 pm/%RH in the range of 30-90 %RH.

2.5 Sensor characterization

The detection limit of the proposed sensor is calculated as the ratio of sensor resolution (R) to the sensitivity of the sensor (S). The sensor resolution depends upon the different sources of noise involved in the measurement and determined by the Eq. (2.3) [31]:

$$R = 3 \sqrt{\sigma_{amp-noise}^2 + \sigma_{temp-induced}^2 + \sigma_{spec-res}^2} \quad (2.3)$$

where

$$\sigma_{amp-noise} \approx \frac{\Delta\lambda}{4.5(SNR)^{0.25}} \quad (2.4)$$

σ is the standard deviation of resulting spectral variation and $\Delta\lambda$ is the full-width half maximum of the mode amplitude derived from the Q factor by $Q = \lambda / \Delta\lambda$. The Q factor of the 171 μm coated microsphere calculated from the transmitted

spectrum was 1.69×10^4 and the FWHM calculated by fitting the resonance dip with Lorentz equation was 91.06 pm at $\lambda = 1537.164$ nm. We assumed the SNR (Signal to Noise Ratio) of the system is approximately 60 dB, then the $\sigma_{\text{amp-noise}}$ is calculated as 0.636 pm. We also assumed the standard deviation due to temperature stabilization is 10 fm [31]. The spectral resolution of the optical spectrum analyzer used for our experiment is 10 pm $\pm 3\%$. The error in determining the position of the resonant mode is uniformly distributed between -0.3 pm to +0.3 pm and the resulting standard deviation of $\sigma_{\text{spect-res}}$ is 0.1732 pm. The overall sensor resolution is $R = 1.977$ pm. The detection limit of a 171 μm diameter coated microsphere is $1.1 \times 10^{-1} \% \text{RH}$ in the humidity range 38.7 - 65.7%RH and $3.7 \times 10^{-2} \% \text{RH}$ in the humidity range 65.7-81 %RH. It should be noted that the detection limit also depends on the nature of the optical source, where a narrow line width source will improve the detection limit [31]. However, such an improvement is not included or assumed here as in our case we used a broadband source.

2.5.1 Sensor stability

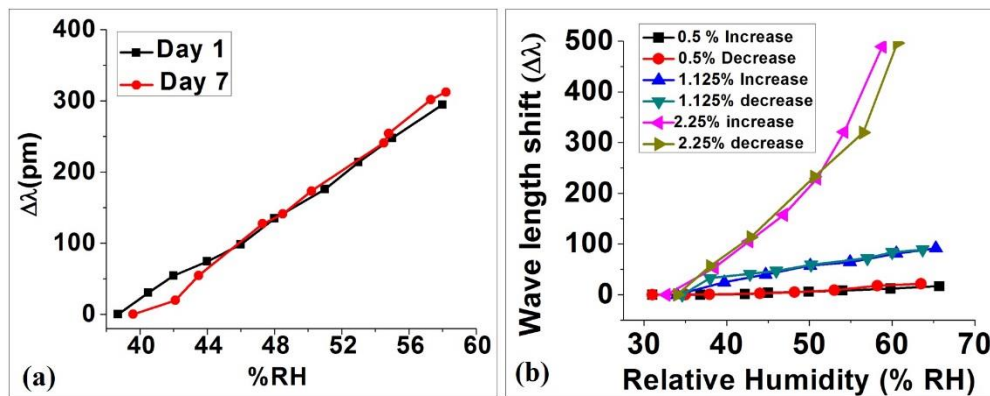


Fig. 2.9 (a) Relative humidity responses of the sensor, measurements recorded seven days apart; (b) studies of the sensor hysteresis: humidity response for the 171 μm microspheres coated with different agarose concentration coatings during RH increase-decrease cycle at 25°C.

To test the stability of the sensor, RH measurements were carried out using the same sensor sample after a time interval of seven days in the RH range from 35% to 65% at a constant temperature. The sample used in this experiment was a 171 μm diameter microsphere coated with a 2.25 % agarose concentration gel. It can be seen in Fig. 2.9 (a), that the performance of the sensor is quite stable over one week with small fluctuations only. Fig. 2.9 (b) illustrates studies of the hysteresis characteristics using data from humidification-dehumidification cycle for the three sensors based on the 171 μm diameter microspheres coated with hydrogel films with agarose concentrations of 0.5, 1.125 and 2.25 wt./vol.%. It can be seen from the figure that all the three sensors demonstrate very small or no hysteresis.

Finally, to investigate the effect of temperature on the RH sensor performance, the humidity in the chamber was set to constant at 41% RH. The temperature was then gradually raised from 16 $^{\circ}\text{C}$ to 27 $^{\circ}\text{C}$. The wavelength shift of the WGM spectrum with temperature is shown in Fig. 2.10. It can be noted that the temperature sensitivity of the sensor is small compared to its RH sensitivity. For a 171 μm diameter sensor coated with 2.25% of agarose hydrogel it is estimated as $\sim 6 \text{ pm}/^{\circ}\text{C}$ in the temperature range of 16 -27 $^{\circ}\text{C}$.

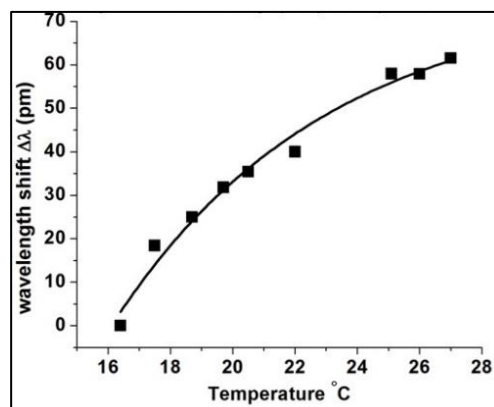


Fig. 2.10. Resonance wavelength shift versus temperature for the 171 μm microsphere coated with 2.25% wt./vol. agarose solution at 41% RH.

2.6 Conclusion

A novel type of relative humidity sensor based on a whispering gallery mode microresonator has been proposed and experimentally demonstrated. WGMs are excited in the silica microsphere dip-coated with an agarose gel evanescently coupled to a tapered fiber. Changes in the refractive index and thickness of the Agarose coating arising due to changes in the surrounding relative humidity lead to a spectral shift of the WGM resonances which can be related to the RH value after a suitable sensor calibration. The RH sensitivity of the proposed sensor depends on the concentration of the agarose gel which determines the initial thickness of the coating deposited on the microsphere. Studies of the coating layers fabricated from gels with three different agarose concentrations of 0.5%, 1.125% and 2.25 wt./vol.% and also by application of coating with the same agarose concentration through repeated coating cycles showed that an increase in the thickness of the coating material results in an increase in sensitivity but also leads to a decrease of quality factor of the micro resonator. The highest sensitivity achieved in our experiments was 518 pm/% RH in the RH range from 30% to 70%. The proposed sensor offers the advantages being very compact in nature, whilst also demonstrating low hysteresis, good repeatability, and a relatively low cross sensitivity to temperature.

Author contributions statement

Arun Kumar Mallik conceived the main idea of the manuscript, designed the experimental setup, carried out the experiments and co-wrote the manuscript. Dejun Liu and Vishnu Kavungal helped in preparation of the agarose coating and

fabrication of the tapered fiber. Gerald Farrell and Qiang Wu provided valuable suggestions and advice. Yuliya Semenova supervised the project and co-wrote the manuscript.

References:

- [1] F. Vollmer, D. Braun, A. Libchaber, M. Khoshshima, I. Teraoka, and S. Arnold, "Protein detection by optical shift of a resonant microcavity," *Appl. Phys. Lett.*, vol. 80, no. 21, pp. 4057–4059, 2002.
- [2] S. Arnold, M. Khoshshima, I. Teraoka, S. Holler, and F. Vollmer, "Shift of whispering-gallery modes in microspheres by protein adsorption," *Opt. Lett.*, vol. 28, no. 4, pp. 272-274, 2003.
- [3] W. Fang, D. B. Buchholz, R. C. Bailey, J. T. Hupp, R. P. H. Chang, and H. Cao, "Detection of chemical species using ultraviolet microdisk lasers," *Appl. Phys. Lett.*, vol. 85, no. 17, pp. 3666–3668, 2004.
- [4] T. Ling and L. J. Guo, "A unique resonance mode observed in a prism-coupled micro-tube resonator sensor with superior index sensitivity.," *Opt. Express*, vol. 15, no. 25, pp. 17424–17432, 2007.
- [5] E. Krioukov, D. J. W. Klunder, A. Driessen, J. Greve, and C. Otto, "Sensor based on an integrated optical microcavity," *Opt. Lett.*, vol. 27, no. 7, 2002.
- [6] V. S. Ilchenko *et al.*, "Strain-tunable high-Q optical microsphere resonator," *Opt. Commun.*, vol. 145, no. 1-6, pp.86-90, 1998.
- [7] N. Lin *et al.*, "Simulation and optimization of polymer-coated microsphere resonators in chemical vapor sensing," *Appl. Opt.*, vol. 50, no. 28, pp. 5465-5472, 2011.
- [8] P. R. Story, D. W. Galipeau, and R. D. Mileham, "A study of low-cost sensors for measuring low relative humidity," *Sensors Actuators B. Chem.*, vol. 25, no. 1-3, pp. 681-685, 1995.
- [9] A. H. P. Raichur, "Fiber optic moisture sensor for baking and drying process control," *Proc. Food Process. Autom. IV, Am. Soc. Agric. Eng.*, pp. 180–189, 1995.
- [10] Z. Chen and C. Lu, "Humidity Sensors: A Review of Materials and Mechanisms," *Sens. Lett.*, vol. 3, no. 4, pp. 274–295, 2005.
- [11] H. E. Posch and O. S. Wolfbeis, "Optical sensors, 13: fibre-optic humidity sensor based on fluorescence quenching," *Sensors and Actuators*, vol. 15, no. 1, pp. 77–83, 1988.
- [12] F. J. Arregui, I. R. Matías, K. L. Cooper, and R. O. Claus, "Simultaneous measurement of humidity and temperature by combining a reflective

- intensity-based optical fiber sensor and a fiber bragg grating,” *IEEE Sens. J.*, vol. 2, no. 5, pp. 482–487, 2002.
- [13] J. M. Corres, I. R. Matias, M. Hernaez, J. Bravo, and F. J. Arregui, “Optical Fiber Humidity Sensors Using Nanostructured Coatings of SiO₂ Nanoparticles,” *IEEE Sens. J.*, vol. 8, no. 3, pp. 281–285, 2008.
 - [14] M. Hernaez, C. R. Zamarreno, I. R. Matias, and F. J. Arregui, “Optical fiber humidity sensor based on surface plasmon resonance in the infra-red region,” in *Sensors & Their Applications Xv*, vol. 178, 01209, 2009.
 - [15] Y. M. Y. Miao *et al.*, “Relative Humidity Sensor Based on Tilted Fiber Bragg Grating With Polyvinyl Alcohol Coating,” *IEEE Photonics Technol. Lett.*, vol. 21, no. 7, pp. 441–443, 2009.
 - [16] A. Gaston, F. Perez, and J. Sevilla, “Optical Fiber Relative-Humidity Sensor with Polyvinyl Alcohol Film,” *Appl. Opt.*, vol. 43, no. 21, pp. 4127, 2004.
 - [17] S. Acikgoz *et al.*, “Use of polyethylene glycol coatings for optical fibre humidity sensing,” *Opt. Rev.*, vol. 15, no. 2, pp. 84–90, 2008.
 - [18] C. Bariáin, I. R. Matías, F. J. Arregui, and M. López-Amo, “Optical fiber humidity sensor based on a tapered fiber coated with agarose gel,” *Sensors Actuators, B Chem.*, vol. 69, no. 1, pp. 127–131, 2000.
 - [19] N. M. Doliba, S. L. Wehrli, A. M. Babsky, N. M. Doliba, and M. D. Osbakken, “Encapsulation and perfusion of mitochondria in agarose beads for functional studies with ³¹P-NMR spectroscopy,” *Magn. Reson. Med.*, vol. 39, no. 5, pp. 679–684, 1998.
 - [20] O. Iglesias, A. Garcia, R. M. Roques, and J. L. Bueno, “cdrying of water gels: Determination of the characteristic curve of agar-agar,” *Drying Technology*, vol. 11, no. 3, pp. 571–587, 1993.
 - [21] J. Mathew, Y. Semenova, G. Rajan, P. Wang, and G. Farrell, “Improving the sensitivity of a humidity sensor based on fiber bend coated with a hygroscopic coating,” *Opt. Laser Technol.*, vol. 43, no. 7, pp. 1301–1305, 2011.
 - [22] Q. Wu, Y. Semenova, J. Mathew, P. Wang, and G. Farrell, “Humidity sensor based on a single-mode hetero-core fiber structure,” *Opt. Lett.*, vol. 36, no. 10, pp. 1752, 2011.
 - [23] P. S. Priambodo, P. S. Priambodo, and R. Magnusson, “Agarose-Gel Based

- Guided-Mode Resonance Humidity Sensor,” *IEEE Sens. J.*, vol. 7, no. 3, pp. 409–414, 2007.
- [24] G. Brambilla, V. Finazzi, and D. J. Richardson, “Ultra-low-loss optical fiber nanotapers,” *Opt. Express*, vol. 12, no. 10, pp. 2258, 2004.
 - [25] T. A. Birks and Y. W. Li, “The Shape of Fiber Tapers,” *J. Light. Technol.*, vol. 10, no. 4, pp. 432–438, 1992.
 - [26] S. Kurihara, H. Torigoe, S. Omura, M. Saito, K. Kurihara, M., & Matsubara, “DNA Fragmentation Induced by a Cytoplasmic Extract from Irradiated Cells,” *Radiat. Res.*, vol. 150, no. 3, pp. 269–274, 1998.
 - [27] M. L. Gorodetsky, A. A. Savchenkov, and V. S. Ilchenko, “Ultimate Q of optical microsphere resonators,” *Opt. Lett.*, vol. 21, no. 7, pp. 453–455, 1996.
 - [28] B. E. Little, J. P. Laine, and H. A. Haus, “Analytic theory of coupling from tapered fibers and half-blocks into microsphere resonators,” *J. Light. Technol.*, vol. 17, no. 4, pp. 704–715, 1999.
 - [29] Y. Miao *et al.*, “Agarose gel-coated LPG based on two sensing mechanisms for relative humidity measurement,” *Appl. Opt.*, vol. 52, no. 1, pp. 90–5, 2013.
 - [30] J. Mathew, Y. Semenova, and G. Farrell, “Experimental demonstration of a high-sensitivity humidity sensor based on an Agarose-coated transmission-type photonic crystal fiber interferometer,” *Appl. Opt.*, vol. 52, no. 16, pp. 3884–3890, 2013.
 - [31] I. M. White and X. Fan, “On the performance quantification of resonant refractive index sensors,” *Opt. Express*, vol. 16, no. 2, pp. 1020, 2008.

3. Study of the influence of the functional coating thickness on sensitivity of the WGM sensor

In the previous chapter a novel highly sensitive relative humidity sensor was proposed and demonstrated experimentally based on a silica microsphere WGM resonator coated with a thin layer of natural hygroscopic polymer agarose. It was demonstrated that when the atmospheric humidity level changes, the refractive index of the coating layer also changes, resulting in the spectral shift of WGM resonances, observed in the transmission spectrum of the light coupling fiber taper. It should be noted however that the WGM spectrum and its sensitivity to humidity for such a sensor also significantly depend on the coating properties, primarily on its thickness. Therefore there is a need to investigate the relationships between the coating thickness of the agarose layer and other parameters of the sensor.

This chapter focuses on the theoretical analysis and experimental investigations of the dependence of sensitivity and spectral Q factor for the proposed sensor on the thickness of agarose coating material. Using the perturbation theory and custom developed MATLAB code, the influence of the agarose coating thickness on the sensitivity of the proposed sensor has been analyzed and the results of the analysis have been verified experimentally. The chapter's main contributions are the development of a reliable theoretical model for predicting the WGMs behavior in coated microspherical resonators for an improved understanding of the WGM phenomena that can be applied to similar sensor structures.

3.1 Study of the influence of the agarose hydrogel layer thickness on sensitivity of the coated silica microsphere resonator to humidity³

Abstract: In this paper, we investigate both theoretically and experimentally the influence of the agarose hydrogel layer thickness on sensitivity of a proposed relative humidity (RH) sensor based on a silica microsphere resonator coated with agarose hydrogel. The operating principle of the sensor relies on excitation of whispering gallery modes (WGMs) in the coated silica microsphere using the evanescent field of a tapered fiber. A change in the ambient relative humidity is detected by measuring the wavelength shift of the WGMs in the transmission spectrum of the tapered fiber. Using perturbation theory, we analyze the influence of the agarose coating thickness on the sensitivity of the proposed sensor and compare the results of this analysis with experimental findings for different coating layer thickness. We demonstrate that an increase in the coating layer thickness initially leads to an increase in the sensitivity to RH and reaches saturation at higher values of the agarose layer thickness. The results of the study are useful for the design and optimization of microsphere sensors parameters to meet a performance specification.

Keywords: Microcavities; Microcavity devices; Fiber optics sensors; Optical resonator; Total internal reflection;

3.2 Introduction

³ Arun Kumar Mallik, Qiang Wu, Gerald Farrell, and Yuliya Semenova, "Study of the influence of the Agarose hydrogel layer thickness on sensitivity of the coated silica microsphere resonator to humidity," Applied Optics, Vol 56 ,4065-4069 (2017)

Optical microspheres with whispering gallery modes (WGMs) have become the focus of many theoretical and experimental studies and the basis for a number of reported ultrasensitive sensors of chemical, physical and biological quantities [1]–[5]. The high Q factor, very small mode volume and narrow spectral lines of the WGMs make the microsphere resonators attractive for the design of highly sensitive and accurate sensor systems. In addition, spherical micro-resonators are attractive because they can be easily fabricated at the tip of an optical fiber and the WGMs can be excited by evanescent light coupling using a simple setup, for example, based on a tapered fiber. The principle of such a sensor operation relies on measurements of the shift of the resonance wavelength against any variation of the microsphere size or any change in the optical properties of the surrounding medium. Arnold *et al.* reported specific detection of proteins absorbed on the surface of a microsphere [1] and showed theoretically that an atomic thickness can lead to a detectable shift of a given resonance frequency. The reports in [2], [3] described refractometric sensors based on microsphere resonators with a sensitivity of up to 30 nm/RIU (refractive index unit), leading to a detection limit for refractive index (RI) in the order of 10^{-7} RIU [3]. Subsequently Ma *et al.* demonstrated temperature and humidity sensing with microsphere resonators [5]. Most of the microsphere sensors reported to date detect the change in the ambient RI because the evanescent “tail” of the WGM, penetrates into the surrounding medium. Typically, the surrounding medium and silica microsphere have a large RI contrast, so that the radiation loss is very small, resulting in very high Q factors [6]. On the other hand, this leads to a limited sensitivity of WGMs to the ambient RI, since the evanescent field is located very close to the microsphere’s surface. This means that chemical molecules with poor adsorbability to the microsphere

surface are difficult to detect using the sensing principle above. Teraoka *et al.* [7] examined the properties of spherical micro-resonators coated with high RI materials and demonstrated that the high RI coating layer enhances the sensitivity of the WGM wavelength shift. They also described a perturbation theory for the wavelength shift of WGM resonances in a microsphere coated with a high RI index layer [7]. Later, Nai Lin *et al.* used this approximate model to calculate the thickness-dependent sensitivity of a zeolite coated microsphere to ammonia gas [4]. They demonstrated that the zeolite coating enhances the typically small microsphere surface-to-mass ratio and most importantly acts as an effective concentrator of the analyte molecules absorbing them within the layer close to the surface.

Recently we proposed and demonstrated an ultrasensitive relative humidity (RH) sensor based on a silica fiber microsphere coated with a thin layer of agarose hydrogel prepared from a 2.25% wt./vol. agarose solution [8]. Agarose is a hygroscopic material, which has proved to be highly stable and can be easily applied to the surface of the device by dip coating. Changes in the surrounding RH induce changes in the RI of the agarose coating layer and thus cause a spectral shift in the WGM resonant wavelengths, which with a suitable calibration can be used for the measurement of RH. Experimental results presented in [8] showed that RH sensitivity of the sensor increases with the increase of the thickness of the agarose coating. On the other hand, increase in the agarose layer thickness also resulted in the decrease of the Q factor due to higher absorption loss within the coating layer, ultimately limiting the sensor's resolution. This paper aims to develop deeper understanding of the relationship between the thickness of the agarose layer and sensitivity of the sensor to RH. We analyze the influence of the

agarose coating thickness on the RH sensitivity of the proposed sensor using perturbation theory and compare the results of this analysis with experimental findings for different coating layer thicknesses. To the best of our knowledge this is the first systematic study on this topic allowing to determine an optimal agarose layer thickness for the best possible trade-off between sensitivity and absorption loss for a given microsphere diameter.

3.3 Theoretical analysis

In our analysis, we use the model based on the perturbation theory for the WGM resonances in a coated microsphere developed in [7] and [4]. Fig. 3.1 shows a schematic diagram of the microsphere of radius a_0 with a surface coating layer of thickness t considered in the model. The RIs of the microsphere and the agarose coating layer are n_1 and n_2 and the RI of the surrounding medium is n_3 .

For simplicity, we consider only fundamental WGM modes ($l = m$ and, $n = 1$, where n , l , and m are the radial, azimuthal and polar mode numbers respectively) of TE polarization.

First, we considered an uncoated silica microsphere ($n_1 = 1.4682$; $n_2 = n_3 = 1$) with a radius $a_0 = 130 \mu\text{m}$ with a WGM resonance near $\lambda = 1551.12 \text{ nm}$ (matching those in our experiment). Solving the characteristic equation for the fundamental mode given in [4] for the above parameters gives $l = m = 757$. Setting the l constant (757), we then introduce the agarose coating in the model by assuming new values for $n_2 = 1.3385$ as the RI of the bulk of the agarose layer and $n_3 = 1.0$ as the surrounding RI. The value of n_2 was measured for the agarose gel experimentally using Abbe refractometer.

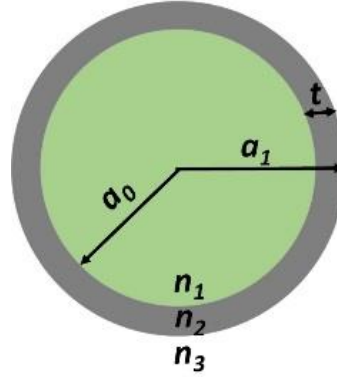


Fig. 3.1 Schematic diagram of the agarose coated microsphere.

The electric field distribution for the WGM mode (TE polarization) in a coated microsphere can be calculated as [4]:

$$E_{l,n} = \begin{cases} A_l \psi_l(n_1 k^{(n)} r) & r < a_0 \\ B_l \psi_l(n_2 k^{(n)} r) + \chi_l \psi_l(n_2 k^{(n)} r) & a_0 < r < a_1 \\ C_l \chi_l(n_3 k^{(n)} r) & r > a_1 \end{cases} \quad (3.1)$$

where A_l , B_l and C_l are constants determined from the boundary conditions for the given mode number.

Fig. 3.2 illustrates the simulated electric field distributions for different values of the agarose layer thickness obtained by solving boundary conditions for the mode with $l = 757$ using MATLAB software.

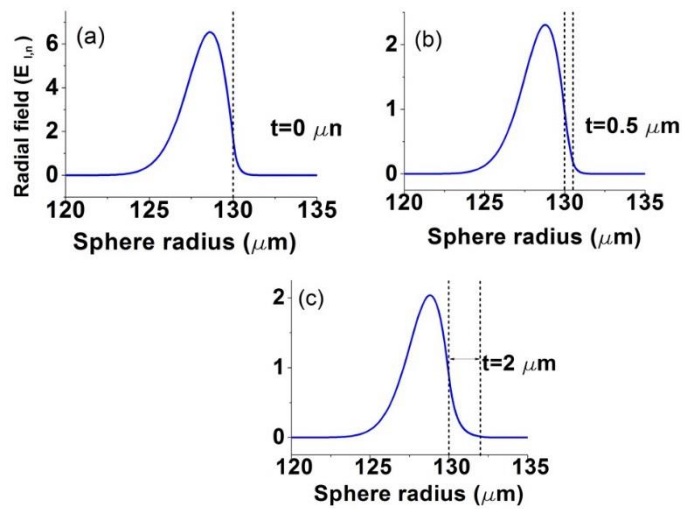


Fig. 3.2 Radial field distributions for the fundamental WGM with $l = m = 757$ and different agarose coating thickness values: (a) $t = 0$; (b) $t = 0.5 \mu m$ and (c) $t = 2 \mu m$.

The RI sensitivity for the TE polarization (S_{TE}) of the coated microsphere can be calculated as [4]:

$$S_{TE} = \frac{n_2 \lambda_R I_2}{n_1^2 I_1 + n_2^2 I_2 + n_3^2 I_3} \quad (3.2)$$

where I_1 , I_2 and I_3 are the fractions of the mode's energy distributed within the silica microsphere, agarose coating layer and the surrounding medium respectively.

Fig. 3.3 shows the simulated dependence for the RI sensitivity of the fundamental WGM above versus the agarose coating layer thickness. One can see from the graph that the estimated RI sensitivity saturates around the value of 1.5 μm of the coating thickness.

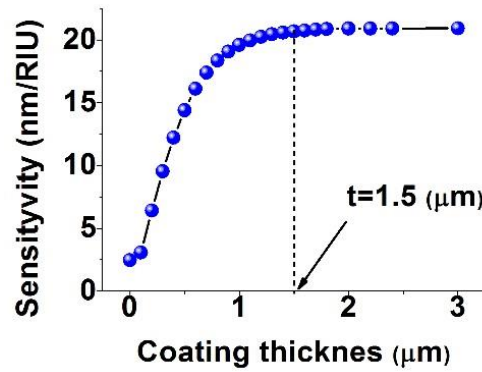


Fig. 3.3 Simulated dependence for the RI sensitivity of the fundamental WGM above versus the agarose coating layer thickness.

3.4 Experimental results and discussion

The microsphere for our experiments was fabricated at the tip of a standard SMF28 single mode fiber by applying a series of electric arc discharges. The sphere diameter in the experiment was measured using an optical microscope as 260 μm . Agarose hydrogel for the coating was fabricated using commercially available agarose powder from Sigma Aldrich (A6013). The hydrogel solution

was prepared by adding 2.25% wt./vol. of the agarose powder into deionized (DI) water followed by stirring at 80 °C temperature until the agarose powder completely dissolved in the DI water. The RI of the agarose gel was measured as 1.3385 with the help of Abbe refractometer. The agarose layer was then applied on the surface of the microsphere by dip coating method. Coating layers with different thickness were realized by repeating the dip coating cycle multiple times (up to six cycles in our experiment). After each coating cycle the microsphere was kept at room temperature for one day to allow for curing. For light coupling to and from the microsphere, an adiabatic tapered fiber was used with a waist diameter of ~3-4 μm . Such a diameter was chosen to ensure the match between the propagation constant of the propagating mode in the taper with that of the WGM mode of interest [9]. The fiber taper was placed in a close proximity with the microsphere inside a chamber in which both humidity and temperature could be controlled.

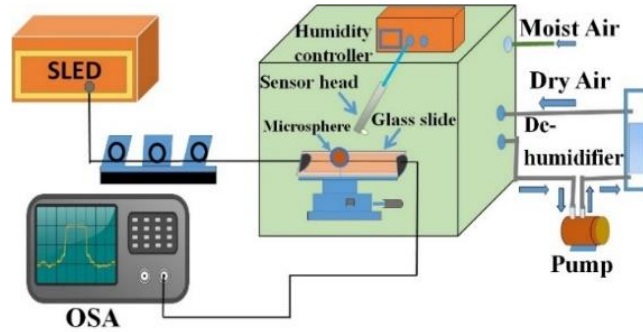


Fig. 3.4 Experimental setup for RH measurements;

Light from the broadband superluminescent light source (SLED) operating in the wavelength range 1530-1570 nm was launched into the fiber taper and the corresponding transmission spectrum was observed at the taper output by means of the OSA with a 10 pm wavelength resolution. The light transmitted through the fiber taper received by a photodetector connected to an oscilloscope as shown in

Fig. 3.4. Experimental transmission spectra were recorded and analyzed for the uncoated microsphere and after each of the subsequent six coating cycles in the RH range from 25 to 50% RH. The value of quality factor was estimated from the experimental spectra as $Q = \lambda_R / \Delta\lambda_{FWHM}$, where λ_R is the resonance wavelength and $\Delta\lambda_{FWHM}$ is the full width at half-maximum of the resonant lobe calculated by fitting the resonant dip with the Lorentz function.

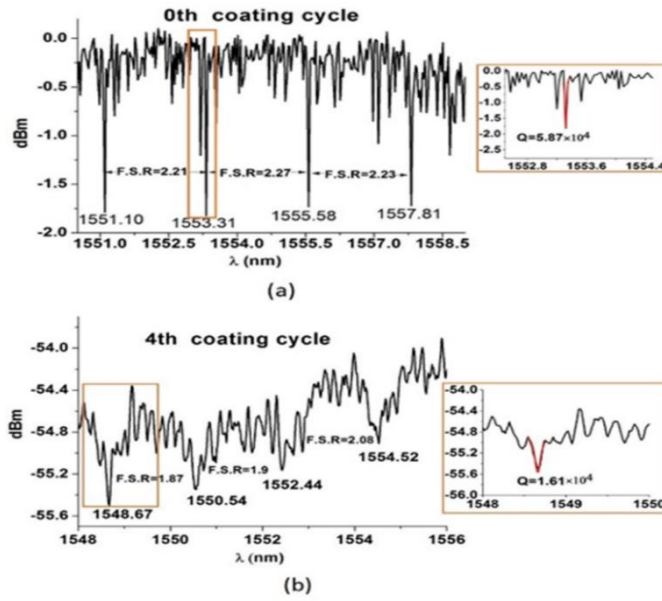


Fig. 3.5 Transmission spectra with the selected WGM resonances: (a) for uncoated silica microsphere with a 260 μm diameter and (b) for the same microsphere after application of four agarose coating layers. Insets illustrate fitting of the selected resonances and estimated Q factors.

Fig. 3.5 (a) and (b) illustrate as an example changes in the quality factor of the microsphere due to application of the agarose coating. The Q for the uncoated microsphere estimated as 5.87×10^4 decreases to $\sim 1.61 \times 10^4$ after four cycles of coating due to the increase in absorption loss within the agarose layer. Fig. 3.6 shows experimentally measured WGM spectra recorded at different humidity levels for the microsphere coated with a single agarose layer. The inset graph illustrates the shift of the selected WGM resonance versus changes in humidity inside the chamber. Any increase in humidity inside the chamber gives rise to the

adsorption of water molecules on the surface of the microsphere; water molecules replace the air inside

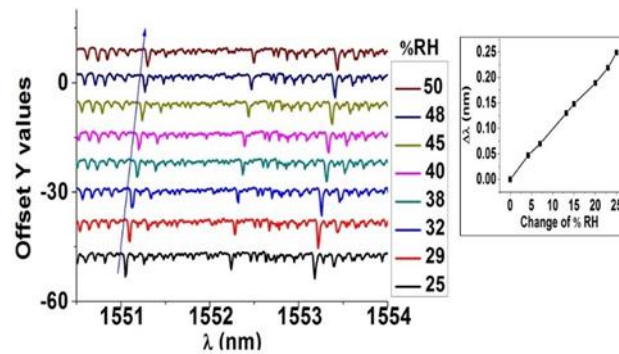


Fig. 3.6 Experimental WGM spectra for the microsphere coated with a single agarose layer recorded at different humidity levels varying from 25 to 50% RH. Inset graph illustrates the WGMs spectral shift versus changes in RH.

the micro pores of the coating layer, which in turn increases the effective RI of the agarose layer. Increase in RH from 25% to 50% at a constant room temperature resulted in a redshift in the WGM spectrum and the value of the spectral shift increased with the increase of the number of agarose coating cycles (the coating thickness) as shown in Fig 3.7 (a). Fig. 3.7 (b) summarizes the experimental data related to RH sensitivity and Q factor values versus the number of coating cycles for all the studied samples.

As expected, the quality factor decreases monotonically with the increase of the coating thickness due to the increased absorption. The measured RH sensitivity, on the other hand, initially grows with the increase of the coating thickness and reaches saturation at higher coating thickness value. This result agrees well with that predicted by the model (Fig. 3.3). Correlation between the experimental and theoretical modeling results allows for an approximate estimate of the agarose layer thickness achieved by the technique described above. Since we have estimated the Q factor of the microsphere after each consecutive coating cycle, it is possible to derive the layer

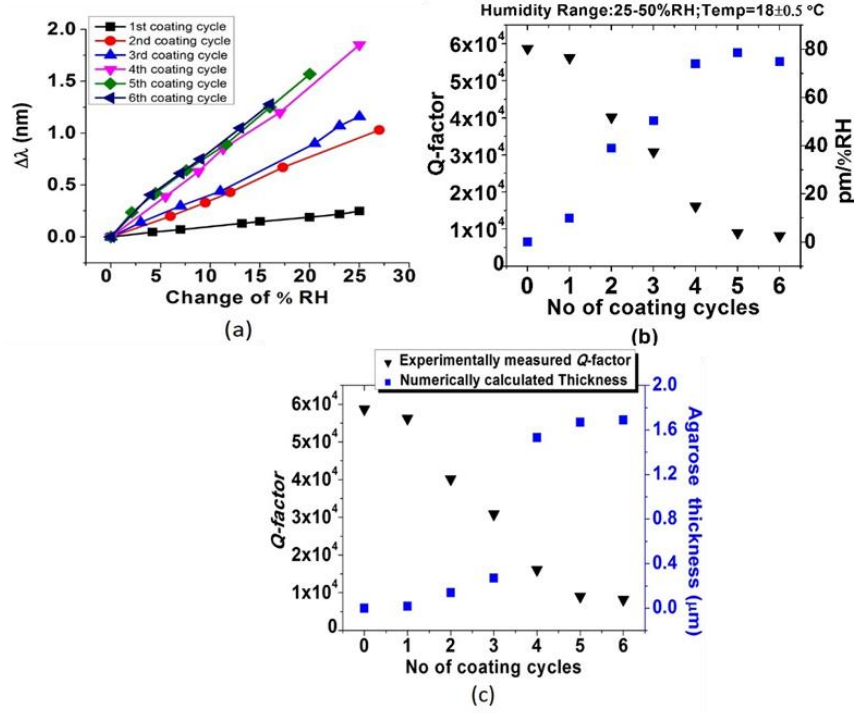


Fig. 3.7 (a) Measured WGM wavelength shift versus RH changes for different thickness of the Agarose coating; (b) Q factor and RH sensitivity from experimental data and (c) experimental Q factor and calculated agarose coating layer thickness as a function of the number of coatings.

thickness by comparing the resonance wavelength difference for every coating cycle, for a certain mode at certain RH and temperature for this, we consider the effective index of the resonance mode, determined by the refractive indices of both silica and agarose, and the energy fraction of the mode distributed in both parts:

$$\frac{1}{Q} \approx \eta_1 \frac{1}{Q_{\text{uncoated}}} + \eta_2 \frac{1}{Q_{\text{coated}}} \quad (3.3)$$

where

$$\eta_1 = \frac{n_1^2 I_1}{n_1^2 I_1 + n_1^2 I_1 + n_1^2 I_1}, \eta_2 = \frac{n_2^2 I_1}{n_1^2 I_1 + n_1^2 I_1 + n_1^2 I_1} \quad (3.4)$$

Assuming the agarose coating is smooth and defect free so that intrinsic loss is negligible, the total Q factor mainly depends on the absorption loss within the agarose layer and can be expressed as $Q_{\text{coated}} \approx 2\pi n_2 / \alpha_2 \lambda_R$, where α_2 is the propagation loss in the agarose coating (the approximate value for the agar

material loss coefficient per unit length is 0.5 dB/cm [10]), n_2 is the coating RI and λ_R is the resonant wavelength. By comparing the results of simulations for the fraction of energy (η_2) within agarose coating with the value of Q factor measured experimentally, the coating thickness corresponding to each number of coating cycles is derived and plotted in Fig. 3.7 (c) along with the experimental Q factor values for each number of the coating cycles. With increasing the number coating cycles of agarose the absorption loss is also increased significantly, as a result the total Q factor decreases [4].

3.5 Conclusion

In this paper, we carried out a theoretical analysis of the sensitivity of the proposed sensor based on perturbation theory and compared the results the simulations with our experimental findings for the coating layers of different thickness. It is concluded, that an increase in the coating thickness initially leads to an increase in the RH sensitivity and then reaches saturation at agarose coating layers with greater thickness ($> 1.6 \mu\text{m}$ in our experiments). The results of the study are useful for the design and optimization of the microsphere sensor parameters for a specified performance.

Author contributions statement

Arun Kumar Mallik developed the numerical simulation model, carried out the experiments and co-wrote the manuscript. Qiang Wu and Gerald Farrell provided suggestions regarding simulation model and methodology. Yuliya Semenova conceived the idea and co-wrote the manuscript.

References:

- [1] S. Arnold, M. Khoshshima, I. Teraoka, S. Holler, and F. Vollmer, “Shift of whispering-gallery modes in microspheres by protein adsorption,” *Opt. Lett.*, vol. 28, no. 4, p. 272, 2003.
- [2] P. Zijlstra, K. L. Van Der Molen, and A. P. Mosk, “Spatial refractive index sensor using whispering gallery modes in an optically trapped microsphere,” *Appl. Phys. Lett.*, 2007.
- [3] N. M. Hanumegowda, C. J. Stica, B. C. Patel, I. White, and X. Fan, “Refractometric sensors based on microsphere resonators,” *Appl. Phys. Lett.*, vol. 87, no. 20, pp. 1–3, 2005.
- [4] N. Lin *et al.*, “Ultrasensitive chemical sensors based on whispering gallery modes in a microsphere coated with zeolite,” *Appl. Opt.*, vol. 49, no. 33, pp. 6463–6471, 2010.
- [5] Q. Ma, L. Huang, Z. Guo, and T. Rossmann, “Whispering-Gallery Mode Silica Micro-Sensors for Temperature and Gas-Phase Concentration Measurements,” in *27th AIAA Aerodynamic Measurement Technology and Ground Testing Conference*, 2010.
- [6] M. L. Gorodetsky, A. A. Savchenkov, and V. S. Ilchenko, “Ultimate Q of optical microsphere resonators,” *Opt. Lett.*, vol. 21, no. 7, pp. 453–455, 1996.
- [7] I. Teraoka and S. Arnold, “Enhancing the sensitivity of a whispering-gallery mode microsphere sensor by a high-refractive-index surface layer,” *J. Opt. Soc. Am. B*, vol. 23, no. 7, p. 1434, 2006.
- [8] A. K. Mallik, D. Liu, V. Kavungal, Q. Wu, G. Farrell, and Y. Semenova, “Agarose coated spherical micro resonator for humidity measurements,” *Opt. Express*, vol. 24, no. 19, pp. 21216–21227, 2016.
- [9] J. C. Knight, G. Cheung, F. Jacques, and T. A. Birks, “Phase-matched excitation of whispering-gallery-mode resonances by a fiber taper,” *Opt. Lett.*, vol. 22, no. 15, p. 1129, 1997.
- [10] J. E. Browne, K. V. Ramnarine, A. J. Watson, and P. R. Hoskins, “Assessment of the acoustic properties of common tissue-mimicking test phantoms,” *Ultrasound Med. Biol.*, vol. 29, no. 7, pp. 1053–1060, 2003.

4. Sensing of low humidity levels with the agarose-coated WGM microresonator

The present chapter extends the study of humidity measurement based on 2.25% wt./vol. agarose coated microsphere resonator to detect low concentrations of water vapor in air. Over 70% of commercially available relative humidity sensors are polymer-based capacitive sensors [1]. They are typically cost-efficient, offer good linearity and stability within the humidity range from 20% to 80%RH. However, in the low humidity range (below 20%RH) capacitive sensors exhibit increasingly nonlinear characteristics, poor sensitivity, large hysteresis and permanent offset values with the decrease of measurable humidity values. Many manufacturers of such sensors often report a drop in sensor's accuracy in a low humidity range (the value of maximum error). In many applications, such as fabrication of pure materials [2], detection of a trace moisture content in natural gas pipelines, drying of solid materials, in meteorology [3], at high altitudes (climate change studies), or in cosmonautical observations [4][5], the measurement of low humidity is essential.

The previous two chapters have largely dealt with measurements of high humidity levels from 30 %RH to 70 %RH using the developed agarose-coated WGM sensor. It should be noted that in chapters 2 and 3 the sensor's resolution and corresponding water detection limit were determined by the interrogation method involving a broadband light source and a standard optical spectrum analyzer. This chapter explores a significantly different interrogation approach, namely frequency detuning method in order to overcome the limitations in the resolution imposed by the optical spectrum analyzer. Detailed experimental demonstration of

the sensor's capability to measure very low concentrations of water in air is presented including studies of the sensor stability, repeatability, hysteresis, response time and temperature dependence. The results and conclusions of this chapter can be applied for enhancing the resolution and detection limits of similar WGM sensors of other measurands.

4.1 A Coated Spherical Microresonator for Measurement of Water Vapor Concentration at PPM Levels in Very Low Humidity Environments⁴

Abstract: This paper presents a novel approach to measurements of low relative humidity (RH) values based on the whispering gallery modes (WGMs) effect in a small silica microsphere coated with a thin layer of agarose hydrogel. The light from a narrow linewidth tunable laser with a few GHz tuning range is launched into an adiabatic tapered fiber, which excites WGMs in the agarose layer via evanescent coupling. Adsorption and desorption of water vapor by the agarose layer in response to changes in ambient humidity lead to changes in the layer's refractive index, which in turn leads to a spectral shift of the WGM resonances. We experimentally demonstrate the WGMs spectral shift over a range of RH values from 1%RH to 25%RH. The proposed sensor displays linear response and is capable of measurement of low concentrations of water vapor (corresponding to about 11.7 ± 0.32 ppm water molecules in air). In addition, the proposed sensor offers the advantages of a very small form factor and good repeatability. Detailed

⁴Arun Kumar Mallik, Gerald Farrell, Dejun Liu, Vishnu Kavungal, Qiang Wu, and Yuliya Semenova, "A coated spherical micro resonator for measurement of water vapor concentration at ppm levels in very low humidity environments," *Journal of Light wave technology*, vol-36,2667 - 2674 (2018).

studies of the sensor stability, cross sensitivity to temperature, response times, and hysteresis are also presented.

Key Terms—Fiber optic sensor, micro-optical devices, optical microresonator, whispering gallery modes.

4.2 Introduction

Whispering gallery mode (WGM) optical micro-resonators are well known for their compactness, ultra-high-quality factors and small mode volumes. A large amount of research has been carried out in the field of physical, chemical, and biological quantities detection using such resonators [6]–[10]. WGMs are high angular momentum modes which can be excited by trapping light inside a dielectric structure with circular symmetry, such as a microsphere, by repeated (near-) total internal reflections. Resonances occur when light retains the same phase after each cycle of propagation. The spectral positions of the WGM resonances are strongly dependent on the geometry of the dielectric resonator (diameter, sphericity), the optical properties of the resonator material and on the refractive index (RI) of the surrounding the resonator medium. This makes such a device suitable for sensing of the surrounding RI or various chemical or biological species if a suitable functional coating is applied to its surface. For example, polymer-coated spherical microresonators have been previously developed for chemical vapor sensing [6], where a change in the polymer RI was induced by adsorption of ammonia molecules from the local environment. There are different approaches to fabrication of dielectric microresonators. Silica microspheres are easily fabricated by surface tension during melting of a silica fiber tip, resulting in a clean, smooth surface with low optical loss and negligible scattering.

Relative humidity (RH) is one of important environmental conditions usually specified for cleanroom operations in the semiconductor, aerospace, food, and pharmaceutical industries. Humidity measurement in industry is often critical because incorrect humidity levels may significantly influence product quality and production efficiency. Fiber-optic humidity sensors have some notable advantages over conventional electronic humidity sensors, such as miniature size, light weight, immunity to electromagnetic interference, water and corrosion resistance and radiation tolerance. Several types of fiber optic humidity sensors have been proposed and demonstrated to date, including those based on fluorescence [11], fiber Bragg gratings [12], interferometry [13] and surface plasmon resonance [14]. Recently we proposed and experimentally demonstrated a humidity sensor based on a spherical silica WGM resonator coated with a layer of hygroscopic agarose layer [15].

Most of the reported sensors have focused on measurements of relatively high levels of humidity, typically above 30 %RH, whereas only a very few studies to date have considered sensing low humidity levels. Measurement of humidity values below 25%RH is important in many industrial applications, for example, in monitoring of industrial gases, where the presence of even low levels of water vapor can cause the formation of aggressive chemicals and corrosion of pipes and containers [16]. Alvarez-Herrero *et al.* proposed a low relative humidity sensor based on a side-polished fiber coupled to a TiO₂ waveguide operating at a wavelength 633 nm with sensitivity of up to 0.5 nm/%RH and an estimated resolution of 0.2% RH in the range from 0 - 15% RH [17]. Ma *et al.* [18] proposed and demonstrated a very low humidity (<10%) WGM sensor coated with a SiO₂

nano-particles, capable of detecting a change of 1 ppm of water molecules but suffering from poor stability of the coating and a significant hysteresis.

In this paper we demonstrate a novel approach to measurements of very low RH values based on the WGMs effect in a small silica microsphere coated with a thin layer of agarose hydrogel. While measurement of humidity in the higher RH region (30% to 70%RH) using an agarose-coated microsphere was previously demonstrated in our earlier work [15], the approach proposed here utilizes a significantly different interrogation method overcoming the limitation of the optical spectrum analyser's (OSA) resolution. This study aims to develop deeper understanding of the influence of different low relative humidity levels on the spectral positions of the WGM resonances and their spectral shifts. The experimental demonstration of the sensor's capability to measure very low concentrations of water in air and the results of studies of stability, repeatability, hysteresis, response time and temperature dependence make the sensor's performance well suited for measurements of low levels of relative humidity.

4.3 Sensing Principle

WGMs in a microsphere can be characterized by a set of integers: n , l , and m , which represent the radial, azimuthal, and polar mode numbers, respectively. When $l = m$ and, $n = 1$, the mode is referred to as a fundamental. A WGM can have either a transverse electric (TE) or transverse magnetic (TM) polarization, which can be selectively excited by controlling the polarization of the coupled light. For simplicity, we only consider the TE polarization. Using a ray optics interpretation, when the light is trapped inside the microsphere, the condition for a WGM resonance is

$$2\pi n_{eff}R = l\lambda_R \quad (4.1)$$

where λ_R is the resonance wavelength, n_{eff} is the effective refractive index of the microsphere and R is its radius. Any fractional change in either refractive index or radius will result in a shift in the WGM resonance wavelength. This shift can be expressed as

$$\frac{\Delta\lambda_R}{\lambda_R} = \frac{\Delta n_{eff}}{n_{eff}} + \frac{\Delta R}{R} \quad (4.2)$$

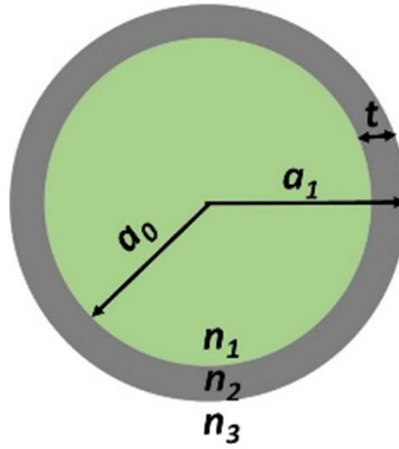


Fig. 4.1 Schematic diagram of the agarose coated microsphere.

Teraoka *et al.* studied the properties of spherical micro-resonators coated with high RI materials and demonstrated that a high RI coating layer enhances the sensitivity of the WGM wavelength shift to both surrounding RI and the resonator's radius. They also described a perturbation theory for the wavelength shift of WGM resonances in a microsphere coated with a high-RI layer [19]–[21]. Later, Nai Lin *et al.* used this approximate model to calculate the thickness-dependent sensitivity of a zeolite coated microsphere to ammonia gas [22]. They demonstrated that the zeolite coating enhances the typically small microsphere surface-to-mass ratio and shows good sensitivity to ammonia. In our studies, we used the same model to determine the resonance conditions of the agarose coated

microsphere. Fig. 4.1 shows a schematic diagram of the sphere of radius a_0 with an agarose coating layer of thickness t . The RIs of the microsphere and the agarose coating are n_1 and n_2 and the RI of the surrounding medium is n_3 .

The characteristic equation for the resonant wavelength λ_R of the WGM with the mode number l is given by [21]:

$$\eta_0 \frac{\chi'_l(n_3ka_1)}{\chi_l(n_3ka_1)} = \frac{B_l\psi'_l(n_2ka_1) + \chi'_l(n_2ka_1)}{B_l\psi_l(n_2ka_1) + \chi_l(n_2ka_1)} \quad (4.3)$$

where

$$B_l = \frac{\eta_1\psi'_l(n_1ka_0)\chi_l(n_2ka_0) - \psi_l(n_1ka_0)\chi'_l(n_2ka_0)}{\psi'_l(n_2ka_0)\psi_l(n_1ka_0) - \eta_1\psi_l(n_2ka_0)\psi'_l(n_1ka_0)} \quad (4.4)$$

where $\eta_1 = \frac{n_1}{n_2}$, for TE mode, $k = 2\pi/\lambda_R$ is the wave number for 1st order radial WGM, $a_l = a_0 + t$ is the total radius of the microsphere including the agarose layer. ψ_l and χ_l are the l_{th} orders of spherical Ricatti-Bessel and spherical Ricatti-Neumann functions, respectively. Each value of l represents multiple values of λ_R that satisfy the characteristic equation. The electric field distribution of the TE WGMs in the coated microsphere can be described as [21]:

$$E_l = \begin{cases} A_l\psi_l(n_1kr) & r < a_0 \\ B_{1l}\psi_l(n_2kr) + B_{2l}\chi_l(n_2kr) & a_0 < r < a_1 \\ C_l\chi_l(n_3kr) & r > a_1 \end{cases} \quad (4.5)$$

where A_l , $B_l = \frac{B_{1l}}{B_{2l}}$ and C_l are constants and can be determined by matching the boundary conditions for a specific azimuthal mode number l .

4.4 Experiments and discussion

4.4.1 Experimental investigation of the humidity response

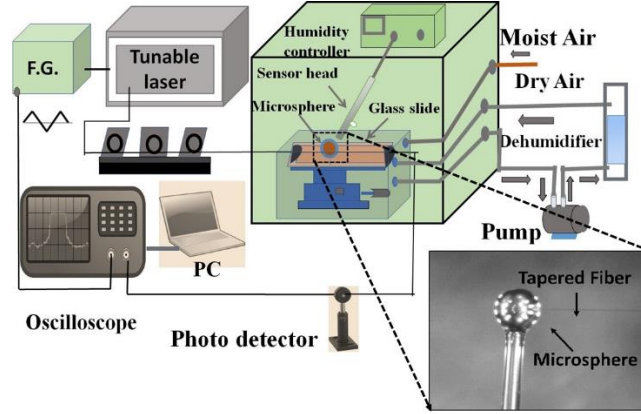


Fig. 4.2 Schematic representation of experimental setup for humidity measurements. The dotted line of the box indicates the location of microsphere and the coupling taper, shown in the inset image.

A schematic representation of the proposed humidity sensor and its characterization setup are shown in Fig. 4.2. First, an adiabatic tapered fiber was fabricated from a standard SMF-28 single mode fiber by using a customized micro heater brushing technique [23]. In our experiment the tapered waist diameter is approximately 3~4 microns.

To improve mechanical stability, the fabricated fiber taper was fixed on a glass slide at a height of ~5 mm from the slide surface using two drops of UV curable epoxy (Norrland). The microsphere for our experiments was fabricated at the tip of a short fiber section (also an SMF-28 fiber). The cleaved end of the fiber was placed inside a fusion splicer (Sumitomo, Type-36). A series of electric arc discharges were applied to the cleaved end of the fiber, so that its tip was gradually softened and became spherical in shape due to surface tension. The diameter of the microsphere measured with an optical microscope was $162 \pm 0.15 \mu\text{m}$. Agarose hydrogel was prepared using white agarose powder from Sigma Aldrich (A6013) by adding 2.25% wt./vol. of the agarose powder into deionized (DI) water followed by stirring at 80 °C temperature until the powder completely dissolved in the DI water. The refractive index of the Agarose gel was measured

as 1.3385 with the help of Abbe refractometer. The microsphere sample was then mounted on a computer- controlled translation stage. The pulling speed of the microsphere from the hot agarose gel was set to 1 mm/sec. The coated microsphere was kept at room temperature for one day before use to allow for drying. For the humidity experiments, the sphere was mounted on an x-y-z translational stage to bring its equator region into direct contact with the tapered fiber to excite WGMs, as shown in Fig. 4.2. The gap between the fiber taper and microsphere may significantly influence the coupling efficiency of the sensor. To ensure the most efficient and stable coupling for our experiment, direct contact between the tapered fiber and the microsphere surface was used to ensure stable coupling conditions.

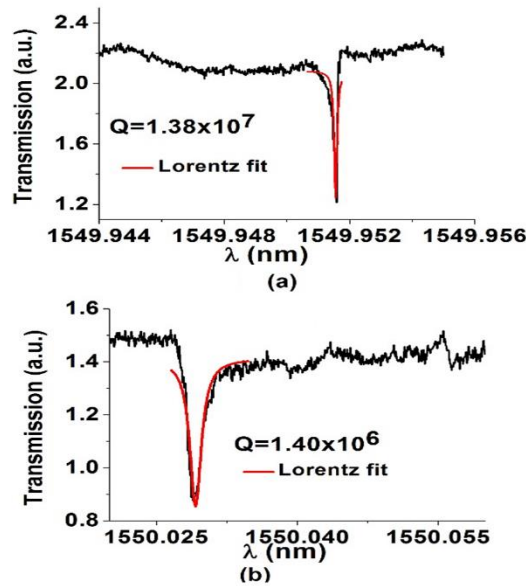


Fig. 4.3 Q factor estimate for the 162 μm diameter silica sphere (a) before and (b) after its coating with agarose.

The characterization of the WGM transmission spectrum of the fiber taper was performed with the help of a tunable external cavity laser (Tunics Plus) with a linewidth of 150 kHz and operating wavelength range of 1490-1640 nm. The wavelength of the tunable laser was swept finely and continuously within 3 GHz

around the selected WGM resonance. A sawtooth current modulation realized by the function generator produced repeated sweeps across the spectral width of the WGM resonance. The output end of the tapered fiber was connected to a photo detector. The transmitted optical power was monitored and measured in real time with a high-speed oscilloscope connected to the photodetector, and the transmitted power data were recorded as a function of time using a customized LabVIEW program. The polarization controller was adjusted manually to achieve maximum light coupling efficiency. Fig. 4.3 (a) illustrates the WGM transmission spectrum of the uncoated microresonator and a Lorentzian fitting of the spectral dip used to estimate the value of its Q factor. The Q factor of the WGM resonance is calculated as 1.38×10^7 using the formula $Q = \lambda_R / \Delta\lambda_{FWHM}$, where λ_R is the resonance wavelength and $\Delta\lambda_{FWHM}$ is the full width at half-maximum of the Lorentz function. After application of the agarose coating, the Q factor of the microsphere decreases to 1.40×10^6 as a result of the increase in loss due to absorption and surface scattering of the coating layer. This result is consistent with that reported in our recent study of the Q factor dependence on the agarose coating thickness [15]. Accurate control of the agarose coating thickness plays an important role in fabrication of the proposed humidity sensor. The sensitivity to humidity increases with the increase of the coating thickness eventually saturating beyond the threshold value, determined by the parameters of the microsphere.

On the other hand, the quality factor of the microsphere decreases with the increase of the coating thickness. This therefore leads to the need to ensure an optimal trade of between the quality factor and the sensitivity of such type of a sensor in real world applications. In addition to the development of the technique for the agarose thickness control, several other issues, such as sensor packaging

and simple interrogation, need to be addressed for the development of practical devices. The corresponding studies are currently on-going. Since the dip coating technique used to apply the agarose hydrogel on the surface of the microsphere does not allow for an accurate control over the layer thickness, we estimated the layer thickness by means of a comparative experiment as follows. A single mode fiber was coated with an agarose layer using the same hydrogel solution and the same technique as applied previously to the microsphere. The coated fiber then was cleaved to improve the visibility of the coating layer and an SEM image of the cross-section was taken. Fig. 4.4 illustrates an SEM image of the cleaved fiber end showing an estimated agarose layer thickness of $3.55\ \mu\text{m}$.

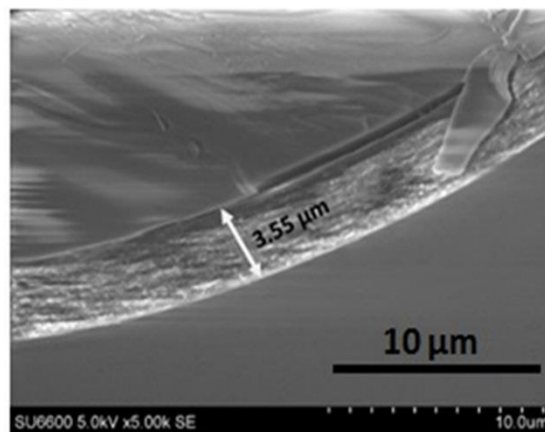


Fig. 4.4 SEM image of the agarose coated-fiber cross section.

To investigate the humidity response of the agarose-coated microsphere resonator, the sensor was placed inside a temperature controlled humidity chamber (ETS5503) with the total volume of 106 liters, shown in Fig. 4.2. The accuracy of the humidity setting within this chamber is $\pm 2\ \%RH$, which was inadequate for studies in a lower humidity range. To overcome this, the sensor sample together with the coupling taper and the humidity controller was placed inside a smaller (5-liter in volume) enclosure which in turn was placed inside the larger humidity chamber as shown in Fig. 4.2. Reducing the effective chamber volume allowed

the use of a dedicated humidity controller to achieve much better setting accuracy. Temperature control was realized by means of the larger chamber. The RH values inside the small chamber were controlled by a calibrated humidity and temperature sensor controller (ETS 520) with a resolution $\pm 0.1\%$ RH. Due to the reduced chamber volume, it was possible to accurately characterize the sensor's response in the relative humidity range between ~ 1 and 25% RH.

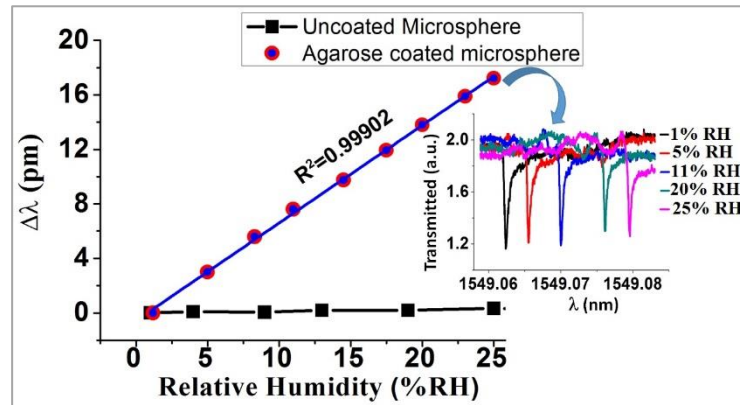


Fig. 4.5 Wavelength shift of the WGM resonance versus RH for the micro-resonator before and after its coating with agarose. Inset graph illustrates the experimental transmission spectra of the coated micro-resonator corresponding to different RH values.

Fig. 4.5 shows a comparison between the experimentally measured humidity responses of the WGM resonance for the same microsphere before and after it was coated with an agarose layer. The proposed sensor's estimated sensitivity is $0.71\text{ pm}/\%RH$ in the humidity range $1\text{--}25\%$ RH at the temperature of $17 \pm 0.2^\circ\text{C}$. Any increase in humidity inside the chamber gives rise to the adsorption of water molecules on the surface of the microsphere. Physically some of the water molecules replace the air inside the micropores of the coating layer due to the hygroscopic nature of the material and capillary forces, which in turn gives rise to an increase in the effective refractive index of the agarose layer. The inset of Fig. 4.5 illustrates measured transmission spectra of the microresonator coated with agarose corresponding to the increasing RH values. As can be seen from the graph,

an increase in RH inside the chamber from 1% to 25% resulted in a redshift of the WGMs by 16.6 pm. The linear regression value of $R^2 = 0.99902$ demonstrates the high linearity of the sensor's response within 1-25% RH range.

It should be noted that although the measurable RH range for the proposed sensor is relatively narrow, since it is limited by the maximum detuning range (3 GHz) of the laser source used in the experiment, studies of the sensor performance at higher RH values confirm that its sensitivity is almost constant (~ 0.71 pm/%RH) in a much broader humidity range of up to 78% RH. Beyond 80% RH its sensitivity increases to 1.32 pm/%RH, possibly due to accumulation of water molecules on the surface of the coating, leading to the non-linear changes of the refractive index.

The simulated radial field distribution for the fundamental WGM of the Agarose coated sphere is shown in Fig. 4.6 (a). From (4.3) and (4.4) it was determined that the nearest possible solution for the fundamental resonant mode corresponding to the experimental value is $l = 463$ and the corresponding WGM resonance wavelength $\lambda_R = 1549.966$ nm. The parameters used in the numerical simulation are as follows: microsphere radius $a_0 = 81.0$ μm , RI of silica $n_1 = 1.447^5$, RI of the Agarose coating $n_2 = 1.3385$, RI of the surrounding air $n_3 = 1.0$ and Agarose layer thickness $t = 3.55$ μm . Using the method described in [17] we estimated that under the above conditions, approximately a 4.37% fraction of the light energy is distributed inside the agarose coating layer [21]. The experimental value of the spectral shift due to humidity was correlated to the numerically calculated change in the RI of the coating without the change in the azimuthal mode number l . Using the model described earlier, we obtained an estimate of the total change in the

⁵ Here the refractive index of silica has taken 1.447 according to the decision by reviewer.

agarose layer RI $\Delta n_{\text{agarose}} = 4.7 \times 10^{-4}$ RIU within the studied humidity range. The plot in Fig. 4.6 (b) shows the calculated data for the agarose layer RI versus relative humidity.

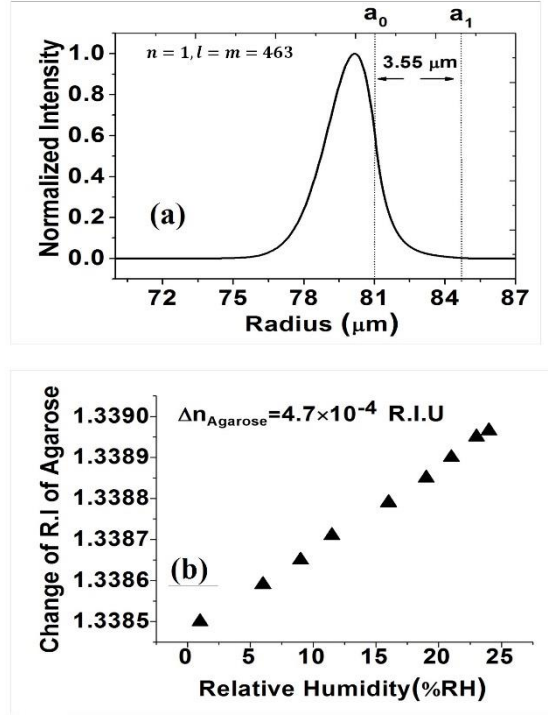


Fig. 4.6 (a) Simulated electric field intensity distributions for the fundamental WGM; (b) change of the Agarose layer RI corresponding to the RH changes (calculated using the theoretical model) with $n = 1, l = m = 463$ with $a_0 = 81.0 \mu\text{m}$ and agarose layer thickness $t = 3.55 \mu\text{m}$.

The detection limit (DL) for a sensor represents the smallest measurable physical parameter change and it can be expressed as $DL = R/S$, where R is the resolution of the sensor and S is its sensitivity. R can be calculated as

$$R = 3 \sqrt{\sigma_N^2 + \sigma_T^2 + \sigma_{SR}^2} \quad (4.6)$$

where σ_N , σ_T , σ_{SR} represent the standard deviations associated with amplitude noise, temperature and detector spectral resolution respectively [24]. We assumed the signal-to-noise ratio of the system is approximately 60 dB, so that σ_N is calculated as 10.47 fm. The standard deviation due to temperature stabilization is taken as $\sigma_T = 10$ fm [20]. The standard deviation associated with the spectral

resolution of the tunable laser whose linewidth of 150 kHz at 1550 nm $\sigma_{SR} = 1.2$ fm [24]. The overall sensor resolution is then calculated as $R = 43.58$ fm. Hence, the DL for the microsphere with a 3.55 μm thick agarose layer is calculated as $6.13 \times 10^{-2} \% \text{RH}$ within the 1-25 %RH humidity range. We estimated the concentration of water molecules inside the 5-liter volume chamber as 190.47 ppm at 1% RH [25]. Hence, the minimum detection limit of water molecules is estimated as 11.7 ppm.

4.4.2 Stability tests

To test the longer-term stability of the sensor's performance, RH measurements were carried out using the same sensor sample after a time interval of one week followed by two more weeks from the initial tests in the same RH range from 1 % to 25 % at a constant temperature of 17 ± 0.2 °C.

It can be seen from Fig. 4.7 (a), that the performance of the sensor is very stable over the two-week period with less than 1% fluctuations from the initial test values, the sensor was tested for repeatability by continuously increasing and decreasing relative humidity inside the chamber from ~12 to 25% RH for several times. Fig. 4.7 (b) illustrates a series of tests where the sensor was exposed to continuously increasing and decreasing relative humidity levels from 12 to 25% RH inside the chamber and the estimated response and recovery times for the sensor. The increase of humidity in the experiment was achieved by natural means whereas the dehumidification was controlled by pumping dry air inside the chamber, so that the latter process took less time within each of the test cycles. As one can see from the figure, the sensor demonstrates good repeatability and a short recovery time in the order of seconds. It should be noted that the response and

recovery times include those of the chamber itself and given the volume of the chamber it is likely that the actual response and recovery times of the sensor are much shorter. Results of studies of the sensor's hysteresis are presented in Fig. 4.7 (c) and 4.7 (d).

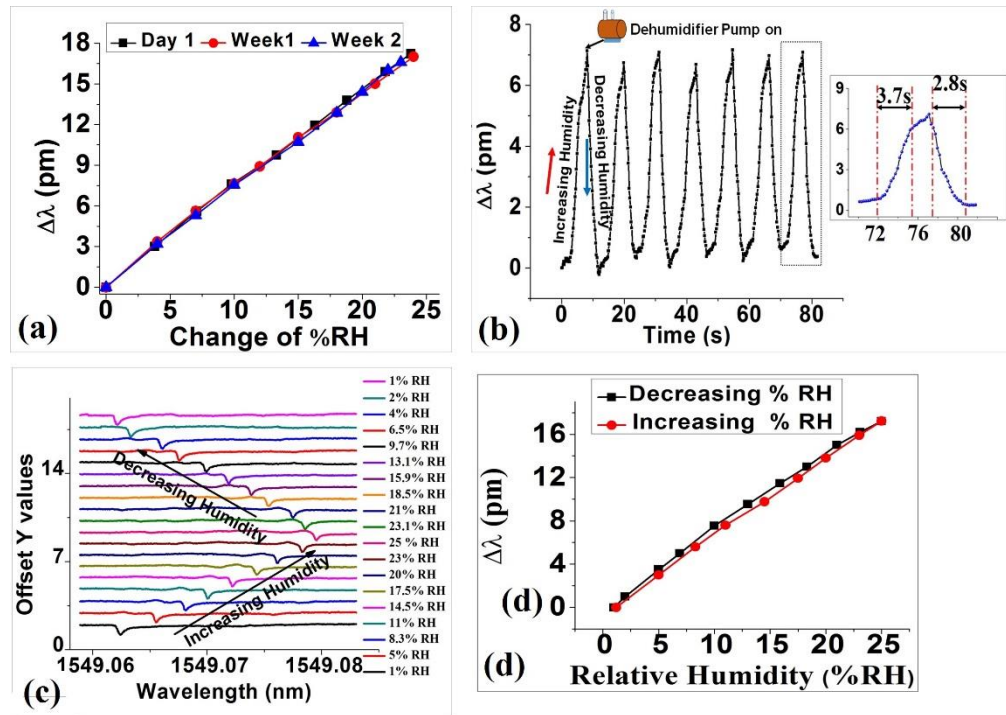


Fig. 4.7 (a) RH responses of the sensor taken within 2 weeks; (b) Studies of repeatability and estimates for response and recovery times; (c) WGM spectra at different RH levels at increasing and decreasing humidity at 17 °C; (d) WGM resonance shift versus RH at 17 °C.

It is clear from the graph that the proposed sensor has a very small hysteresis effect even with a relatively thick 3.55 μm agarose coating. The error due to hysteresis is found to be less than 2% (Fig. 4.7 (d)). This is likely due to the difference between the rates of adsorption and desorption of water molecules at the surface of the agarose layer. This also leads to slight deviation from linearity of the sensor's response observed in Fig. 4.7 (d). It is clear from the graph that the proposed sensor has very small hysteresis. It should be noted that both response and relaxation times and hysteresis properties for the proposed sensor are

significantly better than those reported in [18][26] for a WGM microsphere resonator in a low humidity range.

4.4.3 Response time

The sensor's response time was evaluated in detail. The response time is defined as the time it takes for the wavelength shift to reach 90% of its maximum value when the RH is increased from 0% to a target RH value. The temperature of both chambers was maintained constant and monitored by the ETS 520 controller. Several experimental techniques have been proposed to determine the response time of humidity sensors, with the most popular but simple method based on monitoring of a rapid human breathing cycle [27], [28]. Since our experiments concerned the sensor's performance in the low RH range, this technique was not applicable in our case, since human breath is associated with much higher than 25% RH levels of humidity.

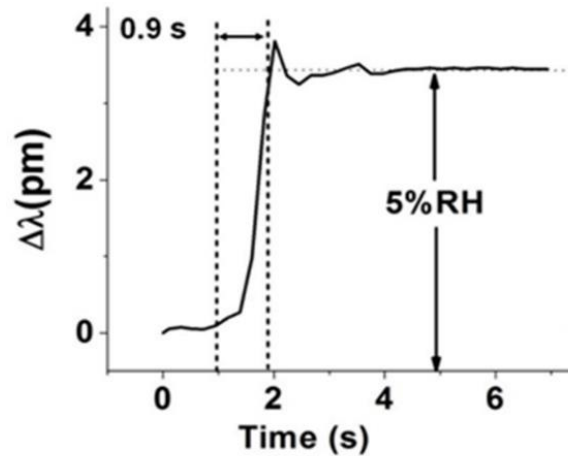


Fig. 4.8 Temporal response of the sensor.

The response time calculated from the experiments carried out in the humidity chamber was approximately 3.7 second as shown in Fig. 4.7 (b). It should be noted however that our humidity controlled chamber also is not ideal for studying

the response time of the sensor because the flows of the humid/dry air in and out of the chamber are very slow. Therefore, in this study we used the following simple method to estimate the response time of the sensor. The difference between the RH settings in both the large and small chambers was maintained constant at 5% RH. The sensor's response was monitored continuously while the cover of the small chamber was rapidly removed allowing the RH levels of both small and big chambers to equalize. The results of this experiment are presented in Fig. 4.8

The sensor's temporal response was plotted by processing a series of digitized oscilloscope images (1000 data points per frame) using a PC to determine the position of the WGM dip corresponding to each of the snapshot images. The frequency of the snapshots was limited to ~5 frames/sec by the speed of transfer and processing of each data set. The estimated response time of the agarose-coated $162 \pm 0.15 \mu\text{m}$ diameter microsphere from Fig. 4.8 was calculated as 0.9 s.

4.4.4 Temperature effects

The influence of temperature on the RH sensor performance was investigated in the range from 20°C to 36°C at three different humidity levels, i.e. 10 %RH, 15 %RH and 25 %RH, set inside the smaller chamber. The lower temperature value of the studied range is determined by the room temperature since the humidity chamber does not have a means of cooling, while the upper temperature limit of 36°C is determined by the gelling temperature of agarose (36°C - 42°C). As the temperature of the larger chamber was gradually raised from 20°C to 36°C in small steps, the wavelength shift of the WGM spectrum was recorded using a high speed digital oscilloscope connected to a PC. The overall temperature response for the agarose coated microsphere is shown in Fig. 4.9 (a). The

estimated temperature sensitivity values calculated from the Fig. 4.9 (a) are 2.3 pm/°C at 25 %RH, 2.25 pm/°C at 15 %RH and 2.5 pm/°C at 10 % RH. We estimated the linearity error of temperature was approximately 3.5 %. The temperature sensitivities at higher RH levels (15 and 25%) are very similar; but the sensor displays slightly higher temperature response at 10% RH. One possible explanation for the observed higher temperature sensitivity at 10 %RH humidity is that because at lower levels of humidity the pores of the agarose layer are mostly filled with air, it results in a greater refractive index contrast between the agarose layer and air, and thus greater sensitivity to any changes in the surrounding refractive index [29].

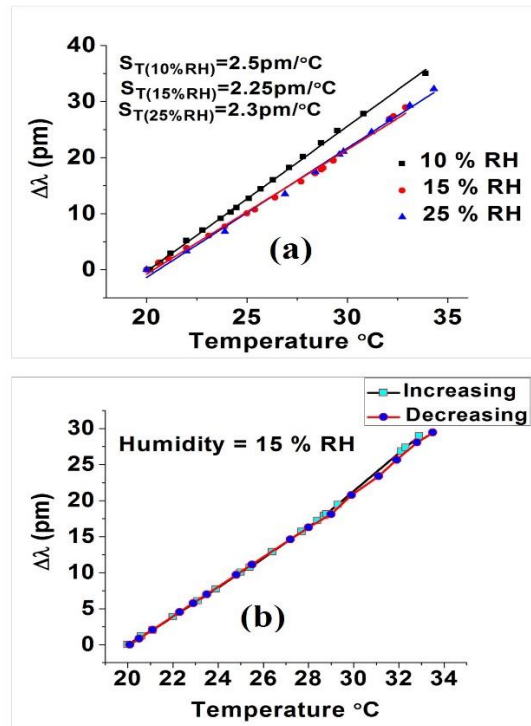


Fig. 4.9 Resonant wavelength shift versus temperature for the $162 \pm 0.15 \mu\text{m}$ microsphere coated with 2.25% wt./vol. agarose solution: (a) 10% RH, 15 % RH and 25% RH; (b) Hysteresis of temperature response at 15% RH.

While the cross-sensitivity of the proposed sensor to temperature at low humidity is quite high it should be noted that our proposed sensor has several orders of magnitude smaller temperature cross-sensitivity compared with some other types

of fiber optic humidity sensors, such as long period gratings [30] or fiber Bragg grating-based humidity sensors [31]. Fig. 4.9 (b) illustrates the temperature increasing and decreasing responses of the same sensor sample at 15% RH. It is found the responses are in a good agreement with each other with negligible hysteresis.

4.5 Conclusion

A novel approach to measure ultra-low concentrations of water vapor, corresponding to low RH values, using an agarose coated microsphere resonator based on the WGMs effect has been proposed and experimentally demonstrated in the humidity range from 1 to 25% RH. The WGMs are excited in a silica microsphere dip-coated with an agarose gel by evanescent coupling to an adiabatic tapered fiber and observed in the transmission spectrum of the taper. The spectral shift of the WGM resonances is induced by the adsorption or desorption of water molecules at the microsphere surface, resulting in a change of RI of the agarose coating. The demonstrated experimentally sensitivity of the sensor is 0.71 pm/%RH with an estimated detection limit of 11.7 ± 0.32 ppm after considering 2% hysteresis error and 3.5 % linear error of temperature using the present setup, which we believe is the highest DL for water vapor detection reported to date. The proposed sensor is very compact and demonstrates good repeatability and stability. The response time of the sensor is 0.9 s, which is very promising for applications where a fast response is required at low levels of humidity. The cross sensitivity to temperature at different humidity levels is investigated. The sensor's temperature sensitivity is almost constant above 15% RH. A more detailed study of the proposed sensor is currently ongoing with the aim to improve the sensing time as

well as optimize the coating thickness, which determines the sensitivity and dynamic range.

Author contributions statement

Arun Kumar Mallik designed and performed the experiments, carried out numerical simulations, analyzed the data and co-wrote the manuscript. Dejun Liu and Vishnu Kavungal helped in preparation of the agarose solution and fabrication of the tapered fiber. Yuliya Semenova supervised the project and revised the manuscript in consultation with Gerald Farrell and Qiang Wu.

References

- [1] Z. M. Rittersma, “Recent achievements in miniaturised humidity sensors - A review of transduction techniques,” *Sensors and Actuators, A: Physical.*, vol. 96, no. 2-3, pp. 196-210, 2002.
- [2] T. Hübert, C. Tiebe, M. Detjens, and J. Majewski, “On-site calibration system for trace humidity sensors,” *Meas. J. Int. Meas. Confed.*, vol. 91, pp. 251-257, 2016.
- [3] P. R. Story, D. W. Galipeau, and R. D. Mileham, “A study of low-cost sensors for measuring low relative humidity,” *Sensors Actuators B. Chem.*, vol. 25, no-1-3, pp. 681-685, 1995.
- [4] A.-M. Harri *et al.*, “Mars Science Laboratory relative humidity observations: Initial results,” *J. Geophys. Res. Planets*, vol. 119, no. 9, pp. 2132-2147, 2014.
- [5] K. Rübner, D. Balköse, and E. Robens, “Methods of humidity determination Part II: Determination of material humidity,” in *Journal of Thermal Analysis and Calorimetry*, vol. 94, pp. 675, 2008.
- [6] N. M. Hanumegowda, C. J. Stica, B. C. Patel, I. White, and X. Fan, “Refractometric sensors based on microsphere resonators,” *Appl. Phys. Lett.*, vol. 87, no. 20, pp. 1–3, 2005.
- [7] V. S. Ilchenko *et al.*, “Strain-tunable high-Q optical microsphere resonator,” *Opt. Commun.*, vol. 145, no. 1-6, pp. 86-90, 1998.
- [8] T. Ioppolo, M. Kozhevnikov, M. V. Otugen, and V. Sheverev, “Performance of a Whispering Gallery Mode Resonator-Based Micro-Optical Force Sensor,” in *45th AIAA Aerospace Sciences Meeting and Exhibit*, 2007.
- [9] C. Y. Chao, W. Fung, and L. J. Guo, “Polymer microring resonators for biochemical sensing applications,” *IEEE J. Sel. Top. Quantum Electron.*, vol. 12, no. 1, pp. 134-142, 2006.
- [10] F. Vollmer, D. Braun, A. Libchaber, M. Khoshshima, I. Teraoka, and S. Arnold, “Protein detection by optical shift of a resonant microcavity,” *Appl. Phys. Lett.*, vol. 80, no. 21, pp. 4057–4059, 2002.
- [11] H. E. Posch and O. S. Wolfbeis, “Optical sensors, 13: fibre-optic humidity sensor based on fluorescence quenching,” *Sensors and Actuators*, vol. 15,

no. 1, pp. 77–83, 1988.

- [12] F. J. Arregui, I. R. Matías, K. L. Cooper, and R. O. Claus, “Simultaneous measurement of humidity and temperature by combining a reflective intensity-based optical fiber sensor and a fiber bragg grating,” *IEEE Sens. J.*, vol. 2, no. 5, pp. 482–487, 2002.
- [13] J. M. Corres, I. R. Matias, M. Hernaez, J. Bravo, and F. J. Arregui, “Optical Fiber Humidity Sensors Using Nanostructured Coatings of SiO₂ Nanoparticles,” *IEEE Sens. J.*, vol. 8, no. 3, pp. 281–285, 2008.
- [14] M. Hernaez, C. R. Zamarreno, I. R. Matias, and F. J. Arregui, “Optical fiber humidity sensor based on surface plasmon resonance in the infra-red region,” in *Sensors & Their Applications Xv*, vol. 178, 012019, 2009.
- [15] A. K. Mallik, D. Liu, V. Kavungal, Q. Wu, G. Farrell, and Y. Semenova, “Agarose coated spherical micro resonator for humidity measurements,” *Opt. Express*, vol. 24, no. 19, pp. 21216–21227, 2016.
- [16] J. Majewski, “Polymer-based sensors for measurement of low humidity in air and industrial gases,” no. 8, pp. 74–77, 2016.
- [17] A. Alvarez-Herrero, H. Guerrero, and D. Levy, “High-Sensitivity Sensor of Low Relative Humidity Based on Overlay on Side-Polished Fibers,” *IEEE Sens. J.*, vol. 4, no. 1, pp. 52–56, 2004.
- [18] M. Qiulin, L. Huang, Z. Guo, and T. Rossmann, “Spectral shift response of optical whispering-gallery modes due to water vapor adsorption and desorption,” *Meas. Sci. Technol.*, vol. 21, no. 11, 115206, 2010.
- [19] J. C. Knight, G. Cheung, F. Jacques, and T. A. Birks, “Phase-matched excitation of whispering-gallery-mode resonances by a fiber taper,” *Opt. Lett.*, vol. 22, no. 15, pp. 1129, 1997.
- [20] I. Teraoka, S. Arnold, and F. Vollmer, “Perturbation approach to resonance shifts of whispering-gallery modes in a dielectric microsphere as a probe of a surrounding medium,” *J. Opt. Soc. Am. B*, vol. 20, no. 9, pp. 1937-1946, 2003.
- [21] I. Teraoka and S. Arnold, “Enhancing the sensitivity of a whispering-gallery mode microsphere sensor by a high-refractive-index surface layer,” *J. Opt. Soc. Am. B*, vol. 23, no. 7, pp. 1434, 2006.
- [22] N. Lin *et al.*, “Ultrasensitive chemical sensors based on whispering gallery modes in a microsphere coated with zeolite,” *Appl. Opt.*, vol. 49, no. 33, pp.

6463–6471, 2010.

- [23] G. Brambilla, V. Finazzi, and D. Richardson, “Ultra-low-loss optical fiber nanotapers,” *Opt. Express*, vol. 12, no. 10, pp. 2258–2263, 2004.
- [24] I. M. White and X. Fan, “On the performance quantification of resonant refractive index sensors,” *Opt. Express*, vol. 16, no. 2, pp. 1020, 2008.
- [25] “The Rotronic Humidity Handbook, Rotronic Instrument corp.,” www.rotronic-usa.com.
- [26] Q. Ma, L. Huang, Z. Guo, and T. Rossmann, “Whispering-Gallery Mode Silica Micro-Sensors for Temperature and Gas-Phase Concentration Measurements,” in *27th AIAA Aerodynamic Measurement Technology and Ground Testing Conference*, 2010.
- [27] J. Mathew, Y. Semenova, and G. Farrell, “Experimental demonstration of a high-sensitivity humidity sensor based on an Agarose-coated transmission-type photonic crystal fiber interferometer,” *Appl. Opt.*, vol. 52, no. 16, pp. 3884–3890, 2013.
- [28] F. J. Arregui, Z. Ciaurriz, M. Oneca, and I. R. Matías, “An experimental study about hydrogels for the fabrication of optical fiber humidity sensors,” *Sensors Actuators B Chem.*, vol. 96, no. 1–2, pp. 165–172, 2003.
- [29] R. Gao, Y. Jiang, and W. Ding, “Agarose gel filled temperature-insensitive photonic crystal fibers humidity sensor based on the tunable coupling ratio,” *Sensors Actuators, B Chem.*, vol. 195, pp. 313–319, 2014.
- [30] L. Wang, Y. Liu, M. Zhang, D. Tu, X. Mao, and Y. Liao, “A relative humidity sensor using a hydrogel-coated long period grating,” *Meas. Sci. Technol.*, vol. 18, no. 10, pp. 3131–3134, 2007.
- [31] S. F. H. Correia *et al.*, “Optical fiber relative humidity sensor based on a FBG with a di-ureasil coating,” *Sensors (Switzerland)*, vol. 12, no. 7, pp. 8847–8860, 2012.

5. Spherical microresonator for ammonia sensing

Ammonia (NH_3) is a highly toxic and corrosive substance that can be found both naturally and produced by humans in various fertilizers, refrigeration systems, during manufacturing of dyes, drugs, synthetic fibers, etc. [1][2]. The lower limit of human NH_3 perception by smell is around 50 ppm [2]. Increasing the concentration of ammonia in air causes severe adverse effects in the human respiratory system, eyes and skin. Ammonia gas is also considered to be one of the major environmental pollutants. There is always a need for a rapid detection of ammonia in the refrigeration industry to prevent the leakage in large scale refrigerating systems. Ammonia gas in ultra-low concentrations also known to cause changes in chemical properties of deep ultra-violet photoresists, important in the semiconductor industry [3].

Stability, selectivity to ammonia, fast response and high measurement accuracy are some of the requirements that modern commercial ammonia sensors have been facing. Very few sensors have been reported to detect ammonia gas concentrations at ppb levels. It is therefore urgent and important to develop a miniature ammonia sensor that offers a rapid detection, repeatability, ultra-high sensitivity and long term stability with high resolution.

This chapter focuses on the development of such a sensor based on a spherical WGM micro resonator. A silica microsphere functionalized with a layer of sol gel silica has been shown to offer an ultra-high sensitivity and selectivity to ammonia in air. Two separate interrogation methods have been investigated to measure the concentrations of ammonia in air from low to ultra-low levels. The interrogation

method based on a broadband light source and optical spectrum analyzer offers a large dynamic range with lower measurement resolution, while the frequency detuning method is employed to measure ultra-low concentrations of ammonia within a relatively narrow range of concentrations. Synthesis of sol gel silica is also discussed in detail. The chapter also presents the results of investigations of the proposed sensor stability, hysteresis, selectivity and its response to relative humidity and temperature. The sensor's response time as well as detection limit have also been studied and analyzed.

5.1 Silica gel coated spherical micro resonator for ultra-high sensitivity detection of ammonia gas concentration in air⁶

Abstract: A silica gel coated microsphere resonator is proposed and experimentally demonstrated for measurements of ammonia (NH₃) concentration in air with ultra-high sensitivity. The optical properties of the porous silica gel layer change when it is exposed to low (parts per million (ppm)) and even ultra-low (parts per billion (ppb)) concentrations of ammonia vapor, leading to a spectral shift of the WGM resonances in the transmission spectrum of the fiber taper. The experimentally demonstrated sensitivity of the proposed sensor to ammonia is estimated as 34.46 pm/ppm in the low ammonia concentrations range from 4 ppm to 30 ppm using an optical spectrum analyser (OSA), and as 800 pm/ppm in the ultra-low range of ammonia concentrations from 2.5 ppb to 12 ppb using the frequency detuning method, resulting in the lowest detection limit (by

⁶Arun Kumar Mallik, Gerald Farrell, Dejun Liu, Vishnu Kavungal, Qiang Wu, and Yuliya Semenova, "Silica gel coated spherical micro resonator for ultra-high sensitivity detection of ammonia gas concentration in air," Scientific Reports, 8, 1620 (2018).

two orders of magnitude) reported to date equal to 0.16 ppb of ammonia in air. In addition, the sensor exhibits excellent selectivity to ammonia and very fast response and recovery times measured at 1.5 and 3.6 seconds, respectively. Other attractive features of the proposed sensor are its compact nature, simplicity of fabrication and potentially low cost.

5.2 Introduction

Ammonia (NH_3) and its compounds are used in the production of liquid fertilizers, in refrigeration, during manufacturing of dyes, drugs, synthetic fibers, in food processing and biological sciences [2],[3]. At room temperature, ammonia is a colorless, highly corrosive and toxic gas with pungent odor. Exposure to high concentrations of ammonia in air causes a burning sensation in the nose, throat and respiratory track. The safe limit of NH_3 concentration that people may work in for more than 8 hours is set to be 25 ppm and 35 ppm for a shorter duration. These thresholds are below the detection limit of a human's sense of smell and therefore some means to sense and also quantify ammonia concentration in the air is needed. Furthermore, sensors with detection thresholds in the order of ppb are very valuable. In the semiconductor industry for example, deep ultraviolet photo resist is extremely sensitive to the presence of airborne molecular gases inside a clean room, where even the presence of ammonia with a concentration of only 17 ppb for 10 minutes will deteriorate the performance of the lithography process[3]. Optical fiber based sensors have some unique advantages over their electrical equivalents such as remote and real time monitoring, immunity to various sources of disturbances e.g. electromagnetic interference, radioactivity and explosive environments which makes them a cost-effective, flexible and inert sensing

solution. Many optical fiber based ammonia sensors have been reported to date, based on different operating principles and with different sensitivities. A surface plasmon resonance based fiber optic ammonia gas sensor has been proposed in [4], [5]. Adolfo *et al.* successfully demonstrated sensing of ammonia concentrations of up to 100 ppm using bromocresol, a pH indicator, attached to an optical fiber [6]. Cao *et al.* also used bromocresol polymer to generate an evanescent field in a U-shaped plastic clad silica multi-mode fiber to sense ammonia [7].

Many of the existing ammonia sensors have been designed to realize detection in the order of ppm, but those are unable to reach ppb level detection, required by some applications. Sensors based on the whispering gallery mode (WGM) effect in spherical microresonators have found many applications for very sensitive detection of molecular adsorption [8], refractive index [9], temperature [10] and gas concentration [11] due to their ultra-high quality factors (Q), low absorption losses and inexpensive fabrication.

WGMs are high angular momentum modes which can be excited by trapping light propagating inside a dielectric structure with a circular symmetry, such as a microsphere, by repeated total internal reflections. The spectral positions of WGM resonances are strongly dependent on the geometry of the dielectric resonator (diameter, sphericity), the optical properties of the resonator material and also on the refractive index (RI) of surrounding the resonator medium. WGMs in a silica micro sphere can be excited by trapping a portion of evanescent field propagating through a fiber taper and the changes in the surrounding RI can be measured by monitoring either reflected or transmitted light through the taper. Recently, we proposed and demonstrated a highly sensitive relative humidity (RH) sensor based

on the similar microsphere coated with a thin layer of agarose hydrogel prepared from a 2.25 % wt./vol. agarose solution [12].

In this paper, we propose and experimentally demonstrate a silica gel coated microsphere for the detection of ammonia vapor concentration in air at a constant relative humidity. The silica microsphere is fabricated at the tip of a short length of SMF-28 fiber and a single layer of silica gel is deposited on the surface of the microsphere by dip coating. WGMs in the microsphere are excited by evanescent coupling of light using an adiabatic fiber taper with a waist diameter of approximately 3-4 μm . Exposure of the silica gel coating layer to ammonia vapor results in changes in its refractive index leading to the corresponding shifts of the WGM resonances. A detailed investigation of the sensor performance has been carried out by its exposure to low concentrations as well as ultra-low concentrations of ammonia vapor inside the test chamber at constant humidity 50 %RH and constant temperature 23 °C conditions.

5.3 Methods

5.3.1 Preparation of porous silica gel

Silica gel in laboratory conditions is typically prepared by sol-gel polymerization of tetra-ethylorthosilicate (TEOS) under hydrolytic conditions using either acids or base catalysis. For our experiments, tetraethylorthosilicate (TEOS), ethyl alcohol and sulphuric acid (H_2SO_4) were purchased from Sigma Aldrich and were used without any further purification. 10 mL of TEOS and 5 mL of ethanol were mixed in a 250 mL measuring flask and kept in a magnetic stirrer for 20 minutes at room temperature. 1.5 mL of 0.1 mol/L H_2SO_4 was poured into the TEOS solution in

the flask under constant stirring. The solution turned to a gel form after 3 hours of continuous stirring.

5.3.2 Microsphere resonator fabrication

The microsphere used for our experiments was fabricated at the tip of a standard single mode fiber by discharging a series of electric arcs. The fiber tip was gradually melted by the arcs and assumed a spherical shape due to surface tension. The sphere diameter was controlled by the number of arcs induced on the tip of the fiber. The fabricated microsphere was then dipped into the silica gel and pulled out very fast. Coated with the porous silica gel, the microsphere was then dried at room temperature for 24 hours. Fig.5.1 shows a scanning electron microscope (SEM) image of the coated microsphere used in our experiment. From Fig.5.1 the sphere diameter is estimated as 282 μm . To allow for coupling of light to and from the microsphere, an adiabatic tapered fiber was fabricated using a customized micro heater brushing technique [13]. In our experiment the tapered waist diameter was approximately 3-4 microns. To improve mechanical stability, the fabricated fiber taper was placed in direct contact with the microsphere and fixed on a glass slide at a height of ~ 5 mm from the slide surface using two drops of UV curable epoxy (Norland).

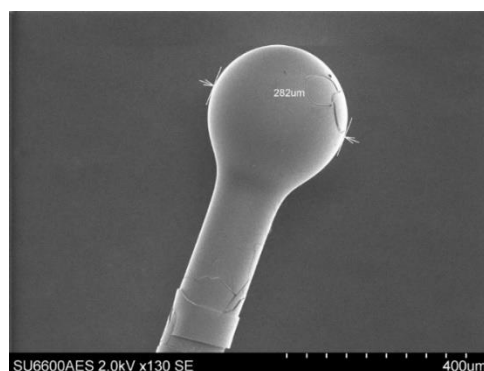


Fig. 5.1 SEM image of porous silica coated microsphere used in experiment

Ammonia, humidity and other gases sensing experiments were carried out in a humidity- and temperature-controlled chamber with a volume of 106 L. In general, for gas vapour sensing experiments, the control of the vapor concentration was achieved by injecting a certain volume of liquid analyte into a test chamber with a known volume using a micro syringe. The resulting concentration of the vapor is calculated using the following equation [14].

$$C_{ppm} = \frac{V_{\mu L} \times D_{gmL^{-1}}}{M_{gmol^{-1}} V_{mL}} \times 2.42 \times 10^7 \quad (5.1)$$

where, C_{ppm} is the required vapor concentration, $V_{\mu L}$ is the volume of the liquid analyte, $D_{gmL^{-1}}$ is the density of the liquid, V_{mL} is the volume of the chamber and $M_{gmol^{-1}}$ is the molecular weight of the liquid analyte. All the subscripts are the corresponding units of measurement. The temperature and humidity inside the test chamber were maintained constant at 23 °C and 50 %RH, respectively throughout the ammonia and volatile organic compounds (VOCs) experiments.

5.3.3 Two methods for characterization of the sensor performance.

The characterization of the proposed ammonia gas sensor was carried out using two different interrogation methods. In one of the methods we used a superluminescent (SLD) light source (Thorlabs S5FC1005S), a polarization controller and an optical spectrum analyzer (OSA, Advantest Q8384) to measure the total WGM resonance wavelength shift against the wide range of low concentrations of ammonia from 4 ppm to 30 ppm as shown in Fig. 5.2 (a). For concentrations below 4 ppm, a frequency detuning method was used, with the corresponding experimental setup shown in Fig. 5.2 (b), consisting of an external

cavity laser (Tunics Plus, linewidth 300 kHz, with operating wavelength range 1490-1640 nm) and a photo detector connected to high speed digital oscilloscope (Agilent MSOX-2022A) to record the WGM spectrum. In the frequency detuning method the tunable laser was swept finely and continuously within 3 GHz across the selected WGM resonance with the help of a sawtooth current modulation realized by the function generator (F.G). The former interrogation method has a wider dynamic range for measurements with a limited resolution while the latter (frequency detuning) method allows for a higher measurements resolution in a narrow range.

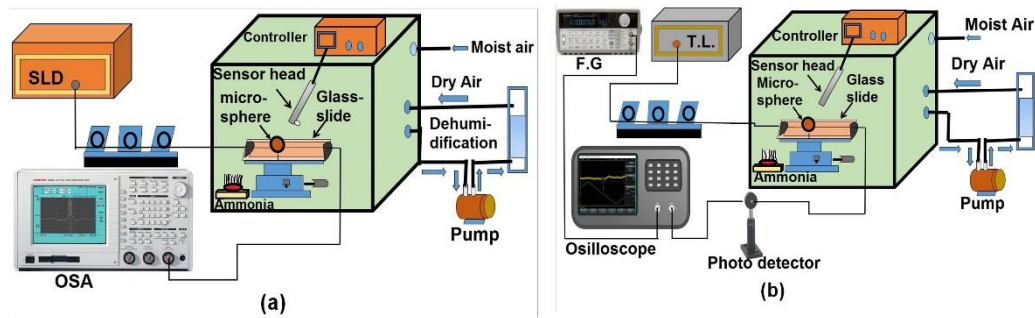


Fig. 5.2 Experimental setup for ammonia sensing using (a) OSA interrogation system; (b) frequency detuning method.

In both experimental setups, the sensor sample a coated microsphere, was mounted on an XYZ nano-positioning stage and then slowly brought in contact with the tapered fiber inside the humidity chamber as shown in Fig. 5.2. In both cases the temperature and moisture inside the chamber were controlled by the chamber's controller system (ETS 5503).

5.4 Results

5.4.1 Experimental investigation of the sensor in a wider range of low (>4-30 ppm) ammonia concentrations using an OSA

In the optical setup shown in Fig.5.2 (a) the light from the broadband SLD was launched into one of the ends of the fiber taper and the corresponding transmission spectrum was observed at the output end by means of an OSA. The wavelength resolution of the OSA was 10 pm. The microsphere was gradually and carefully brought in direct contact with the tapered fiber until the WGM resonances were clearly observed in the transmission spectrum of the fiber taper. The input light polarization was adjusted using a manual polarization controller to achieve maximum light coupling efficiency.

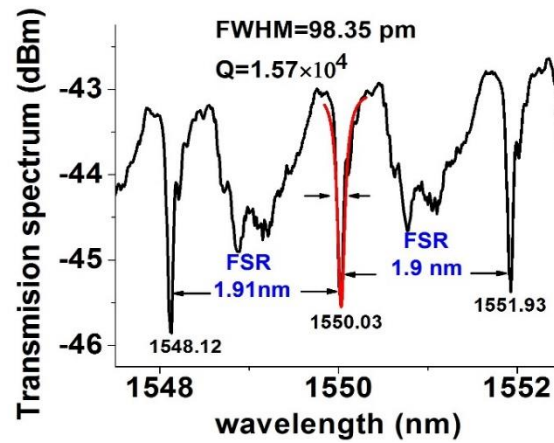


Fig. 5.3 Transmission spectrum recorded by the OSA for a coated microsphere with a 282 μm diameter

Fig. 5.3 illustrates a typical transmission spectrum recorded with the OSA. As can be seen from Fig. 3, periodic transmission dips with a quality factor (Q) in the order of 10^4 and the free spectral range (F.S.R) of ~ 1.9 nm can be clearly observed.

To investigate the response of the porous silica coated microsphere to ammonia vapors with different concentrations, small amounts of ammonium hydroxide (NH_4OH) liquid were injected into and removed from the gas chamber in sequence, in order to create several low concentrations corresponding to 4 ppm,

8 ppm, 12 ppm, 22 ppm and 30 ppm of ammonia in air. As shown in Fig. 5.4 (a), the WGM resonant wavelengths experience a red shift when the sensor is exposed to ammonia vapors. The spectral response of the sensor to an 8 ppm concentration of ammonia is summarized in Fig. 5.4 (b), where multiple WGM spectra are compiled on a single graph to illustrate their shift in time after the sensor was exposed to the ammonia vapor.

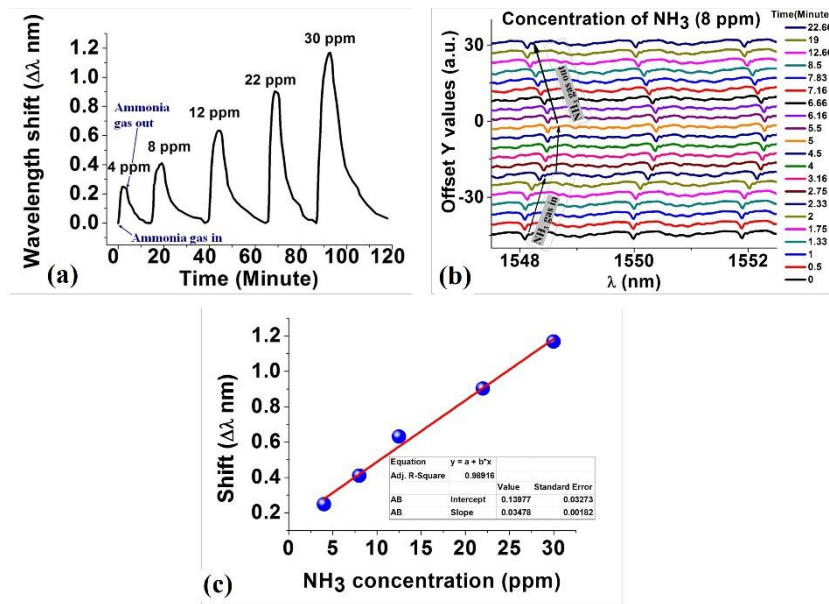


Fig. 5.4 (a) WGM spectral shift during sensor's exposure to different concentrations of NH_3 ranging from 4 ppm to 30 ppm. (b) Sensor's temporal response to the ammonia concentration of 8 ppm. Inset figure illustrates the wavelength shift for a selected WGM resonance in response to exposure to 8 ppm concentration of ammonia. (c) Sensor's response as a function of NH_3 concentration.

The main reason behind the shift is a change in the effective refractive index of the silica coating when NH_3 molecules are adsorbed on the surface of the sphere. A higher concentration of NH_3 leads to a larger red shift in the WGM spectrum. When the gas is removed from the chamber by opening an exhaust valve, the resonance wavelengths recover to their original positions. The maximum spectral shift of the WGM resonances in response to a certain ammonia concentration is plotted as a function of ammonia concentration in Fig. 5.4 (c) and is found to be close to linear with sensitivity estimated as 34.8 pm/ppm. It is important to note

that the measured time response is not that of the sensor alone but also includes the time taken for the vapor concentration to stabilize inside the chamber.

5.4.2 Experimental investigation of the sensor in the ultra-low ammonia concentrations range using frequency detuning method:

The output spectrum of the proposed sensor has a high Q factor, typical for many WGM based sensors, potentially providing the capability to detect ultra-small concentrations of vapor phase ammonia inside the chamber. However the relatively low resolution of the OSA employed in the experiments described above means that we cannot fully utilise the high Q factor available and in turn this limits the ability of the sensor to measure ultra-small concentrations of ammonia vapor. To overcome this issue many researchers employ a tunable laser with frequency detuning method to characterize WGM resonators [10], [15]–[17]. A schematic diagram of our experimental setup employing the frequency detuning method is shown in Fig. 5.2 (b).

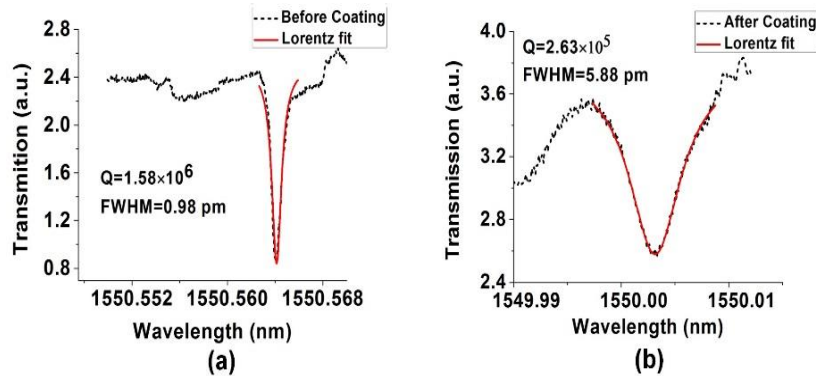


Fig. 5.5 Q factor estimates for the 282 μm diameter silica sphere (a) before and (b) after its coating with porous silica gel.

The transmitted power data was recorded as a function of time using a customized LabVIEW program. The Q factor of a typical WGM resonance for the same coated microsphere and tapered fiber system, determined using the frequency

detuning setup was calculated as 1.58×10^6 using the formula $Q = \frac{\lambda_R}{\Delta\lambda_{FWHM}}$, where λ_R is the resonance wavelength and $\Delta\lambda_{FWHM}$ is the full width at half-maximum of the Lorentz function before coating (Fig. 5.5 (a)). After coating the microsphere with silica gel, its Q factor is reduced to 2.63×10^5 as a result of increasing absorption and surface scattering losses in the coating layer (Fig. 5.5 (b)).

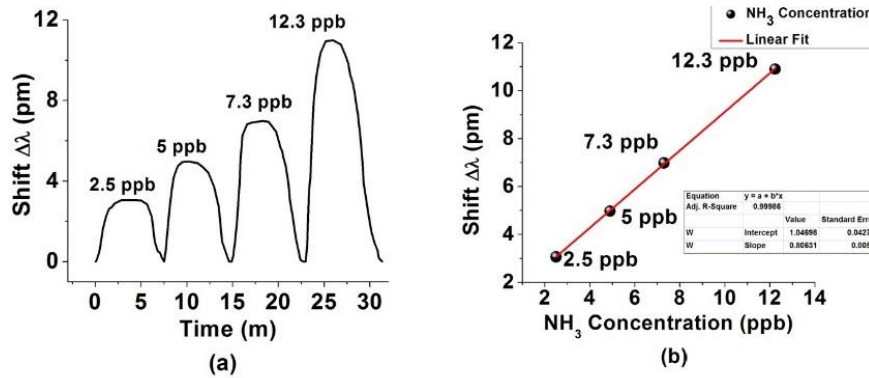


Fig. 5.6 (a) Wavelength shifts of the WGM resonance versus time during the sensor's exposure to various vapor phase ammonia concentrations. (b) A linear fit of the wavelength shift data

Four different ammonia solutions with ultra-low concentrations of 2.5 ppb, 5 ppb, 7.3 ppb and 12.3 ppb were prepared using the method described in Section 3.3 and a series of experiments was carried out to characterize the sensor's response. Similar to the previous experiment, WGM resonances show a red shift in response to the presence of ultra-low concentrations of ammonia and remain stable during the time of exposure. After opening the chamber exhaust door, the WGM spectrum returns to its original position. The temperature and humidity inside the chamber were kept constant throughout the experiments. Fig. 5.6 (a) illustrates the shift of the WGM spectrum in response to a series of injections of ultra-low concentrations of ammonia vapor. The linear regression value $R^2 = 0.99986$ illustrates the high linearity of the sensor's response within the range from 2.5 ppb to 12.3 ppb of ammonia vapor concentrations as shown in Fig. 5.6 (b). The

average sensitivity of the sensor within the studied range of concentrations is estimated as 800 pm/ppm.

5.5 Discussion

To investigate the selectivity of the sensor's response towards ammonia, similar experiments were carried out with other gases generated by volatile liquids such as acetone, methanol, benzene and n, n-dimethyl formide, and the corresponding results are presented in Fig. 5.7. The diagram in Fig. 5.7 graphically compares the sensor's response (maximum wavelength shifts) for the different vapor types expressed as a percentage of the response to a 4 ppm concentration of ammonia. As one can see from the diagram, the concentration of NH_3 vapor as low as 4 ppm results in a much stronger response, whereas the other vapors require a much higher (>500 ppm) concentration to achieve a much smaller response. Thus it can be concluded that the silica gel coated microsphere resonator exhibits a high selectivity to ammonia and can be considered as an excellent optical sensor for detection of ammonia vapor even in the presence of other gases.

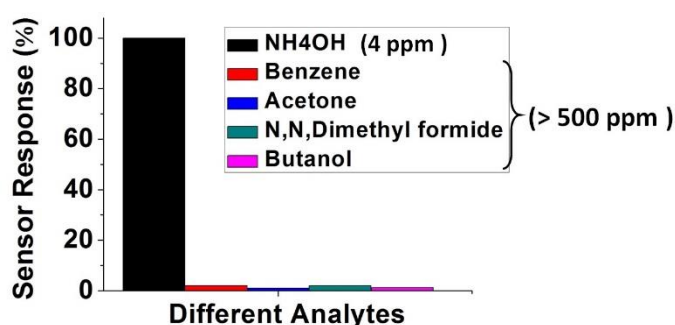


Fig. 5.7 (a) Sensor's response to various volatile organic compounds.

Stability and repeatability of performance are two important characteristics influencing practical applications of any optical sensor. To test the longer-term stability of the sensor's response, ammonia sensing experiments, using an SLD

light source and an optical spectrum analyzer, were carried out for the same sensor sample with a time interval of 10 days. In both experiments the concentrations of ammonia were 4 ppm, 8 ppm, 12 ppm, 22 ppm and 30 ppm at a constant temperature of 23 °C and 50 %RH. It can be seen from Fig. 5.8 (a), that the performance of the sensor is very stable within 10 days period with only small fluctuations. In addition to the stability tests, the sensor was tested for repeatability by exposing it to 12 ppm of ammonia under the same environmental conditions inside the chamber three times consecutively.

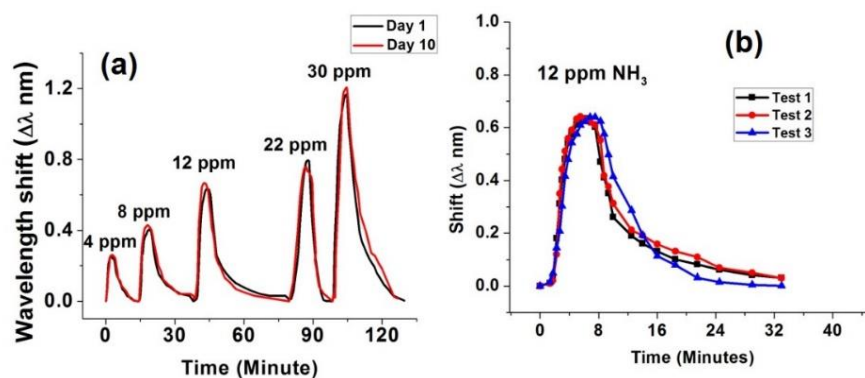


Fig. 5.8 (a) Time responses of the sensor to NH₃ recorded with a 10-days interval. (b) Sensor's responses to 12 ppm of ammonia during three consecutive tests at constant humidity and temperature.

Due to the porous nature of the silica gel coating and its excellent ability to adsorb water, the sensor can also be used to measure the concentration of water vapor in air [18]–[21]. To study the sensitivity of our sensor to relative humidity (RH) we carried out experiments using the same setup, shown in Fig. 5.2 (b). The airtight test chamber shown in the figure is equipped with an inlet and an outlet. The upper inlet is made for the entry of the moist air into the chamber and the outlet is used for dragging the moist air to the dehumidifier through a pump. The dehumidifier box contains anhydrous calcium sulfate which absorbs moisture from the air. The compressed dry air is pumped in to regulate the RH in the

chamber. Humid air was obtained by passing dry air through an ultrasonic humidification system (ETS5462). Controlling the ratio of humid air and compressed dry air in the chamber gives a fixed RH level. The chamber controller system allows for the independent setting of both temperature and relative humidity inside the chamber. The accuracy of the chamber is $\pm 2\%$ RH with the reference electronic humidity sensor resolution of 0.1% RH. Each humidity measurement was recorded five minutes after the RH level reached a set value to allow for the humidity throughout the chamber to stabilize. The sensor response was recorded using the the setup shown in Fig. 5.2 (b) for a range of RH values from 30% to 65% RH. The corresponding results for the 282 μm diameter microsphere coated with silica gel are shown in Fig. 5.9. As can be seen from the figure, an increase in the surrounding RH leads to a red shift of the WGM spectrum. This could be explained by the fact that when the surrounding RH increases, the silica coating absorbs more water from the environment within the air pores which leads to an increase of the effective refractive index of the coating and the microresonator overall. The corresponding RH sensitivity values (S_{RH}) estimated from the graph are 0.3 pm/%RH with high linearity characterized by the regression value of $R^2 = 0.9997$.

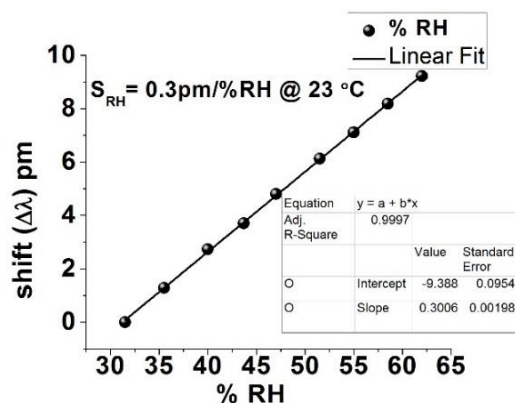


Fig. 5.9 WGM spectral shift versus RH change from 30-65%RH silica gel coated on 282 μm microsphere at 23 $^\circ\text{C}$.

Sensor's response to ammonia gas at different relative humidity levels was also investigated and the result is shown in Fig. 5.10. The graph illustrates the resonant wavelength shift due to exposure to 5 ppb of ammonia at different humidity values in the range from 30% RH to 70% RH at constant temperature inside the chamber. Frequency detuning method was used to record the data. As can be seen from the figure, response of the proposed sensor to ammonia gas decreases gradually with increase of humidity, possibly due to the increased competition from the water molecules being adsorbed on the porous silica surface, thus reducing the number of adsorbed ammonia molecules.

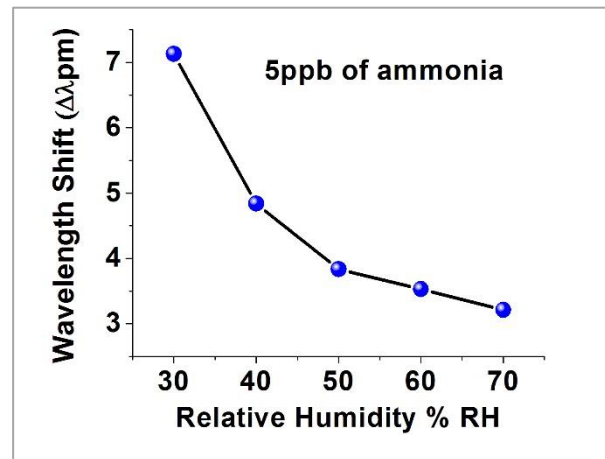


Fig. 5.10 WGM spectral shift versus different RH change from 30-70%RH silica gel coated on 282 μm microsphere at 23 °C against 5 ppb of ammonia.

The detection limit (DL) is a vital parameter used to quantify the device sensing capability. The detection limit represents the smallest measurable physical parameter change and it can be expressed as [22]:

$$DL = \frac{R}{S} \quad (5.2)$$

where R is the resolution of the sensor and S is the sensor sensitivity. R can be calculated as

$$R = 3\sqrt{\sigma_N^2 + \sigma_T^2 + \sigma_{SR}^2} \quad (5.3)$$

where σ_N , σ_T , σ_{SR} represent the standard deviations of the random effects associated with amplitude noise, temperature and detector spectral resolution, respectively. The estimates of DL for both detection methods used in our experiments are explained in Table 5.1. The corresponding standard deviations in the table were calculated in accordance with reference [23].

Table 5.1 Detection limit calculation for the silica gel coated microsphere sensor:

Parameters	Detection techniques	
	OSA	Frequency detuning
σ_N (pm)	0.694	0.041
σ_{SR} (pm)	0.1732	0.001
σ_T (pm)	0.01	0.01
S (pm/ppm)	34.8	800
R (pm)	2.145	0.128
DL (ppb of NH₃)	62	0.16

In the case of the tunable laser, the spectral deviation of the laser with a line width less than 1 MHz is estimated as $\sigma_{SR}=0.001$ pm. Hence, the ammonia DL for the proposed sensor is calculated as 62 ppb when using the OSA method, and as 0.16 ppb when using the frequency detuning method for the same coated sphere sensor sample. Similarly, the DL for humidity measurement is estimated as 4.2×10^{-1} RH in the humidity range of 30-65 %RH.

The response and recovery times are two important parameters for any sensor. The response time is the time taken by the sensor to reach 90% of the total shift in the resonance wavelength after its exposure to ammonia vapor inside the chamber, while the recovery time is the time taken to reach 90% of the change in

wavelength after withdrawing the vapor from the chamber. For the response and recovery time estimations it is not possible to use the optical spectrum analyzer due to its slow wavelength sweep cycles.

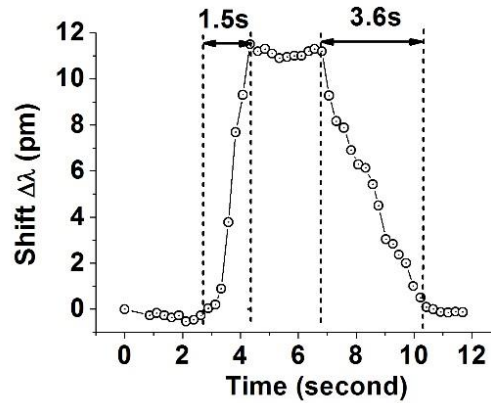


Fig. 5.11 Dynamic response-recovery curve of the sensor to NH_3 at constant room temperature 23°C and constant humidity of 50% RH.

To capture and process the changes in the WGM transmission spectrum with higher speed we used a tunable laser, photo-detector and the high-speed digital oscilloscope. A customized Labview programme was developed to capture the output screen image of the oscilloscope with a speed of 5 frames per second with each frame containing 1000 data points. The response and recovery times of the sensor were measured in response to NH_3 concentration of 12 ppb at constant temperature of 23°C and humidity of 50%RH inside the test chamber. The response time is calculated to be approximately 1.5 seconds, whereas the recovery time was measured to be 3.6 seconds as can be seen from Fig. 5.11, demonstrating the dynamic response of the sensor based on the oscilloscope image analysis. It should be noted that the response and recovery times include those of the chamber itself and given the volume of the chamber it is very likely that the actual the response times of the sensor are considerably better.

Table 2 below summarizes the performance of several fiber optic ammonia sensors reported in the literature utilizing different physical principles in

comparison with our proposed sensor. As can be seen from the table, our proposed sensor offers the detection limit of two orders of magnitude better than any of the optical fiber sensors reported to date.

Table 5.2 Comparative study of performance of various optical ammonia sensors.

Optical technique	Range (ppm)	Response / recovery times (sec)	Detection Limit (ppb)	Ref.
Bromocresol purple coated U-shaped plastic fiber	145-3528	10	10,000	[6]
Silica gel coated micro fiber coupler	0.25-10.4	50/35	5	[24]
Surface plasmon resonance, Ag/SnO ₂	10-100	n/a	154	[25]
Nanostructured dye-doped polypyrrole	12-216	50	5,000	[26]
Mach-Zehnder interferometer using graphene	40-360	0.5	300	[27]
Graphene-coated microfiber Bragg grating	0-100	n/a	200	[28]
Silica gel coated microsphere (this work)	0.0025-0.0123	1.5/3.6	0.16	

5.6 Conclusion

A compact optical sensor based on a whispering gallery mode micro resonator for detection of vapor phase ammonia concentration has been proposed and experimentally demonstrated. WGMs are excited in the silica microsphere dip-coated with silica gel and evanescently coupled to an adiabatic fiber tapered. A change in the refractive index of the coating arising due to its exposure to low

concentrations of ammonia in air leads to a spectral shift of the WGMs. Two different interrogation methods have been applied to study the sensor's response to ammonia vapor in two different ranges of concentrations: a wider, low concentrations, range and a narrow range of ultra-low concentrations. The highest sensitivity achieved in our experiments was 34.78 pm/ppm to ammonia concentration using an OSA, and 800 pm/ppm for the ultra-low concentrations of ammonia using a frequency detuning method. Studies of cross sensitivity to humidity have shown a sensitivity 0.3 pm/%RH in the RH range from 30% to 65% at a constant temperature of 23° C. The proposed sensor offers the advantages of compact size, low cost and high sensitivity. Experimental studies reveal an excellent performance for the proposed sensor in terms of its selectivity to ammonia in the presence of other volatile organic compounds with an ammonia detection limit calculated as 0.16 ppb and a fast response and recovery times in the order of seconds.

Author contributions statement

Arun Kumar Mallik carried out all experimental work, performed analysis of the experimental results with the help of other authors and co-wrote the manuscript. Yuliya Semenova developed the main concept, supervised the project and co-wrote the manuscript. Dejun Liu and Vishnu Kavungal helped in preparation of the agarose solution and fabrication of the tapered fiber. Manjusha Ramakrisnan helped in preparation of the sol-gel silica coating. Gerald Farrell and Qiang Wu co-supervised the project and gave valuable advice on analyzing the data. All authors provided critical feedback and helped shaping the research presented in the manuscript.

References:

- [1] B. Timmer, W. Olthuis, and A. Van Den Berg, “Ammonia sensors and their applications - A review,” *Sensors and Actuators, B: Chemical*. 2005.
- [2] C. Malins *et al.*, “Personal ammonia sensor for industrial environments,” *J. Environ. Monit.*, vol. 1, no. 5, pp. 417–422, 1999.
- [3] G. Dean, K., Miller, D., Carpio, R., Piterson, J. & Rich., “Effects of airborne molecular contamination on duv photo resists,” *J. photo Polym. Sci. Technol.*, vol. 10, pp. 425–443, 1997.
- [4] S. K. Mishra, D. Kumari, and B. D. Gupta, “Surface plasmon resonance based fiber optic ammonia gas sensor using ITO and polyaniline,” *Sensors Actuators, B Chem.*, vol. 171–172, pp. 976–983, 2012.
- [5] Z. Jin, Y. Su, and Y. Duan, “Development of a polyaniline-based optical ammonia sensor,” *Sensors Actuators, B Chem.*, vol. 72, no. 1, pp. 75–79, 2001.
- [6] A. J. Rodríguez Rodríguez, D. A. May-Arrioja, R. F. Domínguez Cruz, C. Ruíz Zamarreño, R. I. Matías Maestro, and F. Arregui San Martín, “Fiber optic ammonia sensor using bromocresol green pH indicator,” in *Proceedings of IEEE Sensors*, 2014, vol. 2014–Decem, no. December, pp. 1146–1149.
- [7] W. Cao and Y. Duan, “Optical fiber-based evanescent ammonia sensor,” *Sensors Actuators, B Chem.*, vol. 110, no. 2, pp. 252–259, 2005.
- [8] S. Arnold, M. Khoshshima, I. Teraoka, S. Holler, and F. Vollmer, “Shift of whispering-gallery modes in microspheres by protein adsorption,” *Opt. Lett.*, vol. 28, no. 4, pp. 272, 2003.
- [9] N. M. Hanumegowda, C. J. Stica, B. C. Patel, I. White, and X. Fan, “Refractometric sensors based on microsphere resonators,” *Appl. Phys. Lett.*, vol. 87, no. 20, pp. 1–3, 2005.
- [10] Q. Ma, L. Huang, Z. Guo, and T. Rossmann, “Whispering-Gallery Mode Silica Micro-Sensors for Temperature and Gas-Phase Concentration Measurements,” in *27th AIAA Aerodynamic Measurement Technology and Ground Testing Conference*, 2010.
- [11] N. Lin *et al.*, “Simulation and optimization of polymer-coated microsphere resonators in chemical vapor sensing,” *Appl. Opt.*, vol. 50, no. 28, pp. 5465,

2011.

- [12] A. K. Mallik, D. Liu, V. Kavungal, Q. Wu, G. Farrell, and Y. Semenova, "Agarose coated spherical micro resonator for humidity measurements," *Opt. Express*, vol. 24, no. 19, pp. 21216–21227, 2016.
- [13] G. Brambilla, V. Finazzi, and D. Richardson, "Ultra-low-loss optical fiber nanotapers," *Opt. Express*, vol. 12, no. 10, pp. 2258–2263, 2004.
- [14] A. Kalita, S. Hussain, A. H. Malik, N. V. V Subbarao, and P. K. Iyer, "Vapor phase sensing of ammonia at the sub-ppm level using a perylene diimide thin film device," *J. Mater. Chem. C*, vol. 3, no. 41, pp. 10767–10774, 2015.
- [15] S. Soria *et al.*, "High-Q polymer-coated microspheres for immunosensing applications," *Opt. Express*, vol. 17, no. 17, pp. 14694, 2009.
- [16] A. Giannetti, S. Berneschi, F. Baldini, F. Cosi, G. N. Conti, and S. Soria, "Performance of eudragit coated whispering gallery mode resonator-based immunosensors," *Sensors (Switzerland)*, vol. 12, no. 11, pp. 14604–14611, 2012.
- [17] A. Rasoloniaina *et al.*, "Controlling the coupling properties of active ultrahigh-Q WGM microcavities from undercoupling to selective amplification," *Sci. Rep.*, vol. 4, 4023, 2014.
- [18] Z. Zhao and Y. Duan, "A low cost fiber-optic humidity sensor based on silica sol-gel film," *Sensors Actuators, B Chem.*, vol. 160, no. 1, pp. 1340–1345, 2011.
- [19] L. Sun *et al.*, "Investigation of humidity and temperature response of a silica gel coated microfiber coupler," *IEEE Photonics J.*, vol. 8, no. 6, 2016.
- [20] R. Gao, Y. Jiang, and W. Ding, "Agarose gel filled temperature-insensitive photonic crystal fibers humidity sensor based on the tunable coupling ratio," *Sensors Actuators, B Chem.*, vol. 195, pp. 313–319, 2014.
- [21] and S. T. Nobuaki Tsuda, Hideki Fukano, "High-sensitivity humidity sensor composed of optical fiber coated with sol-gel derived porous silica," in *Opto Electron. Commun. Conf. (OECC) held jointly with 2016 Int. Conf. on Photonics Switch. (PS), IEEE*, 2016.
- [22] I. M. White and X. Fan, "On the performance quantification of resonant refractive index sensors," *Opt. Express*, vol. 16, no. 2, pp. 1020, 2008.
- [23] I. M. White and X. Fan, "On the performance quantification of resonant

- refractive index sensors,” *Opt. Express*, vol. 16, no. 2, p. 1020, 2008.
- [24] L. Sun *et al.*, “High sensitivity ammonia gas sensor based on a silica-gel-coated microfiber coupler,” *J. Light. Technol.*, vol. 35, no. 14, pp. 2864–2870, 2017.
 - [25] A. Pathak, S. K. Mishra, and B. D. Gupta, “Fiber-optic ammonia sensor using Ag/SnO(2) thin films: optimization of thickness of SnO(2) film using electric field distribution and reaction factor,” *Appl. Opt.*, vol. 54, no. 29, pp. 8712–8721, 2015.
 - [26] F. Tavoli and N. Alizadeh, “Optical ammonia gas sensor based on nanostructure dye-doped polypyrrole,” *Sensors Actuators, B Chem.*, vol. 176, pp. 761–767, 2013.
 - [27] B. Yao *et al.*, “All-optical Mach-Zehnder interferometric NH₃ gas sensor based on graphene/microfiber hybrid waveguide,” *Sensors Actuators, B Chem.*, vol. 194, pp. 142–148, 2014.
 - [28] Y. Wu *et al.*, “Graphene-coated microfiber Bragg grating for high-sensitivity gas sensing,” *Opt. Lett.*, vol. 39, no. 5, pp. 1235, 2014.

6 Spherical microresonators for multi-parameter sensing

In the previous chapters it was demonstrated that WGM sensors based on silica microsphere resonators functionalized with suitable polymer layers (i.e., agarose and silica gel) can be used for measurements of relative humidity and ammonia concentrations with high accuracy and excellent resolution. Monitoring of these two environmental parameters is of great importance in many industries both for minimizing the adverse effects on human health as well as for maintaining production levels and quality of products. However, to continuously monitor both of the parameters, two separate sensors with separate interrogation systems are required. Every additional sensor used to measure different parameter will increase the overall cost of the sensor system. A great deal of attention has been paid to reducing the overall cost of multi-parameter sensing systems by the researchers, particularly in the field of fiber optic sensors where the cost of interrogation unit is typically higher than that for other sensor technologies.

This chapter proposes a novel approach to the development of a multi parameter sensor capable of measurements of relative humidity and ammonia concentration in air simultaneously. The sensor consists of an array of two microspheres one of which is coated with agarose and another with silica gel, coupled to a single adiabatic tapered fiber in the transmission spectrum of which WGMs associated with both the microspheres can be observed. The spectral shifts of each of the two groups of modes are directly proportional to the ambient RH and ammonia concentration changes. The proposed method has the potential for expansion to sensing of a larger number of parameters reducing the overall cost of interrogation.

Detailed investigation on the cross sensitivity between the different parameters and temperature effects has also been carried out.

6.1 Whispering gallery mode micro resonators for multi-parameter sensing applications⁷

Abstract: A novel fiber optic sensing configuration for simultaneously measuring ammonia vapor (NH_3) concentration and relative humidity (RH) in air is proposed and experimentally demonstrated. The system comprised two silica whispering gallery mode (WGM) microsphere resonators coated with different polymer layers. One of the microspheres was dip-coated with sol gel silica polymer and another with a 0.5 % wt./vol. agarose hydrogel. WGMs in both microspheres were excited simultaneously by evanescent coupling using a single adiabatic fiber taper. The optical properties of both coating layers change due to their exposure to ammonia and water molecules in the surrounding atmosphere, resulting in the spectral shifts of the WGM resonances relevant to each of the microspheres. By measuring the relevant WGMs spectral shifts, NH_3 concentration in air and RH can be determined simultaneously. The experimentally demonstrated sensitivity of the proposed sensor array to ammonia was estimated as 19.07 pm/ppm (NH_3 molecules in air) and its sensitivity to relative humidity as 1.07 pm/% RH. Detailed studies of the coatings cross-sensitivity and temperature dependence are also presented. The proposed sensor array is compact, highly sensitive and potentially low cost.

⁷ Arun Kumar Mallik, Gerald Farrell, Manjusha Ramakrishnan, Vishnu Kavungal, Dejun Liu, Qiang Wu, and Yuliya Semenova, "Whispering gallery mode micro resonators for multi-parameter sensing applications", Optics Express ,accepted for publication (2018).

6.2 Introduction

Whispering gallery mode (WGM) microsphere resonators have been successfully investigated as sensors in numerous areas including refractive index, temperature, force, electromagnetic field, gas, and bio sensing in recent years due to their high quality factors (Q), low mode volume and inexpensive fabrication processes [1]–[7]. The WGM operating principle relies on strong confinement of light through total internal reflection inside the microcavity and retaining the same phase after each cycle of propagation. Silica microspheres are shaped by natural surface tension forces during fabrication, resulting in a clean, smooth silica surface with very minimal loss and negligible scattering, making such silica microspheres suitable for the next generation of high-performance optical sensors. The spectral positions of WGM resonances are strongly dependent on the geometry of the dielectric resonator (diameter, sphericity), the optical properties of the resonator material and also on the refractive index (RI) of the medium in the environment surrounding the resonator. Either a very small deformation of the microcavity or a minute change in material properties (such as RI) can be easily quantified by monitoring the WGM resonance wavelength shift. Much of the research effort to date has been focused on using a single WGM resonator to sense a single physical, chemical or biological quantity, with only limited research focused on multi-parametric sensing [8]. However, in real life applications simultaneous sensing of multiple parameters is often required. Many effective techniques have been developed to realize multi-parametric measurements with fiber optic sensors. For example, simultaneous measurement of humidity and temperature has been proposed using a combination of a long period grating (LPG) inscribed in a fiber

loop mirror [9], a combination of a fiber Bragg grating (FBG) and Fabry-Perot interferometer cavity [10], a FBG and photonics crystal fiber interferometer [11], a LPG partially coated with PAH/PAA poly electrolyte complexes [12], Nafion-crystal violet film based optical sensor is to measurement of humidity and ammonia in air simultaneously [13], nano porous layer of alumina is also proposed for sensing of both humidity and ammonia gas [14] and many others. All the above-mentioned sensing techniques rely on measurements of characteristic wavelength shifts in the spectra of the sensors influenced by the physical parameters of interest. Some of these configurations suffer from complexity of interrogation and a poor wavelength resolution. WGM microsphere resonators have advantage over the sensors above due to their high Q factors (up to 10^9) [15], resulting in much higher wavelength resolution and low detection limits. Recently we proposed and demonstrated an highly sensitive relative humidity (RH) sensor based on a silica microsphere coated with a thin layer of agarose hydrogel [16]. We have also demonstrated a silica gel coated silica microsphere for a very low detection limit ammonia sensing and a silica gel coated optical fiber sensors for highly sensitive detection of ammonia in water [17][18]. Ammonia is a colorless, highly corrosive and toxic gas with pungent smell which has adverse effects on human health including burning nose, throat and respiratory track irritation even after a long term exposure at lower concentrations of ammonia [19], [20]. Therefore, some means to sense and also quantify ammonia concentration in air is needed. Similarly, humidity is one of the important environmental conditions which plays a very significant role in agriculture, the food industry, clinical medicine, manufacturing, civil engineering, textile manufacture, the semiconductor industry and many other fields. Humidity measurement in

industries is critical because it may affect the quality of the product, for example the shelf-life of foodstuffs. Hence, humidity sensing is very important, especially in the control systems for industrial processes. In many of the applications listed above, a means for simultaneous measurement of ammonia concentration in air and RH is required. For example, a recent study by Wei *et al.* demonstrated a strong influence of both NH_3 concentration and ambient RH on the immune system of broiler chickens, highlighting the need for simultaneous monitoring and control of both parameters in the atmosphere of poultry or animal houses [21].

In this article, we propose a novel fiber optic sensor's configuration for simultaneous measurement of both ammonia concentration and relative humidity in air. To realize this we excited WGMs in two microspheres coupled to the same optical fiber taper. The two microspheres have nearly the same diameter of 250 μm and 255 μm and were used to measure ammonia and humidity simultaneously. An adiabatic tapered fiber with the uniform waist diameter of $\sim 3\text{-}4\ \mu\text{m}$ was used to simultaneously couple the light into both microspheres forming a small array. One of the microspheres was coated with a layer of sol-gel silica whose optical properties are very sensitive to ammonia, while the second microsphere was coated with a highly hygroscopic layer of 0.5 % wt./vol. agarose hydrogel. To the best of our knowledge this study is the first experimental demonstration of multi-parametric sensor based on the WGM phenomenon that offers simultaneous high resolution measurement of both ammonia concentration in air and relative humidity. A study of the temperature sensitivity of the proposed sensing system was also performed showing minimal temperature dependence compared to other fiber optic sensors.

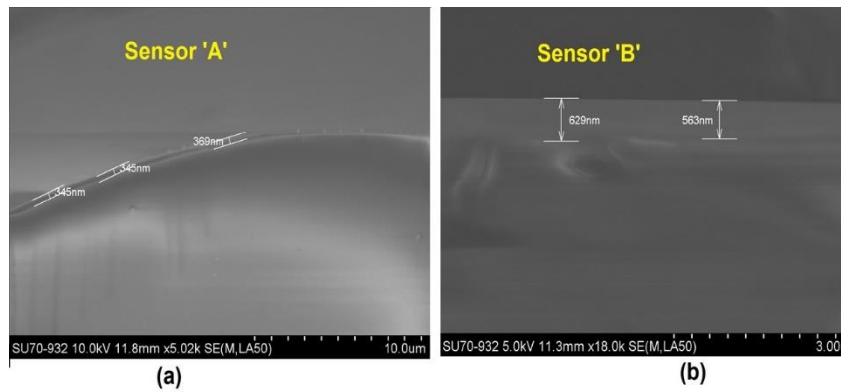


Fig. 6.1 SEM images of cross sections of singlemode fibers coated with (a) silica sol-gel; (b) 0.5% wt./vol. agarose hydrogel

6.3 Sensor Fabrication and Experimental setup

In our experiment the agarose hydrogel for the coating was made from a commercially available agarose powder from Sigma Aldrich (A6013). The hydrogel solution was prepared by adding 0.5% wt./vol. of the agarose powder mixed in deionized (DI) water, followed by continuous stirring at 80°C temperature until all the agarose powder was completely dissolved in the DI water. Preparation of the sol-gel silica coating was carried as described in [22]. The sol-gel was prepared by hydrolysis and condensation of TEOS (Tetraethyl ortho silicate) in presence of water and ethanol. The molar ratio of TEOS, ethyl alcohol and DI water was 1:4:16 mixed in a 250-mL measuring flask and kept at continuous stirring conditions for 1.5 hour. 3-4 drops of hydrochloric acid (HCL) were used as catalyst. The solution was kept for two days at room temperature. Both silica microspheres were fabricated at the tip of an unjacketed cleaved single mode fiber using the electric arc of a fusion splicer, as described in [16]. After applying a series of 3 electric discharge arcs to the cleaved surface of the fiber tip using a fusion splicer, the fiber tip assumed spherical shape due to surface tension. Two microspheres of almost the same diameter (250 μm and 255 μm) were

prepared for our experiments. agarose and silica coating layers were applied separately on each of the microsphere's surfaces by dip coating method with the pulling speed of 2 mm/sec. For identification we labeled the silica gel coated microsphere as sensor 'A' and the agarose coated microsphere as sensor 'B'. Both microspheres were kept dry at room temperature for 24 hours before the experiments. The coating thickness was estimated by analyzing the SEM images of cross-sections of single mode fiber ends dip coated with the respective gels using the same method and pulling speed (2 mm/sec), similarly dried and cleaved. Fig.6.1 shows the SEM images of the respective cleaved surfaces where the thickness of the coating is measured as ~300 - 400 nm for the silica gel and ~500-600 nm for agarose.

To allow for coupling of light in and out of the microspheres, an adiabatic tapered fiber was fabricated using a customized micro heater brushing technique [23]. In our experiment the tapered waist diameter was approximately 3-4 microns. To improve mechanical stability, the fabricated fiber taper was placed in direct contact with the microspheres and fixed on a glass slide at a height of ~5 mm from the slide surface using two drops of UV curable epoxy (Norrrland). A schematic diagram of the experimental setup is shown in Fig.6.2.

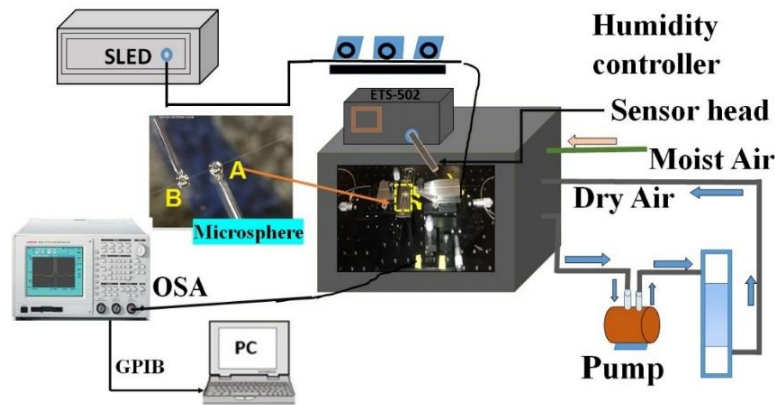


Fig. 6.2 Experimental setup for multi parameter sensor characterization.

The experimental set up consisted of a broadband light source (Thorlabs S5FC1005S), polarization controller, optical spectrum analyzer (OSA, Advantest Q8384) and a temperature controlled humidity chamber (ETS 5503). Each coated microsphere was mounted on an XYZ nano-positioning stage and then slowly brought in contact with the tapered fiber inside the humidity chamber.

6.4 Results and discussion

Light from the broadband superluminescent light source (SLD) operating in the wavelength range 1530-1570 nm was launched into the fiber taper and the corresponding transmission spectrum was observed at the taper output by means of the OSA. The wavelength resolution of the OSA was 10 pm. The WGM excitation in both microspheres was achieved by evanescent coupling to the tapered fiber. At first, the silica gel coated microsphere (sensor A) was gradually and carefully brought in direct contact with the tapered fiber until the WGM resonances were clearly observed in the transmission spectrum of the fiber taper. The input light polarization was adjusted using a manual polarization controller to achieve maximum light coupling efficiency.

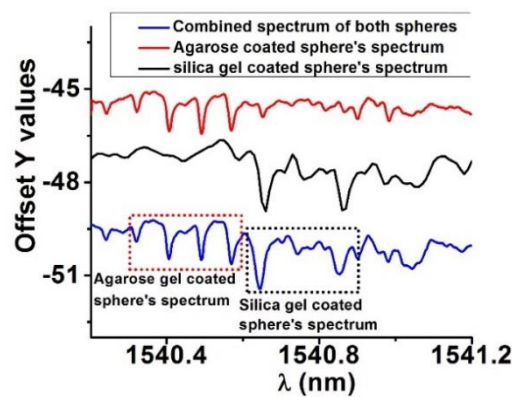


Fig. 6.3 Transmission WGM spectra for both sensors separately and when both microspheres are coupled simultaneously.

The transmission spectrum after coupling sensor A is shown in Fig.6.3, where WGM resonances near 1540 nm can be clearly seen. Without changing the setup, the second microsphere (sensor B) was positioned near the silica gel coated sphere and coupled to same tapered fiber. The resulting transmission spectrum showing the WGM resonances due to both microspheres is labelled “A+B” in Fig. 6.3. Red curve “sensor B” in Fig.6.3 illustrates the WGM spectrum of the tapered fiber when only sensor B is coupled. As one can see from the figure, both groups of “A” and “B” resonances are clearly visible and distinguishable in the combined “A+B” spectrum.

The optical properties of the agarose coating are very sensitive to relative humidity, while those of the silica coating strongly depend on the ammonia concentration in the surrounding atmosphere and to a lesser extent on its relative humidity. Therefore changes in either of the parameters will result in spectral shifts of the WGM resonances, which can be expressed as:

$$\begin{bmatrix} \Delta\lambda_A \\ \Delta\lambda_B \end{bmatrix} = \begin{bmatrix} K_{11} & K_{12} \\ K_{21} & K_{22} \end{bmatrix} \begin{bmatrix} \Delta_{RH} \\ \Delta_{NH3} \end{bmatrix} \quad (6.1)$$

where K_{11} and K_{12} are the linear coefficients representing sensitivity of sensor A to relative humidity and ammonia concentration respectively. Similarly, K_{21} and K_{22} are the ammonia sensitivities of sensor B. After experimental calibration of the sensors and determining the values of the coefficients, it is possible to independently find both humidity and ammonia concentration.

Experimental measurements of humidity inside the humidity and temperature controlled chamber were carried out with both sensors A and B in the range of relative humidity values from 40 % to 70 %RH at constant temperature of $25 \pm 0.1^\circ\text{C}$. The sensing mechanism for both sensors A and B are based on the change

of effective refractive index and thickness of the coating layer due to adsorption of water vapor by the coating surface. This process leads to the air inside the micro pores of the coating layer being replaced with water molecules under capillary forces. As a result, the effective refractive index and thickness of the coating increases and WGMs experience a red spectral shift. Fig. 6.4 represents the WGM spectra of both sensors at different levels of relative humidity in the chamber. A commercial electronic hygrometer was used as a reference for humidity measurement inside the chamber. The Q factors of the selected WGMs for sensors A and B in Fig.6.4 were estimated using equation $Q = \lambda_R / \Delta\lambda_{FWHM}$, where λ_R is the resonance wavelength and $\Delta\lambda_{FWHM}$ is the full width at half-maximum of the resonant lobe calculated by fitting the resonant dip with the Lorentzian function. The quality factors were calculated as $Q = 5.22 \times 10^4$ for sensor A and $Q = 9.81 \times 10^4$ for sensor B, respectively.

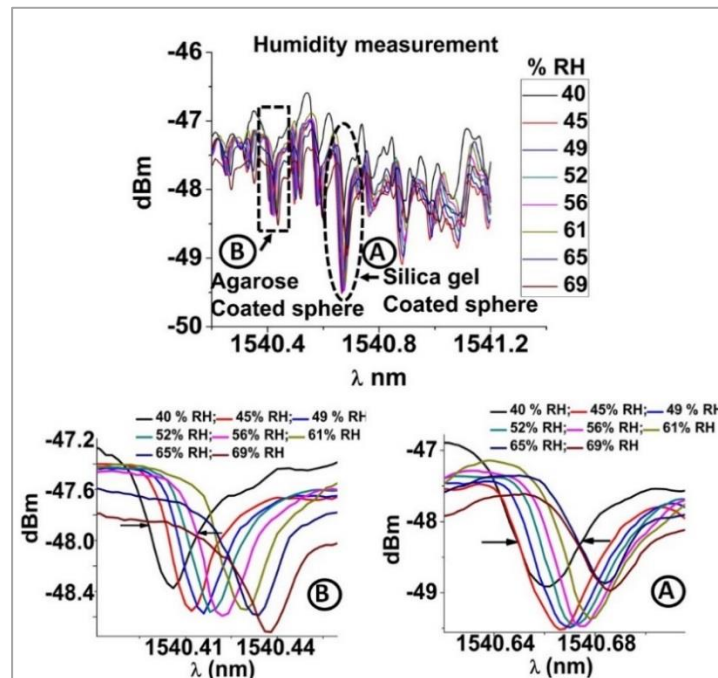


Fig. 6.4 Transmission spectrum for sensors A and B simultaneously at different humidity levels inside the chamber. The inset graphs are enlarged selected portions of the overall spectrum for sensors 'A' and 'B' at constant temperature of $25 \pm 0.1^\circ\text{C}$

It should be noted the measured values of the Q factor shown in Fig.6.4 are lower compared to those reported in the literature for silica microspheres [2], [3]. One of the reasons is the limitations of the experimental setup employed in our experiment, which consisted of a broadband light source and optical spectrum analyzer with a wavelength resolution of 10 pm. Another reason might be the increased absorption and scattering loss due to the applied coatings on the surfaces of the microspheres. Fig.6.5 is a plot of the spectral shifts of the selected WGM resonances for sensors A and B as functions of relative humidity inside the chamber. One can see from the graph that both dependences are very close to linear and the corresponding sensitivities to humidity are $K_{11} = 0.8$ pm/%RH for sensor A and $K_{21} = 1.07$ pm/%RH for sensor B.

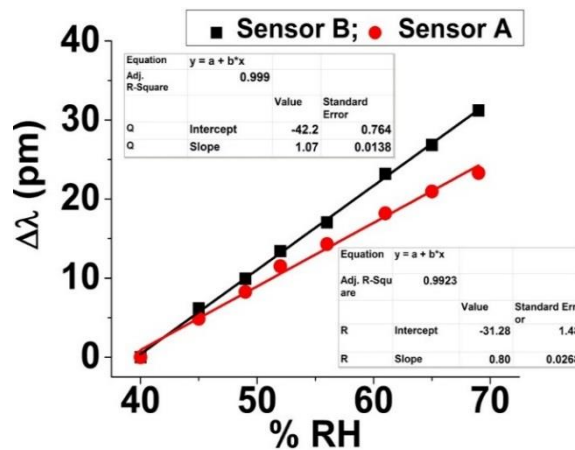


Fig. 6.5 Linear fitted graph of the selected WGM wavelengths versus relative humidity for both the silica gel coated (sensor A) and agarose coated (sensor B) microspheres.

The same experimental setup was used to investigate the optical responses of the sensors A and B to different concentrations of ammonia vapors at constant temperature of $25 \pm 0.1^\circ\text{C}$ and constant humidity of 40% RH inside the chamber. A small amount of ammonium hydroxide (NH_4OH) liquid was injected into and then removed from the gas chamber after the measurement, in order to create three low

ammonia vapor concentrations corresponding to 0.46 ppm, 1.46 ppm, and 2.19 ppm of ammonia in air. Spectral data was recorded using an OSA connected to a PC through a GPIB cable and a customized LabView program. It should be noted that the WGM spectral shift dynamics depends on the diffusion rate of ammonia vapors inside the chamber.

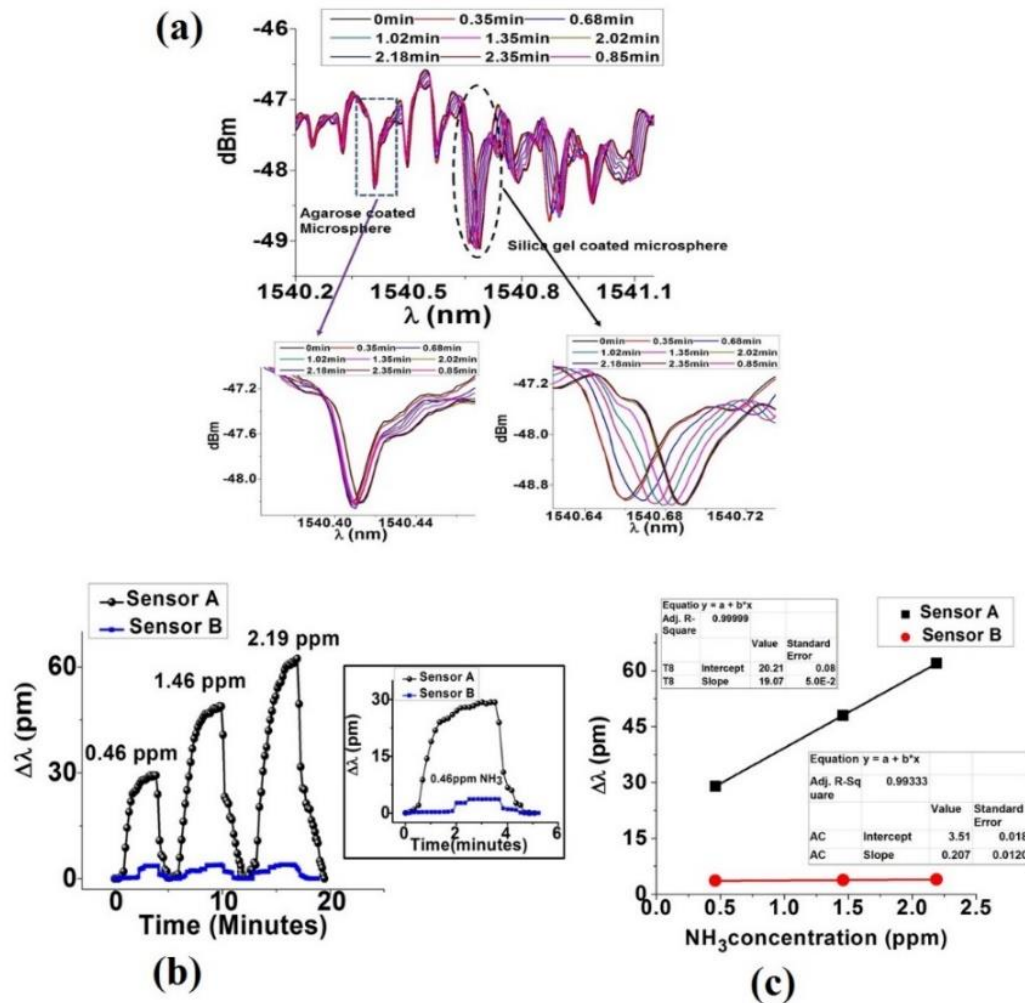


Fig. 6.6 (a) Transmission spectrum for the sensor system recorded at different times after injection of ammonia vapor in concentration of 46 ppm inside the chamber at constant temperature of $25 \pm 0.1^\circ\text{C}$ and humidity 40% RH. Insets represent the enlarged portions of the spectrum corresponding to sensors A and B; (b) A and B WGM spectral shifts in response to three different concentrations of ammonia (0.46 ppm, 1.46 ppm and 2.19 ppm) after injection of the vapors inside the chamber. Inset figure illustrates the response to 0.46 ppm concentration of ammonia only; (c) WGM spectral shifts for the sensors A and B as a function of ammonia concentration.

Fig.6.6 (a) illustrates the spectrum for both the microspheres coupled to the same tapered fiber after injection of ammonia vapor at 0.46 ppm concentration inside

the chamber. As can be seen from the figure and inset A (dotted oval in the main graph), the WGM resonance associated with the silica gel coated microsphere experiences red shift during the sensor's exposure to ammonia vapor. The corresponding spectral shift of the WGM resonance associated with sensor B (inset B, dotted rectangle in the main graph) also occurs in the direction towards the longer wavelengths but is much smaller. Fig.6.6 (b) illustrates the dynamics of the WGM spectral shifts for both of the microspheres as they were exposed to 0.46 ppm, 1.46 ppm and 2.19 ppm concentrations of ammonia inside the chamber. The inset graph in Fig.6.6 (b) shows that the total shift of the selected WGM resonance wavelength for sensor A was approximately 95 times larger than that for the sensor B during their an exposure to 0.46 ppm ammonia vapor concentration. This is due to presence of silanol group on the surface of silica gel coated sphere producing ae dipole interaction between hydroxyl group and NH_3 . The adsorption of these ammonia molecules on the surface of silica gel microsphere increases themuch higher sensitivity of the effective refractive index of silica gel coating more than to ammonia compared to that of the agarose layer on the surface of B microsphere. When the gas was removed from the chamber by opening its exhaust valve, the WGM resonances returned back to their original positions. Total spectral shifts of the WGM resonances for both the microspheres are plotted as a function of ammonia concentration in Fig.6.6 (c). The ammonia sensitivity coefficients K_{12} and K_{21} were derived from the linear fits of the experimental data as $K_{12}=19.07$ pm/ppm and $K_{22}=0.2$ pm/ppm at constant temperature of $25\pm0.1^\circ\text{C}$ and 40% RH humidity.

It should be noted that the above sensitivity coefficients for both of the sensors were determined at a constant ammonia concentration (0.46 ppm) and humidity

(40%RH) level respectively, and at first were assumed to be independent. It is possible, however that both coatings have some cross-sensitivity issues, so that the values of the linear coefficients are not fully independent. In particular, the porous nature of the silica gel coating layer is more likely to make it susceptible to the presence of water molecules, affecting its sensitivity to ammonia at a different RH. To investigate this, we carried out an additional study of response of the silica gel coated microsphere towards ammonia at several different relative humidity levels, namely at 10, 22, 35, 45, 60 and 75% RH.

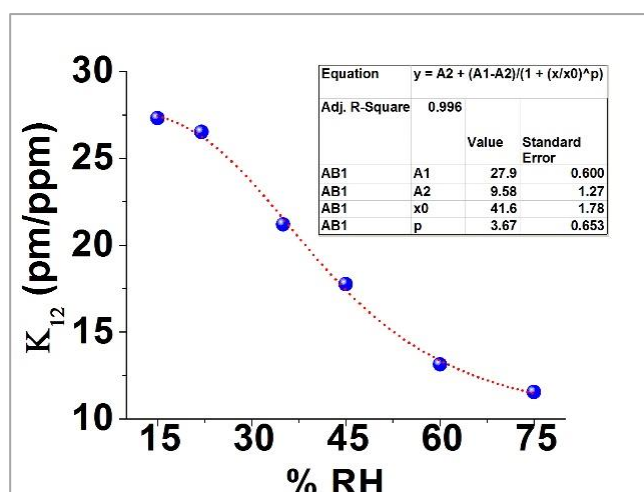


Fig. 6.7 K_{12} as a function of RH at constant temperature of 25°C

Fig.6.7 shows the dependence of the sensor A sensitivity to ammonia (coefficient K_{12}) as a function of relative humidity at constant temperature of 25°C. The same values of ammonia concentrations as in the previous experiments were used in this study. As one can see from Fig.6.7, sensitivity to ammonia for sensor A is a non-linear function of relative humidity in the chamber. Ammonia sensitivity decreases with an increase of relative humidity saturating above 60% RH. This is likely because ammonia molecules are more easily adsorbed by the surface water rather than the silica coating. Similarly, at lower humidity levels, a greater number of ammonia molecules are adsorbed directly on the surface of the silica coating

pores resulting in greater change of the coating's effective refractive index due to ammonia. The fit of the experimental results with a logistic function in Fig.6.7 gives the approximate sensitivity of the sensor A in presence of humidity in the range from 15% RH to 75% RH with less than $\pm 1\%$ error.

It is clear that K_{12} in Eq. (6.1) is not a constant independent of the humidity level. However, the dependence of K_{12} on the humidity level is predictable and can be determined from the following approximate equation:

$$K_{12} = 9.58 + \frac{18.32}{1 + \left(\frac{\%RH}{41.6}\right)^{3.67}} \quad (6.2)$$

Since K_{12} can no longer be considered as a constant, it appears that Eq. (1) can no longer be used for accurate detection of both parameters changing independently in the surrounding the sensor system atmosphere

substituting the K_{12} coefficient's values in Eq. (6.1) we get:

$$\begin{bmatrix} \Delta\lambda_A \\ \Delta\lambda_B \end{bmatrix} = \begin{bmatrix} K_{11} & 9.58 + \frac{18.32}{1 + \left(\frac{\%RH}{41.6}\right)^{3.67}} \\ K_{21} & K_{22} \end{bmatrix} \begin{bmatrix} \%RH \\ \%NH_3 \end{bmatrix} \quad (6.3)$$

To determine the value of K_{12} unambiguously one only needs to have an accurate value for the %RH level, which Sensor B can provide, and which is not dependent on the level of ammonia.

Thus to determine the %RH and ammonia concentrations levels requires a two step approach. Assuming both sensors are calibrated, then as first step use Sensor B to measure %RH and then as a second step use the value of the %RH to determine the value of the coefficient K_{12} and then directly determine the ammonia concentration using this value and the measured wavelength shift for Sensor A.

A study of the influence of temperature on the performance of the proposed sensor array was also carried out using the same environmental chamber. The temperature inside the chamber was gradually increased in a step like fashion from 20°C to 40 °C. Each WGM spectrum was recorded when the temperature inside the chamber was stable at the set point. Fig.6.8 shows the temperature responses of sensors A and B at 40 % RH. The linear fits of the experimental data allow to determine the temperature sensitivities as 5.8 pm/°C for sensor A and 6.7 pm/°C for sensor B.

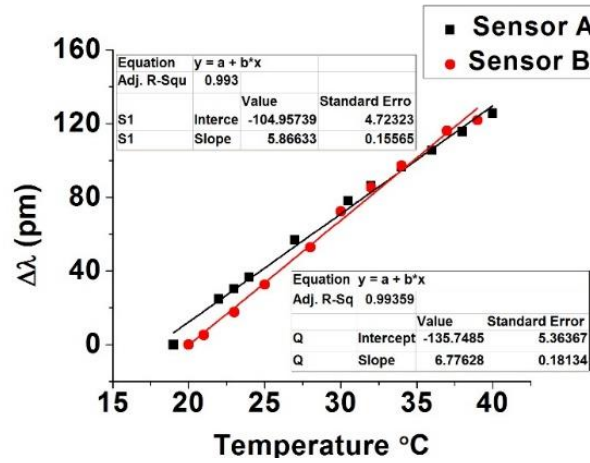


Fig. 6.8 Temperature dependence of the WGM spectral shift for sensors A and B at constant humidity of 40% RH.

The detection limit (DL) for a sensor represents the smallest measurable physical parameter change and it can be expressed as $DL = R/S$, where R is the resolution of the sensor and S is its sensitivity. R can be calculated as

$$R = 3\sqrt{\sigma_N^2 + \sigma_T^2 + \sigma_{SR}^2} \quad (6.4)$$

where σ_N , σ_T , σ_{SR} represent the standard deviations associated with the amplitude noise limited SNR of the detection system, temperature fluctuations and detector spectral resolutions respectively [24]. We assumed the signal-to-noise ratio of the system to be approximately 60 dB, so that σ_N is calculated as 0.2 pm and 0.1 pm

for sensors A and B, respectively [24]. The standard deviation due to temperature stabilization is taken as $\sigma_T = 0.01$ pm for both the sensors. The error in determining the position of the resonant mode is uniformly distributed between -0.3 pm and +0.3 pm and the resulting standard deviation associated with the standard deviation of the spectral resolution of the broadband source is $\sigma_{SR} = 0.17$ [24] in both cases. The overall sensor resolution calculated for sensor A is $R = 0.8$ pm and for sensor B is $R = 0.6$ pm. The corresponding DLs for sensors A and B are listed in Table 6.1

Table 6.1 Individual detection limit estimates for sensor A and B at 40 %RH

	Humidity	Ammonia
Sensor A	1 %RH	42 ppb
Sensor B	0.56 %RH	3000 ppb

6.5 Conclusion

In conclusion, a novel approach to simultaneous measurement of ammonia vapor and humidity in air has been proposed and demonstrated experimentally. WGMs were excited at the same time in the array of two microspheres coated with different polymers, namely, silica gel and agarose hydrogel, coupled to a single adiabatic fiber taper. The experimental results revealed that the silica gel coated microsphere was more sensitive to ammonia than the agarose coated microsphere. Similarly, the agarose coated sphere had better sensitivity to humidity than the silica gel coated microsphere. It has been demonstrated that by monitoring the spectral positions of two WGM resonances relevant to each of the microspheres, it was possible to simultaneously determine ammonia concentration and relative

humidity in the surrounding the array atmosphere. The maximum measurement resolutions of the two parameters were estimated as 42 ppb for ammonia and $5.6 \times 10^{-1} \%RH$ for humidity at the temperature of $25 \pm 0.1^\circ C$. The proposed method offers the advantages interrogation using a single fibre along with a compact sensor size, high resolution and simple fabrication. The potential applications can be expanded to sensing of other chemical and biological quantities utilizing various coatings and possibly increasing the number of sensors within the array.

Author contributions statement

Arun Kumar Mallik carried out all experimental work, performed analysis of the experimental results with the help of other authors and co-wrote the manuscript. Yuliya Semenova developed the main concept, supervised the project and co-wrote the manuscript. Dejun Liu and Vishnu Kavungal helped in preparation of the agarose solution and fabrication of the tapered fiber. Manjusha Ramakrisnan helped in preparation of the sol-gel silica coating. Gerald Farrell and Qiang Wu co-supervised the project and gave valuable advice on analyzing the data. All authors provided critical feedback and helped shaping the research presented in the manuscript.

References:

- [1] N. M. Hanumegowda, C. J. Stica, B. C. Patel, I. White, and X. Fan, "Refractometric sensors based on microsphere resonators," *Appl. Phys. Lett.*, vol. 87, no. 20, pp. 1–3, 2005.
- [2] Q. Ma, T. Rossmann, and Z. Guo, "Whispering-gallery mode silica microsensors for cryogenic to room temperature measurement," *Meas. Sci. Technol.*, vol. 23, 129501, 2010.
- [3] T. Ioppolo, M. Kozhevnikov, V. Stepaniuk, M. V. Ötügen, and V. Sheverev, "Micro-optical force sensor concept based on whispering gallery mode resonators," *Appl. Opt.*, vol. 47, no. 16, pp. 3009, 2008.
- [4] T. Ioppolo, U. Ayaz, and M. V Otugen, "Tuning of whispering gallery modes of spherical resonators using an external electric field," *Opt. Express*, vol. 17, no. 19, pp. 16465-16479, 2009.
- [5] V. S. Ilchenko *et al.*, "Strain-tunable high-Q optical microsphere resonator," *Opt. Commun.*, vol. 145, no. 1-6, pp. 86-90, 1998.
- [6] N. Lin *et al.*, "Simulation and optimization of polymer-coated microsphere resonators in chemical vapor sensing," *Appl. Opt.*, vol. 50, no. 28, p. 5465, 2011.
- [7] F. Vollmer, D. Braun, A. Libchaber, M. Khoshsim, I. Teraoka, and S. Arnold, "Protein detection by optical shift of a resonant microcavity," *Appl. Phys. Lett.*, vol. 80, no. 21, pp. 4057–4059, 2002.
- [8] F. Vollmer, S. Arnold, D. Braun, I. Teraoka, and A. Libchaber, "Multiplexed DNA quantification by spectroscopic shift of two microsphere cavities," *Biophys. J.*, vol. 85, no. 3, pp. 1974-1979, 2003.
- [9] H. Liu, H. Liang, M. Sun, K. Ni, and Y. Jin, "Simultaneous measurement of humidity and temperature based on a long-period fiber grating inscribed in fiber loop mirror," *IEEE Sens. J.*, vol. 14, no. 3, pp. 893-896, 2014.
- [10] F. J. Arregui, I. R. Matías, K. L. Cooper, and R. O. Claus, "Simultaneous measurement of humidity and temperature by combining a reflective intensity-based optical fiber sensor and a fiber bragg grating," *IEEE Sens. J.*, vol. 2, no.5, pp. 482-487, 2002.
- [11] J. Mathew, Y. Semenova, and G. Farrell, "Fiber optic hybrid device for simultaneous measurement of humidity and temperature," *IEEE Sens. J.*,

- vol. 13, no. 5, pp. 1632-1636, 2013.
- [12] A. Urrutia, J. Goicoechea, A. L. Ricchiuti, D. Barrera, S. Sales, and F. J. Arregui, "Simultaneous measurement of humidity and temperature based on a partially coated optical fiber long period grating," *Sensors Actuators, B Chem.*, vol. 227, pp. 135-141, 2016.
 - [13] I. M. Raimundo Jr. and R. Narayanaswamy, "Simultaneous determination of relative humidity and ammonia in air employing an optical fibre sensor and artificial neural network," *Sensors Actuators, B Chem.*, vol. 74, no. 1-3, pp. 60-68, 2001.
 - [14] E. C. Dickey, O. K. Varghese, K. G. Ong, D. W. Gong, M. Paulose, and C. A. Grimes, "Room temperature ammonia and humidity sensing using highly ordered nanoporous alumina films," *Sensors*, vol. 2, no. 3, pp. 91-110, 2002.
 - [15] M. L. Gorodetsky, A. A. Savchenkov, and V. S. Ilchenko, "Ultimate Q of optical microsphere resonators," *Opt. Lett.*, vol. 21, no. 7, pp. 453-455, 1996.
 - [16] A. K. Mallik, D. Liu, V. Kavungal, Q. Wu, G. Farrell, and Y. Semenova, "Agarose coated spherical micro resonator for humidity measurements," *Opt. Express*, vol. 24, no. 19, pp. 21216-21227, 2016.
 - [17] A. K. Mallik, G. Farrell, D. Liu, V. Kavungal, Q. Wu, and Y. Semenova, "Silica Gel Coated Spherical Micro resonator for Ultra-High Sensitivity Detection of Ammonia Gas Concentration in Air," *Sci. Rep.*, vol. 8, no. 1, p. 1620, Dec. 2018.
 - [18] D. Liu *et al.*, "High sensitivity sol-gel silica coated optical fiber sensor for detection of ammonia in water," *Opt. Express*, vol. 24, no. 21, pp. 24179-24187, 2016.
 - [19] C. Malins *et al.*, "Personal ammonia sensor for industrial environments," *J. Environ. Monit.*, vol. 1, no. 5, pp. 417-422, 1999.
 - [20] B. Timmer, W. Olthuis, and A. Van Den Berg, "Ammonia sensors and their applications - A review," *Sensors and Actuators, B: Chemical.*, vol. 107, no. 2, pp. 666-677, 2005.
 - [21] F. X. Wei *et al.*, "Ammonia concentration and relative humidity in poultry houses affect the immune response of broilers," *Genet. Mol. Res.*, vol. 15, no. 2, pp. 3160-3169, 2015.

- [22] A. Buckley and M. Greenblatt, "The sol-gel preparation of silica gels," *J. Chem. Educ.*, vol. 71, no. 7, pp. 599-602, 1994.
- [23] G. Brambilla, V. Finazzi, and D. J. Richardson, "Ultra-low-loss optical fiber nanotapers," *Opt. Express*, vol. 12, no. 10, pp. 2258, 2004.
- [24] I. M. White and X. Fan, "On the performance quantification of resonant refractive index sensors," *Opt. Express*, vol. 16, no. 2, pp. 1020, 2008.

7 Conclusions and future work

7.1 Conclusions

The primary goal of this research was to gain fundamental scientific insight into the principles of WGMs in micro-fibre resonators induced by the evanescent field of a tapered fiber and to investigate the use of this effect for sensing of important environmental parameters with a particular focus on measurements of moisture and ammonia concentration in air. Agarose and silica gel are the two coating materials successfully applied on the microsphere's surface to facilitate the humidity and ammonia detection. The proposed WGM microresonator sensors are compact, offer excellent sensitivity, detection limit and stability. The sensors can be easily combined with different interrogation systems making them good candidates for a wide range of industrial sensing applications.

To reach this goal a series of numerical and experimental investigations have been carried out. Firstly, analytical simulation models for both uncoated and coated silica microspheres have been simulated based on perturbation theory. Using the models, the polar, azimuthal and radial modes distributions were solved to provide graphical representations of the WGM modes at the equatorial region of the microsphere. Mode coupling between the tapered fiber and microsphere was simulated numerically and analyzed to optimize the light coupling efficiency during the experiments. Different loss mechanisms that influence the Q factor of the microspheres were also analyzed. Numerical simulation results for the free spectral range of the microsphere's WGM spectra were compared with experimental values in order to validate the numerical models. In order to

understable experimental studies, methods for in-lab fabrication of the silica microspheres with diameters of 100-300 μm , adiabatic fiber tapers with submicron waists, coatings preparation and application techniques have been developed and realized. Several customized experimental setups have been developed for experimental characterization of the proposed WGM sensors for environmental applications. The following are the main conclusions from across the thesis, divided into five sections based on the different objectives and research strands investigated and reported in this thesis.

7.1.1 Conclusions regarding the agarose coated spherical microsphere resonator for sensing of humidity

A compact relative humidity sensor based on a silica microresonator coated with a thin layer of agarose gel has been proposed and experimentally demonstrated. The sensor's operating principle is based on the changes in the refractive index of the agarose coating arising due to changes in the surrounding relative humidity, which leads to a spectral shift of the WGM resonances. The measured WGMs spectral shift can be related to the RH value after a suitable sensor calibration. The main conclusions drawn from this research are as follows:

- A simple dip coating method for functionalizing silica microspheres' surfaces with hygroscopic polymer layers has shown to be effective means for the application of coatings containing different concentrations of agarose, namely 0.5%, 1.125% and 2.25 wt./vol.%.
- The dependency of the sensitivity of the sensor to RH on concentration of the agarose gel in the coating has been studied experimentally, and it

is concluded that the RH sensitivity of the sensor increases with the increase of the agarose concentration in the coating material.

- The highest sensitivity achieved in the experiments was 518 pm/% RH in the humidity range from 30% to 70%RH for the coating containing 2.25 %wt./vol. of agarose.
- The experimental study of the relation between coating thickness and the Q factor of the agarose coated microsphere resonator concluded that the Q factor is gradually decreased with each coating cycle due to an increase of the coupling loss between tapered fiber and microsphere.
- The developed RH sensor based on an agarose coated spherical micro resonator offers is compact in nature, with low hysteresis, good repeatability, and a relatively low sensitivity to temperature (~ 6 pm/ $^{\circ}\text{C}$).

7.1.2 Conclusions regarding the influence of the agarose coating thickness on the sensitivity of the WGM sensor to relative humidity

The influence of the agarose coating thickness on sensitivity to relative humidity has been analyzed theoretically using perturbation theory and the results of the analysis and numerical simulations have been verified experimentally. For the experimental verification, a 260 μm diameter microsphere coated with agarose layers of different thickness was utilized, with the various thickness layers realized using multiple coating cycle. The results of the study are useful for the design and optimization of the microsphere sensor parameters for a specified performance and can be utilized in the design of similar sensors with different types of functional coatings.

- It has been concluded that an increase in the coating thickness initially leads to an increase in the RH sensitivity but this reaches saturation at a certain coating thickness ($\sim 1.6 \mu\text{m}$ in our experiments) and no further increase of RH sensitivity occur.
- Based on a knowledge of the operation of the sensor, it is concluded that a certain coating thickness, the WGM field becomes fully confined within the coating layer so that changes in the coating RI are most efficiently transformed into the spectral shift of the resonance and any further increase in the coating thickness does not lead to increase in sensitivity
- It is concluded that the good correlation between the experimental and theoretical modeling results allows for an approximate estimate of the agarose layer thickness.

7.1.3 Conclusions regarding application of the proposed agarose coated microsphere for sensing of low relative humidity

A novel approach to measure ultra-low concentrations of water vapor in air using an agarose coated microsphere WGM resonator has been proposed and experimentally demonstrated in the humidity range from 1 to 25% RH. The proposed approach is based on the use of a frequency detuning interrogation method in order to overcome the limited resolution of the common interrogation scheme, based on an optical spectrum analyzer. A customized experimental setup for sensor's characterization in the low RH range has been built. The main conclusions from this research are as follows:

- The demonstrated experimental sensitivity of the sensor is 0.71 pm/%RH with an estimated detection limit of 11.7 ± 0.32 ppm, which is the highest DL for water vapor reported to date.
- In addition, the sensor offers the advantages of high linearity of 99.9% ($R^2 = 0.9999$), low ($\pm 2\%$) hysteresis error, less than 3.5% temperature induced error in the range from 20 °C to 35 °C and a fast response (less than 900 ms).
- It is concluded that an increase in the surrounding the sensor humidity level from 0-25% RH leads to an increase of the agarose layer RI up to 4.7×10^{-4} RIU, this is based on the previously developed theoretical model and experimental findings in the low RH range, changes in the refractive index of the agarose layer within the studied RH range have been estimated theoretically.
- The measured response time (~900 ms) is dominated by the slow response of the humidity chamber (the time it takes for the new RH value to stabilize within the chamber's volume). This suggests that actual sensing response should be significantly faster.

7.1.4 Conclusions regarding the silica gel coated spherical microsphere resonator for ammonia sensing applications

A novel sensor based on a silica gel coated microsphere resonator is proposed and experimentally demonstrated for measurements of ammonia concentration in air with ultra-high sensitivity. The silica gel coating preparation method is developed based on the sol gel process. Two distinct interrogation techniques have been demonstrated for measurements of ammonia concentration using the proposed sensor, where one technique allows for the detection of a wide range of ammonia

concentrations. The alternative technique, based on frequency detuning is used to detect ultra-low concentrations of ammonia with higher sensitivity and resolution. Demonstrated excellent repeatability and long term stability of the sensor combined with its compact nature and potentially low cost are the added advantages of the proposed device.

The following conclusions are drawn from the ammonia sensing experiments:

- The maximum ammonia sensitivity demonstrated experimentally using the OSA for sensor interrogation is 34.4 pm/ppm within the range of ammonia concentrations of up to 30 ppm and with estimated DL of 62 ppb.
- The maximum sensitivity to ammonia achievable using the frequency detuning method is 800 pm/ppm within the range 2 to 13 ppb of ammonia molecules in air with the ammonia detection limit estimated as 0.16 ppb.
- It is concluded that the developed silica gel coating has high selectivity to ammonia in the presence of other volatile organic compounds verified by exposing to other VOCs such as Benzene, Acetone, N, N, Dimethyl formide, Butanol.
- It is found that the sensitivity of the sensor to ammonia initially decreases with the increase of humidity level in air stabilizing beyond 70 % RH. It should be noted however, that sensitivity of the sensor to ammonia is significantly higher than that to humidity (~ 2 times) in the low humidity range.
- A possible reason for the diminished response to ammonia with the increase of relative humidity inside the chamber is the increased

competition from the water molecules that are also easily adsorbed on the surface of porous silica gel coating.

- It is shown that the sensor shows very fast response and recovery times measured at 1.5 and 3.6 seconds, respectively.

7.1.5 Conclusions regarding the multi-parameter sensing with silica microsphere resonators

Finally, a new sensor design has been demonstrated for simultaneous high-resolution measurement of two physical parameters relative humidity and ammonia concentration, by coupling two silica microspheres coated with different functional layers to a single adiabatic tapered fiber. One of the microspheres was dip-coated with the silica gel and another with a 0.5 % wt./vol. agarose hydrogel. Since the optical properties of both coating layers change as a result of their exposure to ammonia and water molecules in the surrounding atmosphere, this leads to independent spectral shifts of the WGM resonances, associated with each of the microspheres being clearly distinguishable in the transmission spectrum of the tapered fiber. The following conclusions are drawn from this experiment:

- The silica gel coated microsphere is 95 % more sensitive to ammonia and 25 % less sensitive to relative humidity than the agarose coated microsphere.
- Studies of the sensitivity of both the microspheres to both parameters offers a mean for the determination of the cross-sensitivity coefficients of the characteristic matrix, allowing simultaneous measurement of both relative humidity and ammonia concentration, assuming an appropriate calibration has taken place.

- The maximum measurement resolutions of the two parameters were estimated as 42 ppb for ammonia and 0.56 %RH for humidity at the temperature of 25°C.
- Studies of the temperature dependence of the proposed sensor system showed a sensitivity of 5.8 pm/°C for the silica gel coated microsphere and 6.7 pm/°C for the agarose coated microsphere in the temperature range 20°C-40°C. Both dependencies are linear in nature and thus could be easily calibrated out with the addition of a temperature sensor to the system.
- The proposed technique allows reduction of the cost of multi-parameter sensors interrogation and could be potentially expanded towards a larger number of sensing parameters.

7.2 Future Work

Research described in this thesis has been dedicated to studies of the WGM effect in coated silica fiber microresonators. It resulted in the development of several novel fiber optic WGM sensors for environmental sensing applications. The study has also shown promise for the development of WGM sensors that may be tailored to other specific applications. There remain a number of unanswered research questions and challenges that current work could be extended to address.

7.2.1 Improving the accuracy of measurement for the sensor's response time

The response times for the coated WGM microsphere sensors were found to be 0.9 s [1] in the case of humidity sensor and 1.5 s [2] for the ammonia sensor. It is

likely however that the above response time values in addition to the response of the sensor itself include the time that takes for the ammonia or water molecules to diffuse through the chamber's volume. In all of the experiments described in this thesis, the sensor was mounted on an X-Y-Z nano positioning stage so that and the entire sensor system occupied $\sim 5 \text{ cm}^3$ volume, restricting the smallest volume of the environmental chamber. One possible solution for improving the accuracy of response time characterization is the development of the appropriate methods for sensor packaging and its mount which could lead (among other advantages) to the reduction of the effective environmental chamber volume, surrounding the sensor itself.

7.2.2 Sensor packaging and protection

By the nature of its operation any sensor based on a spherical microresonator requires direct interaction with the environmental conditions; therefore its performance usually degrades over a period of time due to a variety of factors, including different types of contamination, making the sensor unsuitable for long term measurements without special means of protection. Possible contamination agents are dust particles, organic pollutants and chemical vapors. Another important issue in the design of packaging for the WGM microsphere resonators is the need to maintain direct contact between the microsphere and the tapered fiber, whose waist diameter is in the order of $1\text{-}5 \text{ }\mu\text{m}$ to ensure highly efficient light coupling in and out of the resonator. To ensure the light coupling efficiency and its stability over time during the life time of the sensor, different approaches could be examined. A schematic diagram in Fig.7.1 presents one possible approach to packaging of the sensor for gas/humidity sensing applications. In this approach the microsphere (with its fiber "stem") is initially mounted on an X-Y-Z nano

positioning stage and then gradually brought in direct contact with the tapered fiber until the WGMs are clearly observed in the transmission spectrum of the tapered fibre. A separate cleaved fiber section is attached to the opposite pole of the microsphere using a fusion splicer to give maximum mechanical support to the microsphere during the coupling process. A UV glue is used to fix both the fiber taper and the microsphere's stem for long term stability.

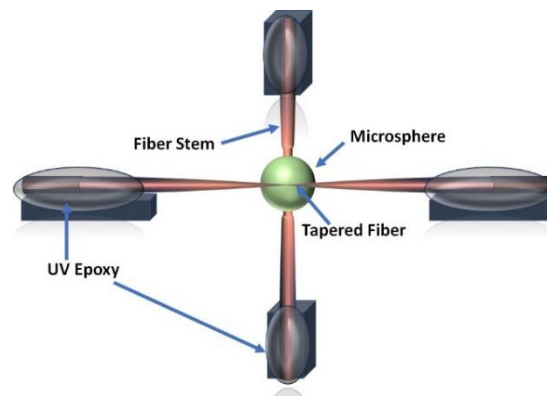


Fig. 7.1 Schematic diagram of one of the possible approaches to packaging of spherical micro resonator

7.2.3 More detailed study of multi parameter sensors based on the WGM effect for different applications

In Chapter 6, a multi parameter sensor for simultaneous measurement of water vapor and ammonia concentration in air was successfully demonstrated. This approach could be potentially extended to detection of additional number of VOCs in air. In general, VOCs have low boiling points and thus evaporate very quickly at room temperature. Their presence in industrial or domestic environments even in relatively low concentrations can cause serious health issues after inhalation of these gases by humans. It is important to monitor the concentration of the vapors to avoid environmental hazards. Some other greenhouses gases including carbon oxide derivatives (CO and CO₂), ammonia,

nitrogen oxides derivatives (NO_x) and sulphur dioxide (SO₂) are also needed to be monitored at ppb levels in air to prevent air pollution.. Sensor technologies with the ability to continuously monitor and accurately measure concentrations of these VOCs in air could provide the solution to control and minimize air pollution. Many techniques have been developed to measure the VOCs concentrations at ppm levels but only a few can offer measurement resolution at concentrations below parts per billion.

Achieve this goal with the proposed multi parameter array of WGM sensors, it is necessary to develop a series of specialized coating materials whose RI would change in proportion to the gas/VOC concentration in the environment with high selectivity. Using sol-gel techniques it may be possible to develop suitable coating materials for a small number of selected gases, so that each coated microsphere would target specific gas or a VOC of interest. This small number of microspheres would be coupled to an adiabatic fiber taper to produce a combined WGM transmission spectrum at the detector. Then tracking the spectral positions of each of the groups of WGMs would provide the information regarding each of the target gas concentrations with high resolution.

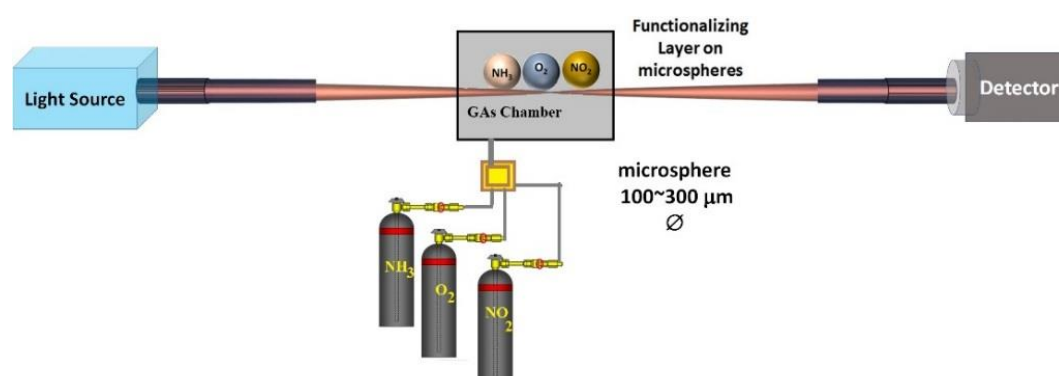


Fig. 7.2 Schematic diagram of the set up for simultaneous measurement of three different gases (NH₃, O₂ and NO₂) using an array of the WGM sensors

As an example, schematic diagram in Fig. 7.2 illustrates a possible setup for experimental characterization of an array of three WGM microsphere resonators for simultaneous measurement of oxygen, ammonia and nitrous oxide concentrations in air. Three different functional coatings targeting NH_3 , O_2 and NO_2 would need to be prepared and applied to the surface of each of the microspheres. As was demonstrated in this thesis, for ammonia sensing application porous silica gel can be used as the functional coating material. As a functional coating for sensing of oxygen, a material based on the mixture of TEOS, Octyl triEOS, Hydrochloric acid (HCl) and Triton X, described in [3], could be used. LuPc₂ (lutetium bisphthalocyanine) coating solution could be used to detect Nitrous oxide [4]. These three microspheres will produce three different groups of WGMs in the transmission spectrum of the coupling fiber. Then the spectral shifts of each of the group of the WGM resonances could be linked to the corresponding changes in the respective gases concentrations.

Another broad field for potential applications of the proposed WGM sensors is in biomedical applications for detections of various disease markers and other bio-analytes.

References:

- [1] A. K. Mallik, G. Farrell, D. Liu, V. Kavungal, Q. Wu, and Y. Semenova, "A Coated Spherical Micro-Resonator for Measurement of Water Vapor Concentration at ppm Levels in Very Low Humidity Environments," *J. Light. Technol.*, 2018.
- [2] D. Liu *et al.*, "Sol-gel silica coated optical fiber sensor for ammonia gas detection," in *ICOON 2016 - 2016 15th International Conference on Optical Communications and Networks*, 2017.
- [3] M. Zolkapli, S. Saharudin, S. H. Herman, and W. F. H. Abdullah, "The influence of sol-gel coated length and withdrawal rate on plastic optical fiber core towards oxygen gas sensing sensitivity," *J. Teknol.*, 2016.
- [4] C. Bariáin, I. R. Matías, C. Fernández-Valdivielso, F. J. Arregui, M. L. Rodríguez-Méndez, and J. A. De Saja, "Optical fiber sensor based on lutetium bisphthalocyanine for the detection of gases using standard telecommunication wavelengths," in *Sensors and Actuators, B: Chemical*, 2003, vol. 93, no. 1–3, pp. 153–158.

Appendix A

Statement of Contribution

For the publications presented within this thesis, the co-authors listed below certify that:

1. Arun Kumar Mallik is the first author for all the publications.
2. As first author, Arun Kumar Mallik undertook all aspects of the research described in each publication, including preparation and submission of the publication and the preparation of any revisions requested by referees, with the support and advice of the co-authors.
3. The co-authors agree to the use of the publications in this thesis.



Prof. Yuliya Semenova



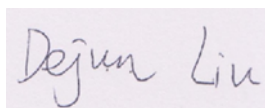
Prof. Gerald Farrell



Dr. Qiang Wu



Dr. Manjusha Ramakrishnan



Mr. Dejun Liu



Mr. Vishnu Kavungal

Appendix B

B. WGMs field distributions in an uncoated microsphere resonator

Electromagnetic field distribution in a dielectric sphere depends on the sphere's effective radius, dielectric loss factor for different modes and the transmission coefficient between the microsphere and the coupling tapered fiber. Fig 1.2 in Chapter 1 shows the microsphere in spherical coordinates where r indicates the radial direction, φ is the azimuthal angle in the y - z plane and θ is the polar angle perpendicular to the y - z plane. The solution of the Helmholtz equation in spherical coordinates can be expressed as (Eq.(1.5) in Chapter 1):

$$\psi_{l,m,n}(r, \theta, \varphi) = N_s \cdot \psi_r(r) \cdot \psi_\theta(\theta) \cdot \psi_\varphi(\varphi) \quad (\text{B-1})$$

where $\psi_r(r)$, $\psi_\theta(\theta)$ and $\psi_\varphi(\varphi)$ represent the fields in the radial, angular/polar and azimuthal directions respectively. The normalization constant, N_s is determined by the division of a volume integral of the square magnitude of the field over the entire volume of the microsphere to the microsphere circumference $2\pi R_0$ [1]. Next, we solve the field distribution for each component of the electric field.

7.3 Radial field distribution

The radial component of the field satisfies the following equation:

$$\frac{d^2\psi_r}{dr^2} + \frac{2}{r} \frac{d\psi_r}{dr} + \left(k^2 n_s^2 - \frac{l(l+1)}{r^2} \right) \psi_r = 0 \quad (\text{B-2})$$

The two independent solutions of Eq. (B-2) are found in the form of spherical Bessel function $j_l(kn_s r)$ and a Neuman function $y_l(kn_s r)$ as:

$$\psi_r = c_1 j_l(kn_s r) + c_2 y_l(kn_s r) \quad (\text{B-3})$$

where

$$\begin{aligned} j_l(kn_s r) &= \sqrt{\frac{\pi}{2kn_s r}} J_{l+0.5}(kn_s r) \quad r \leq R_0 \\ y_l(kn_s r) &= \sqrt{\frac{\pi}{2kn_s r}} Y_{l+0.5}(kn_s r) \quad r > R_0 \end{aligned} \quad (\text{B-4})$$

To validate the solutions (B-4), let us examine them when the sphere's radius approaches 0. From the property of spherical Bessel functions it is known that if $(kn_s r) \ll 1$, $j_l(kn_s r) \rightarrow \frac{(kn_s r)^l}{(2l+1)!}$ then $y_l(kn_s r) \rightarrow -\frac{(2l-1)!}{kn_s r^{l+1}}$ which means $y_l(r)$ is divergent as $r \rightarrow 0$. Since the field must be finite everywhere, the radial field distribution inside the sphere is reduced to

$$\psi_r(r) = A j_l(kn_s r), \quad r \leq R_0 \quad (\text{B-5})$$

The evanescent field outside of the sphere decreases exponentially and the solution for the electric field outside of the sphere calculated from Eq. (B-4) becomes

$$\psi_r(r) = B e^{(-\alpha_s(r-R_0))} \quad (\text{B-6})$$

where $\alpha_s = \sqrt{\frac{l(l+1)}{R_0^2} - k^2 n_0^2}$ and n_0 is the refractive index of the surrounding medium.

Eq. (B-5) and Eq. (B-6) combined together present the radial field of a microsphere as:

$$\psi_r(r) = \begin{cases} A j_l(kn_s r) & r \leq R_0 \\ B e^{(-\alpha_s(r-R_0))} & r > R_0 \end{cases} \quad (\text{B-7})$$

where A and B are constants determined by matching the boundary conditions at the surface. The radial field distribution is related to the mode numbers l and n

that denote the number of maxima of the field along the radial distribution. The characteristic equation for the fundamental mode with a fixed value of l is derived by matching tangential field components at the boundary at the microsphere surface, given as [1]:

$$\left(\eta_s \alpha_s + \frac{1}{R_0}\right) j_l(k n_s R_0) = k n_s j_{l+1}(k n_s R_0) \quad (\text{B-8})$$

$$\text{where } \eta_s = \begin{cases} 1 & TE \\ \left(\frac{n_s}{n_0}\right)^2 & TM \end{cases}$$

Eq. (B-8) has multiple solutions for each value of l . These solutions represent resonance wavelengths of the 1st order mode (fundamental mode), 2nd order mode, and so on. For example, resonance wavelengths that correspond to the 1st and 2nd order modes are 1.608 μm and 1.388 μm , respectively for a 5 μm radius microsphere. The simulated radial electric field distributions for the 1st and 2nd order modes are shown in Fig. B.1. It can be seen from the figure that for the fundamental mode electric field has its maximum close to the surface of the microsphere whereas the maximum of the field for the 2nd order mode is located further away from the microsphere surface. The electric fields outside the sphere decay exponentially.

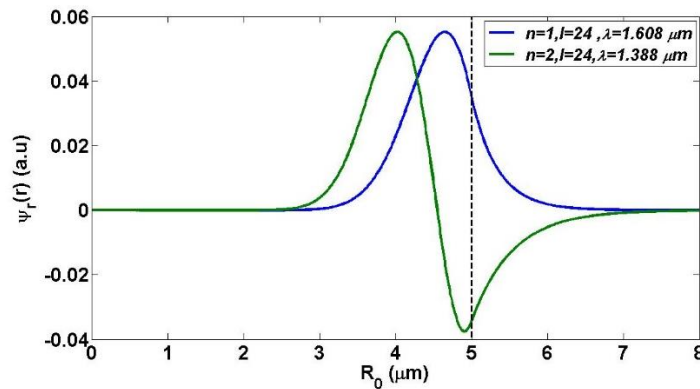


Fig. B.1 Simulated WGM radial field intensity distributions for the 1st order mode $n = 1$, $l = 24$, $\lambda = 1.608 \mu\text{m}$ and 2nd order mode $n = 2$, $l = 24$, $\lambda = 1.388 \mu\text{m}$ for a sphere of radius $R=5 \mu\text{m}$, $n_s = 1.4682$, $n_0 = 1$.

7.4 Azimuthal field distribution

The azimuthal field distribution can be derived as

$$\frac{d^2\psi_\varphi}{d\varphi^2} + m^2\psi_\varphi = 0 \quad (\text{B-9})$$

The solution of Eq. (B-9) is in the form:

$$E_\varphi = N_\varphi \exp(\pm im\varphi) \quad (\text{B-10})$$

$$N_\varphi = \frac{1}{\sqrt{2\pi}}$$

where N_φ is the normalization constant chosen so that the integration of $|\psi_\varphi|^2$ over one revolution is unity.

7.5 Polar field distribution

The polar electric field component satisfies the equation [1]:

$$\frac{1}{\cos\theta} \frac{d}{d\theta} \left(\cos\theta \frac{d}{d\theta} \psi_\theta \right) - \frac{m^2}{\cos^2\theta} \psi_\theta + l(l+1)\psi_\theta = 0 \quad (\text{B-11})$$

The solution of this differential equation assumes the form of

$$\psi_\theta(\theta) \approx p_l^m(\cos\theta) \quad (\text{B-12})$$

where p_l^m are the adjoint Legendre polynomials and m degenerates with l in wavelength, that is for a given polar index, l , there are $2m + 1$ modes that possess the same resonant wavelength. $m = -l, -(l-1), -(l-2), \dots, (l-2), (l-1), l$ and $l - m + 1$ gives the number of intensity maxima in the polar direction. We assume that modes confined to the plane of equator ($\theta \approx 0$, θ is measured from the equator plane) are those that most strongly coupled to the fiber. We make an approximation that $\tan\theta \approx \theta$ and $\frac{1}{\cos^2\theta} \approx \theta$, so that equation (B-11) becomes

$$\frac{d^2}{d\theta^2}\psi_\theta - \theta \frac{d}{d\theta}\psi_\theta - m^2(1+\theta^2)\psi_\theta + l(l+1)\psi_\theta = 0 \quad (\text{B-13})$$

and the solution of Eq.(B-13) is

$$\psi_\theta = N_\theta \exp\left[-\frac{m}{2}\theta^2\right] H_N(\sqrt{m}\theta), m \gg 1 \gg \theta \quad (\text{B-14})$$

where $N = l - m$, $H_N(x)$ are the Hermite polynomials and N_θ is the normalization factor measured as the integral of $|\psi_\theta|^2$ over infinite gives unity.

Hence,

$$N_\theta = \frac{\sqrt{m}}{2^N \sqrt{\pi} N!} \quad (\text{B-15})$$

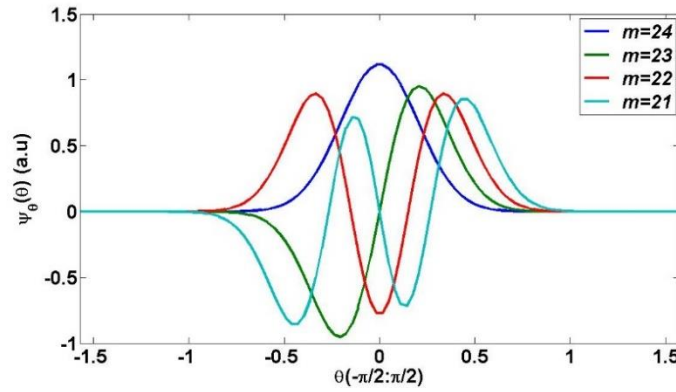


Fig. B.2 Simulated electric field distribution in the polar angular direction $l = 24, m = 24, 23, 22, 21, n = 1$.

The electric field distribution in the direction of polar angle depends on l and m .

The first four polar modes that degenerate at the same wavelength $\lambda = 1.608 \mu\text{m}$ are shown in Fig. B.2.

A contour plot of the field distribution for the 1st order mode ($n = 1, l = m = 24, \lambda = 1.608 \mu\text{m}$) in the radial and azimuthal directions $\psi(r, \varphi)$ is shown in Fig. B.3. As can be seen from the figure the fundamental mode has one maximum in the radial direction near the surface and 48 peaks in the azimuthal direction

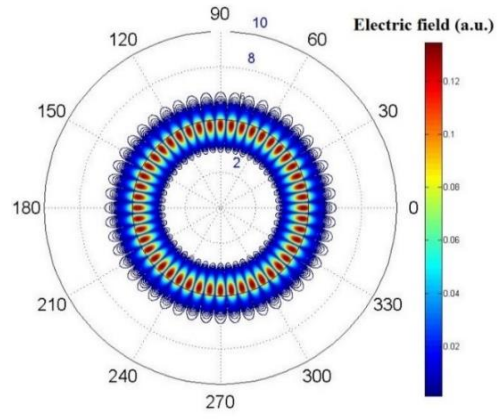


Fig. B.3 The contour plot of electric field distribution in the $r - \varphi$ plane, $n = 1$, $l = m = 24$, $\lambda = 1.608 \text{ } \mu\text{m}$, $R_0 = 5 \text{ } \mu\text{m}$.

Appendix C

WGM field distribution in a microsphere resonator coated with a thin functional layer

In this thesis the main focus was on improving the sensitivity of spherical WGM resonators to changes in concentration of specific molecules in the surrounding the resonator atmosphere, thus analysis of sensitivity was crucial to understanding of the experimental outcomes. For sensing the microspheres were coated with thin layers of different materials, so that the sensitivity of such a WGM sensor was determined both by the RI of the coating layer and its thickness.

The radial field distribution of the transverse electromagnetic (TE) WGM in a coated microsphere as stated in Chapter 1:

$$E_l = \begin{cases} A_l \psi_l(n_s k r) & r \leq R_0 \\ B_{1l} \psi_l(n_f k r) + B_{2l} \chi_l(n_f k r) & a_1 \leq r \leq R_0 \\ C_l \chi_l(n_0 k r) & r \geq a_1 \end{cases} \quad (0-1)$$

where A_l , B_{1l} , B_{2l} and C_l are constant whose values can be determined from the boundary conditions at $r = R_0$ and $r = R_1$. At the interface between the sphere and the coating layer, the radial field value E_l and its derivative E_l' must be continuous.

At $r = R_0$ the radial fields E_l and E_l' are given by Eq. (C.2):

$$\begin{aligned} E_l &= \begin{cases} A_l \psi_l(n_s k R_0) \\ B_{1l} \psi_l(n_f k R_0) + B_{2l} \chi_l(n_f k R_0) \end{cases} \\ E_l' &= \begin{cases} A_l n_s k \psi_l'(n_s k R_0) \\ B_{1l} n_f k \psi_l'(n_f k R_0) + B_{2l} n_f k \chi_l'(n_f k R_0) \end{cases} \end{aligned} \quad (0-2)$$

At the boundary $E_l = E_l'$ and Eq. (C-2) becomes:

$$\begin{aligned} A_l \psi_l(n_s k a_0) &= B_{1l} \psi_l(n_f k R_0) + B_{2l} \chi_l(n_f k R_0) \\ A_l n_s k \psi_l'(n_s k R_0) &= B_{1l} n_f k \psi_l'(n_f k R_0) + B_{2l} n_f k \chi_l'(n_f k R_0) \end{aligned} \quad (0-3)$$

We can rewrite Eq. (C-3) as

$$\frac{\psi_l(n_s k R_0)}{B_{1l}\psi_l(n_f k R_0) + B_{2l}\chi_l(n_f k R_0)} \quad (0-4)$$

$$\begin{aligned} &= \frac{n_s k \psi_l'(n_s k R_0)}{B_{1l} n_f k \psi_l'(n_f k R_0) + B_{2l} n_f k \chi_l'(n_f k R_0)} \\ &\psi_l(n_s k R_0) \{B_{1l} n_f k \psi_l'(n_f k R_0) + B_{2l} n_f k \chi_l'(n_f k R_0)\} \\ &= n_s k \psi_l'(n_s k R_0) \{B_{1l} \psi_l(n_f k R_0) + B_{2l} \chi_l(n_f k R_0)\} \\ &\psi_l(n_s k R_0) B_{1l} n_f k \psi_l'(n_f k R_0) + \psi_l(n_s k R_0) B_{2l} n_f k \chi_l'(n_f k R_0) = \\ &n_s k \psi_l'(n_s k R_0) B_{1l} \psi_l(n_f k R_0) + n_s k \psi_l'(n_s k R_0) B_{2l} \chi_l(n_f k R_0) \\ &\psi_l(n_s k R_0) B_{1l} n_f k \psi_l'(n_f k R_0) - n_s k \psi_l'(n_s k R_0) B_{1l} \psi_l(n_f k R_0) \\ &= n_s k \psi_l'(n_s k R_0) B_{2l} \chi_l(n_f k R_0) \\ &- \psi_l(n_s k R_0) B_{2l} n_f k \chi_l'(n_f k R_0) \\ &B_{1l} k (n_f \psi_l(n_s k R_0) \psi_l'(n_f k R_0) - \\ &n_s \psi_l'(n_s k R_0) \psi_l(n_f k R_0)) = B_{2l} k (n_s \psi_l'(n_s k R_0) \chi_l(n_f k R_0) - \\ &\psi_l(n_s k R_0) n_f \chi_l'(n_f k R_0)) \end{aligned} \quad (0-5)$$

$$\begin{aligned} \frac{B_{1l}}{B_{2l}} &= \frac{n_s \psi_l'(n_s k R_0) \chi_l(n_f k R_0) - n_f \psi_l(n_s k R_0) \chi_l'(n_f k R_0)}{n_f \psi_l(n_s k R_0) \psi_l'(n_f k R_0) - n_s \psi_l'(n_s k R_0) \psi_l(n_f k R_0)} \\ \frac{B_{1l}}{B_{2l}} &= \frac{\frac{n_s}{n_f} \psi_l'(n_s k R_0) \chi_l(n_f k R_0) - \psi_l(n_s k R_0) \chi_l'(n_f k R_0)}{\psi_l(n_s k R_0) \psi_l'(n_f k R_0) - \frac{n_s}{n_f} \psi_l'(n_s k R_0) \psi_l(n_f k R_0)} \\ \frac{B_{1l}}{B_{2l}} &= \frac{\eta_1 \psi_l'(n_s k R_0) \chi_l(n_f k R_0) - \psi_l(n_s k R_0) \chi_l'(n_f k R_0)}{\psi_l(n_s k R_0) \psi_l'(n_f k R_0) - \eta_1 \psi_l'(n_s k R_0) \psi_l(n_f k R_0)} \end{aligned}$$

where $\eta_1 = \frac{n_s}{n_f}$.

Let us find out the field distribution within the coating layer and its surroundings.

At $r = R_1$, the radial fields E_l and E_l' should be continuous and satisfy the Eq.

(C-6).

$$\begin{aligned} E_l &= \begin{cases} B_{1l} \psi_l(n_f k R_1) + B_{2l} \chi_l(n_f k R_1) \\ C_l \chi_l(n_0 k R_1) \end{cases} \\ E_l' &= \begin{cases} B_{1l} n_f k \psi_l'(n_f k R_1) + B_{2l} n_f k \chi_l'(n_f k R_1) \\ C_l n_0 k \chi_l'(n_0 k R_1). \end{cases} \end{aligned} \quad (0-6)$$

At the boundary $E_l = E_l'$ and Eq. (B.6) becomes:

$$\begin{aligned} B_{1l} \psi_l(n_f k R_1) + B_{2l} \chi_l(n_f k R_1) &= C_l \chi_l(n_0 k R_1) \\ B_{1l} n_f k \psi_l'(n_f k R_1) + B_{2l} n_f k \chi_l'(n_f k R_1) &= C_l n_0 k \chi_l'(n_0 k R_1). \end{aligned} \quad (0-7)$$

We can rewrite Eq. (B.7) as

$$\begin{aligned} & \frac{B_{1l}\psi_l(n_fkR_1) + B_{2l}\chi_l(n_fkR_1)}{C_l\chi_l(n_0kR_1)} \\ &= \frac{B_{1l}n_fk\psi_l'(n_fkR_1) + B_{2l}n_fk\chi_l'(n_fkR_1)}{C_ln_0k\chi_l'(n_0kR_1)} \end{aligned} \quad (0-8)$$

$$\begin{aligned} & \frac{\frac{B_{1l}}{B_{2l}}\psi_l(n_fkR_1) + \chi_l(n_fkR_1)}{\chi_l(n_0kR_1)} = \frac{\frac{B_{1l}}{B_{2l}}n_f\psi_l'(n_fkR_1) + n_f\chi_l'(n_fkR_1)}{n_0\chi_l'(n_0kR_1)} \\ & n_0\chi_l'(n_0kR_1) \left\{ \frac{B_{1l}}{B_{2l}}\psi_l(n_fkR_1) + \chi_l(n_fkR_1) \right\} \\ &= \chi_l(n_0kR_1)n_f \left\{ \frac{B_{1l}}{B_{2l}}\psi_l'(n_fkR_1) + \chi_l'(n_fkR_1) \right\} \end{aligned} \quad (0-9)$$

$$\eta_0 \frac{\chi_l'(n_0kR_1)}{\chi_l(n_0kR_1)} = \frac{\frac{B_{1l}}{B_{2l}}\psi_l'(n_fkR_1) + \chi_l'(n_fkR_1)}{\frac{B_{1l}}{B_{2l}}\psi_l(n_fkR_1) + \chi_l(n_fkR_1)}$$

where $\eta_0 = \frac{n_0}{n_f}$.

The constant terms A_l and C_l can be derived from Eq. (C-2) and Eq. (C-7):

$$A_l = \frac{B_{1l}\psi_l(n_fkR_0) + B_{2l}\chi_l(n_fkR_0)}{\psi_l(n_ska_0)} \quad (0-10)$$

$$C_l = \frac{B_{1l}\psi_l(n_fkR_1) + B_{2l}\chi_l(n_fkR_1)}{\chi_l(n_0kR_1)} \quad (0-11)$$

The RI sensitivity for the TE polarization (S_{TE}) in the coated microsphere can be calculated as [2]:

$$S_{TE} = \frac{n_2\lambda_R I_2}{n_1^2 I_1 + n_2^2 I_2 + n_3^2 I_3} \quad (0-12)$$

where I_1 , I_2 and I_3 are the fractions of the mode's energy distributed within the silica microsphere, polymer coating layer and the surrounding medium respectively. The detailed application of Eq. (C.12) has been used in Chapter 3 and Chapter 5.

References:

- [1] B. E. Little, J. P. Laine, and H. A. Haus, “Analytic theory of coupling from tapered fibers and half-blocks into microsphere resonators,” *J. Light. Technol.*, vol. 17, no. 4, pp. 704–715, 1999.
- [2] I. Teraoka and S. Arnold, “Enhancing the sensitivity of a whispering-gallery mode microsphere sensor by a high-refractive-index surface layer,” *J. Opt. Soc. Am. B*, vol. 23, no. 7, p. 1434, 2006.